Argonne National Laboratory

THE MASS TRANSFER OF SINGLE, SOLID URANIUM SPHERES TO FLOWING MOLTEN CADMIUM IN LAMINAR AND TURBULENT FLOW

by

E. Dean Traylor

Printed in USA. Price $5.00. Available from the Clearinghouse for Federal Scientific and Technical Information, National Bureau of Standards, U. S. Department of Commerce, Springfield, Virginia

ANL-7091
Engineering and
Equipment (TID-4500)
AEC Research and
Development Report

ARGONNE NATIONAL LABORATORY
9700 South Cass Avenue
Argonne, Illinois 60439

THE MASS TRANSFER OF SINGLE, SOLID URANIUM SPHERES TO FLOWING MOLTEN CADMIUM IN LAMINAR AND TURBULENT FLOW

by

E. Dean Traylor

Chemical Engineering Division

Based on a Thesis
Submitted to the Faculty of the Graduate School
of The Ohio State University
in Partial Fulfillment of the Requirements for the Degree of
Doctor of Philosophy

September 1965

Operated by The University of Chicago
under
Contract W-31-109-eng-38
with the
U. S. Atomic Energy Commission

A short article, summarizing the work reported here in full is published in Industrial and Engineering Chemistry Fundamentals, Vol. 4, page 119, May 1965.

TABLE OF CONTENTS

TABLE OF CONTENTS

TABLE OF CONTENTS

TABLE OF CONTENTS

TABLE OF CONTENTS

TABLE OF CONTENTS

LIST OF FIGURES

LIST OF FIGURES

LIST OF FIGURES

LIST OF TABLES

LIST OF TABLES

NOMENCLATURE

A_v	counts/minute for vibration index
Δ_a	activity driving force
aH_t	dimensionless number used in packed bed correlation by Gaffney-Drew[2]
A_i	values of J_d at Reynolds number of 3.5×10^4
A	characteristic or appropriate area, cm^2
A_c	cross sectional area, cm^2
A_p	cross sectional area of pipe, cm^2
A_n	nominal sphere area, cm^2
A_s	arithmetic mean area by average of micrometer measurements before and after mass transfer runs, cm^2
A_m	geometrical mean area, cm^2
a	exponent on $N_{Re,s}$
a_1	activity of uranium in liquid cadmium, $N_1\gamma_1$ (atom fraction units)
a_s	activity of uranium at saturation
B	magnetic field strength of magnets in electromagnetic flowmeter, gauss
B_j	values of J_d at a Reynolds number of 7×10^4
b	exponent on N_{Sc} for temperature variation
C_i	values of J_d extrapolated through hump at a Reynolds number of 7×10^4
C_s	concentration of uranium in dissolved cadmium at saturation, g/cc
C_1	concentration of uranium in dissolved cadmium, g/cc
ΔC	concentration driving force ($C_s - C_1$), g/cc, or ($C_1 - C_2$) for equation 3.1
C	concentration of uranium in capillary, percent
ΔC_{max}	maximum concentration driving force ($C_s - 0$), g/cc
C_a	average concentration of uranium in capillary, percent
ΔC_i	concentration driving force when the concentration of the liquid is varied by the addition of uranium, g/cc
C_0	initial concentration, percent
C_{Wa}	weighted average of concentration, percent
C_1	constant in equation 10.6
$\overline{C}$	average concentration in capillary after diffusion, percent
C_d	average discharge coefficient for orifice
C_p	specific heat at constant pressure, cal/mole °K
C/C_0	ratio of extinction phenomena for x-ray diffraction analysis or random orientations of uranium material
d	pipe diameter, cm, or molecular volume for N molecules $(V/N)^{1/3}$
d_p	loop pipe diameter, cm
d_s	average sphere diameter, cm
d_1, d_2, d_3	interatomic distances perpendicular to the direction of diffusion, Å units
D_L	axial mixing coefficient in direction along tube axis, cm^2/sec
D_v	molecular diffusivity, cm^2/sec
D_0	molecular diffusivity at reference temperature, T_0 cm^2/sec; orifice diameter, cm
D	distance or characteristic dimension in equation 3.12 for plates, cm
E	emf generated by liquid metal flowing through electromagnetic flowmeter
$\overline{E}$	average emf generated by liquid metal flowing through electromagnetic flowmeter
E_i	instantaneous emf corresponding to velocity at θ' during coast-down
E_{ss}	steady state emf corresponding to average velocity in loop pipe
f_d	total drag coefficient, f_d (reference 77)
f	Fanning friction factor
F	fractional surface renewal
g	gravitational constant, 980.665 cm sec^{-2}
h	heat transfer coefficient Btu/hr ft^2 °F
H	distance from wall of solute in Harriott's theory, cm
h'	head across orifice, feet
I_0	diffraction of x-rays from an hkl plane of known random structure
I	diffraction of x-rays from plane hkl of uranium for diffraction analysis
J_d	Colburn mass transfer J_d factor, dimensionless
J_d'	Colburn mass transfer J_d factor with N_{Sc}0.58, dimensionless
k	interfacial transfer coefficient, gm/cm^2 sec, g/cc; also mass transfer coefficient in Harriott's theory
K	constant in electromagnetic flowmeter equation 9.7
k_1	mass transfer coefficient, g/cm^2 sec (g/cc)
k_g	mass transfer coefficient based on gas film
L	length of flat plate, cm; also conduction path for emf generated by flowing liquid cadmium
l	length of capillary for diffusion experiment, cm
M_A	molecular weight in general for diffusate in equation 3.9
N_{Gr}	modified Grashof number for mass transfer, $g d_s^3 \Delta C/(\mu/\rho)$
$N_{Re,a}$	Reynolds number based on average pipe velocity, $d_p V_a \rho/\mu$, dimensionless
$N_{Re,s}$	Reynolds number based on the sphere, $d_s V_s \rho \mu$, dimensionless
N	atom fraction of uranium in cadmium
N_{Sh}	Sherwood number, $k_1 d_s/D_v$, dimensionless
N_{Sh}^*	Sherwood number after contributions of natural convection and radial diffusion are subtracted out
N_{Sc}	Schmidt number, $\mu/\rho D_v$, dimensionless
M	downstream gage at orifice radius tap, mm Hg
N_{Pr}	Prandtl number of liquid cadmium, dimensionless
N_{Nu}	Nusselt number, dimensionless
N_A	mass flux from sphere, g/sec cm^2
$P(\alpha,\beta)$	volume fraction of material with various orientations compared to standard of high degree of random orientations
P	pressure, lb/in^2
Q_a	activation energy for diffusion, cal/g mole
q	heat transfer rate, Btu/hr
R	radius of diffusing particle, Å units (10^{-8}) cm
R'	gas constant, cal/g mole
s	rate of eddy production for surface renewal theory
t_i	time corresponding to velocity, V_i
t	time of exposure of solvent elements to solute in surface renewal theory, sec
T	torque, inch-pounds
T°C	temperature, °C
T°K	temperature, °K
T_e	experimental temperature at sphere, °C
u	0.5 for surface renewal theory
V	valve designation
V_i	instantaneous velocity during coast-down at θ_i, cm/sec
$\overline{V}$	average velocity at sphere during coast-down, cm/sec
V_a	average velocity in tube, cm/sec
V_0	velocity over a flat plate, cm/sec
V_f	film velocity, cm/sec
V_{ss}	steady state velocity as checked by electromagnetic flowmeter which is also the same as V_s, cm/sec
V_s	corrected velocity at sphere in the annular space between the sphere and the pipe wall, cm/sec
$(V/N)^{1/3}$	estimate of effective molecular volume for N particles
V_1	molecular volume, cc/mole
$\Delta w'$	weight loss from sphere during coast-down time, gms
Δw	weight loss from sphere used for J_d correlation, gms
Δx_f	film thickness, cm
X	distance along axis of capillary, cm
x	exponent on N_{Sc} in slope analysis of J_d lines; also inches of Hg absolute
z'	used for pressure calculation, $(\Delta P)^{1/2}/C_d$, mm $Hg^{1/2}$
Z	distance along plate, cm, or mm of Hg absolute
α	effective number of neighbors of molecules lying in same plane
β^{at}	function for distribution of eddies from H to infinity as a function of time
Γ	momentum
$\Gamma(\alpha)$	distribution function for lifetime of eddy production in Harriott's theory
μ	viscosity in centipoise, or radius of diffusing particle
ρ	density, g/cc
ρ_{cd}	density of cadmium, g/cc
θ'	coast-down time after motor shut off at pump, sec
θ	time for the length of a mass transfer run, sec
γ	activity coefficient of uranium in atom fraction units in cadmium solution; also ratio of area correction for orifice to pipe
$\overline{\epsilon}$	average fractional rate of coast-down
ϵ_i	instantaneous value of steady flow rate at time θ' during coast-down
$\Psi(N_{Re,s}, N_{Gr}, N_{Sc})$	functional notation for Reynolds, Schmidt, and Grashoff moduli
$\phi(N_{Re})$	function of N_{Re}
ϕ_1	concentration ratio for diffusion analysis for equation 7.14
ϕ_2	equation 7.14
$\phi'(\mu, \rho, D_v)$	Schmidt number function, or function of physical properties

THE MASS TRANSFER OF SINGLE, SOLID URANIUM SPHERES TO FLOWING MOLTEN CADMIUM IN LAMINAR AND TURBULENT FLOW

by

E. Dean Traylor

I. SUMMARY AND ABSTRACT

The mass transfer of normal uranium to molten cadmium was studied in order to extend the present data on mass transfer in aqueous and metal systems and to test previous classical correlations as well as propose others. The relative high density of molten cadmium as compared with water made possible the attainment of very high Reynolds numbers, and afforded the opportunity to extend the mass transfer data into an unknown area.

In this study, a 1/2-inch diameter uranium sphere was used and molten cadmium was pumped past the test spheres at different flow rates. Mass transfer coefficients were determined from weight losses of the test spheres.

The cadmium-uranium system was chosen because it was possible in this system to operate in a temperature range in which uranium was the solid phase in equilibrium with the molten cadmium solution. The J_d data and other derived correlations were compared with previous correlations and data for different systems. The experimental curves for mass transfer from uranium spheres in a flowing cadmium stream have the same general shape as those found previously by Geankoplis and Steele[22] for the mass transfer from 2-naphthol, benzoic acid, and cinnamic acid in water. An exception to this similarity is that a pronounced hump in the J_d factor versus Reynolds' number correlation occurs in the vicinity of 10^5 Reynolds number, i.e., the region where turbulence penetrates to the surface of the sphere, and associated pressure changes occur in the vicinity of the sphere. Geankoplis and Steele observed only a small hump at this point in their correlations.

The driving force for mass transfer was varied for the uranium-cadmium system and the mass fluxes were obtained and plotted versus the concentration and activity driving forces. Extrapolation of these curves to zero driving force yielded finite mass flux rates which were different from the zero value expected at the saturated condition. Steele and Geankoplis[22]

also obtained a finite flux at zero driving force and suggested the attrition from the sphere might account for it. It was shown in this work that neither attrition nor the activity data and activity driving force could account for the finite flux at zero driving force.

Uranium spheres which were heat-treated showed random grain structures and yielded J_d values about 2 to 5 times higher than spheres not heat-treated to give nonrandom structures.

The skin friction, $f/2$, for spheres in organic liquids from Reynolds numbers of 10^2 to 10^3 and at a separate Reynolds number of 1.56×10^5 was 2 to 3 times greater than the J_d for uranium-cadmium. The results of runs with artificially roughened spheres showed that the roughening produced no effect at a Reynolds number of 330. At a Reynolds number of 8.8×10^3 the J_d for the roughened sphere was about 80% higher than for the smooth sphere. This could be attributed to the early onset of the tripping of the boundary layer.

The exponent of the Schmidt number was determined at Reynolds numbers of 735 and 115. The exponent on the Schmidt number was determined to be approximately 0.60. However, the range of variation of the Schmidt number was only 60%.

Prior to this work all liquid metal dissolution data was obtained over a very limited Reynolds number range or at a constant Reynolds number. The present work for the correlation of J_d from 10^2 to 5×10^5 provides for the first time good evidence that the conventional mass transfer expressions can be used for liquid metal systems.

II. INTRODUCTION

A study was initiated in the Chemical Engineering Division at Argonne National Laboratory to obtain information concerning the dissolution of uranium in flowing molten cadmium. This problem was selected to provide additional information useful for other investigations in liquid metal media which are of prime importance in connection with fuel recovery processes being developed for Experimental Breeder Reactor (II) fuel materials. The specific problem, viz., to measure the dissolution rates from uranium spheres into flowing molten cadmium streams was chosen by representatives of Argonne National Laboratory in the Chemical Engineering Division and the Chemical Engineering Department of The Ohio State University. This work was chosen to extend the studies previously made by Geankoplis and Steele[22] at Ohio State University who investigated mass transfer from spheres of various materials (e.g., benzoic acid, cinnamic acid, and 2-naphthol) into flowing water.

The dissolution from uranium spheres to molten cadmium was chosen in belief that such a study could provide sufficient information on corrosion problems or operative mechanisms involved with mass transfer in liquid metals. Spheres were chosen because they were used by other investigators and are frequently encountered in practical applications. Mass transfer to or from spherical bodies is of importance in the dissolution of solid materials, either deliberate, or in a corrosion sense, where molecular diffusion is operative. Furthermore, spheres provide a convenient reference upon which to present a general correlation, since the correlation may be corrected to apply to irregular particles by replacing the test sphere diameter by an equivalent diameter of a sphere which has the same surface area as the irregular particle. Since it was desirable to compare the results of this work with that of other investigators, geometry of the apparatus and the boundary conditions were chosen to be approximately similar. This requirement roughly established the equipment size and shape, but the choice of cadmium as a solvent increased the power and equipment requirements over those of other investigators because of the relatively high density of cadmium (about 7 g/cc) and the fact that operations had to be conducted around 500°C to 600°C.

Figure 1 shows the partial phase diagram for the uranium-cadmium system. The reasons for choosing this system are discussed in detail in Chapter IV. However, it may be observed that above a temperature of 473°C the solubility of uranium in cadmium remains reasonably constant. Thus, one may vary the temperature of the system above 473°C during the mass transfer runs without appreciably changing the concentration driving force. This, in essence, suggests that the exponent on the Schmidt number may be determined independently of the temperature variation of the coefficient of solubility. In addition, above a temperature of 473°C the possible formation

of intermetallics during a mass transfer run is eliminated because saturated solutions are in equilibrium with uranium metals. A big advantage derived from the choice of cadmium as a solvent is that it may be easily contained in mild steels or stainless steels.

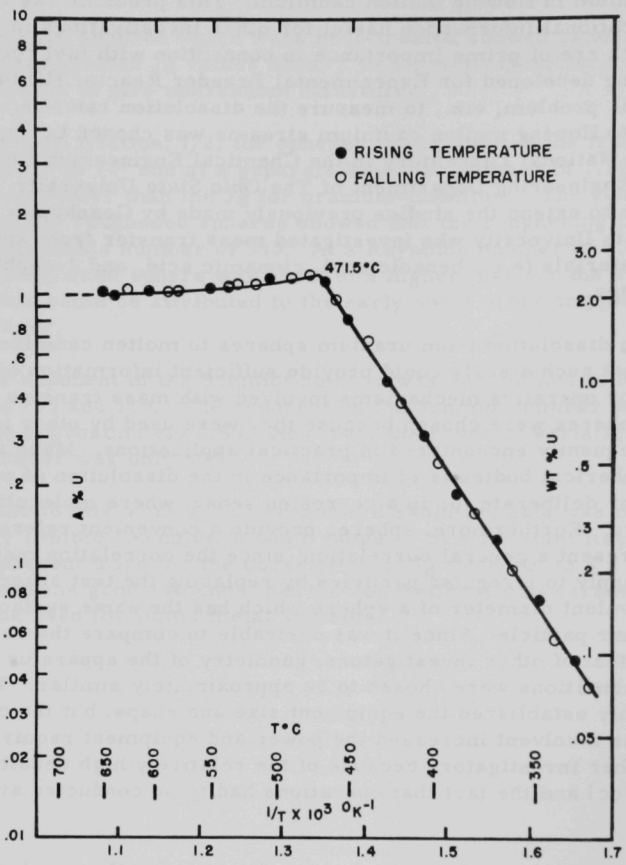

Fig. 1. The Uranium Cadmium Phase Diagram[5]

The principle variables selected for investigation of their effects on the mass transfer rate and the resulting mass transfer correlations were velocity of the flowing cadmium, temperature of the system (hence, variation of physical properties of the solvent), and the degree of saturation of the solvent.

III. LITERATURE SURVEY AND DEVELOPMENT OF THEORY

A. Introduction Remarks

The study of the diffusion of solids into aqueous and organic liquids has received considerable attention in the past years. Several analogies have been presented which seem to be relatively limited in generality. This is due to the nature of turbulent phenomena which cannot be characterized exactly by mathematical treatment nor experimental measurement. It is believed that an extension of experimental work to the area of liquid metals may provide a means of further testing some of the widely used analogies, viz., Chilton-Colburn equations, and possibly provide some insight into mass transfer mechanisms as affected by the general characteristics of liquid metals. This chapter will discuss the older theories of mass transfer as well as more recent concepts. A discussion of the mass transfer coefficient and the relationship between mass and heat transport in liquid metals may also afford a basis for further studies in the diffusional process of dissolution. Attempts will be made to present a mathematical analysis of the kinetics of dissolution, although generally better results have been obtained from semi-empirical equations.

B. Literature Review of Mass Transfer and Dissolution Theories

1. General Discussion of Mass Transfer Theories

Models previously used to explain mass transfer have involved such concepts as presence of stagnant liquid films, turbulent eddy penetration, and interfacial resistance to mass transfer between phases. The concept of a hypothetical liquid film was first suggested by Nernst.[6] Whitman[7] later proposed the film theory to facilitate the interpretation of mass transfer data. Later models for mass transfer were proposed and perhaps the most revolutionary was that of Higbie[8] who suggested the penetration theory. There have been subsequent modifications to this theory, but the fundamental approach used by Higbie seems to be common to most of these. In recent years, some have suggested that the mass transfer between phases occurs at a finite rate across some equivalent resistance at the interface between solid and liquid phases. These investigators have modified earlier interpretations of the various theories to account for this interfacial resistance.

The following discussion attempts to review briefly the essential points of the theories mentioned above to provide continuity and clarification for other elements of this report. The discussion shall include:

(1) Film theory for mass transfer;

(2) Penetration theories in mass transfer;

(3) Random surface renewal theory;

(4) Random eddy penetration model for mass transfer;

(5) Theories pertaining to interfacial resistance between phases; and

(6) General summary and evaluation of mass transfer theories.

a. Film Theories

The original concept of a stagnant film adjacent to the solid phase has already been mentioned as due to Whitman and Nernst.[6] Although experimental evidence indicates that the concept of a completely stagnant film is most likely fictitious, the model helps in understanding the transfer of mass under the influence of a concentration gradient. Usually the transfer of mass flux, N_A (weight/unit time, area) is pictured as occurring across a stagnant film next to the solid wall, i.e., the concentration gradient for molecular diffusion is only effective across the stagnant film. It is assumed that transfer of mass in the film is accomplished by molecular diffusion. The mass flux, N_A, is represented by an equation

$$-N_A = \frac{D_v}{\Delta x_f} (C_1 - C_2) \tag{3.1}$$

where

D_v = molecular diffusivity of diffusate,

Δx_f = film thickness, and

$C_1 - C_2$ = the concentration gradient.

b. Penetration Theory

Higbie[8] originally proposed the penetration theory in his study of liquid and gas phases in absorption processes. In this theory, mass is assumed to be transferred into the liquid phase under unsteady state conditions. The equation which relates the mass flux at a point in the surface of the liquid in contact with a gas phase is given as

$$-N_A = \left(\frac{D_v}{\pi t}\right)^{1/2} (C_1 - C_2) \tag{3.2}$$

where t equals time of contact of liquid and gas phases. The theory was effective in providing further insight into the correct mechanism for mass transport.

c. Random Surface Renewal Theory

Danckwerts[9,10] modified Higbie's theory to apply to absorption in turbulent flow.

$$-N_a = (D_v s)^{1/2} (C_1 - C_2). \tag{3.3}$$

The experimental data were shown to be consistent with 3.3 as indicated by Hanratty.[11] This recent evidence tends to disfavor the concept of the laminar sub-layer and pictures the mass exchange at the solid surface in terms of mass exchange to eddies which penetrate directly to the surface in turbulent motion.

d. Random Eddy Penetration Model for Mass Transfer

Harriott[12] presented a modification of the previous penetration models based upon the random motion of eddy lifetimes and a random distribution of distances from the solid surface. Harriott chose a random sequence of distances, H, and times to fit distributions of the type:

$$p(t) = \frac{1}{\Gamma(\alpha)\beta^{\alpha t}} t^{\alpha-1} \exp\left(\frac{-t}{\beta}\right) \tag{3.4}$$

where α was taken as 1 for the distribution of lifetimes. For distances, α was taken as 1 and 2.

Generally, this theory does not include the effect of flow across a surface. Harriott states that a more critical test of this mass transfer model could be made if more data were available for N_{Sc} of 1,000 to 100,000.

e. Toor's Film-Penetration Model

The penetration theory of Higbie[8] and the random surface renewal theory of Danckwerts[9,10] have been shown to be special cases of a more general theory as shown by Toor.[82] Toor presents a film-penetration model which includes the essential features of the surface renewal theories, viz., the surface renewal rate, the thickness of the region where the surface renewal occurs, and the molecular diffusivity, D_v. Experimental evidence has not yet been obtained to verify this theory or to differentiate between the special cases of Higbie[8] and Danckwerts.[9,10] This has been discussed in section B.2 of this chapter.

f. Theories Pertaining to Interfacial Resistance

Noted discrepancies between experimental data and that predicted by the other theories such as those previously mentioned, have

prompted many investigators to introduce the concept of a resistance to mass flux at the interface between phases.[13,14,15] This deviation is usually attributed to the absence of thermodynamic equilibrium at the interface between phases. According to Scott,[16] the concentration profiles at the interface are related by a coefficient which relates the mass flux, N_A, to the concentration in each phase and allows the mass flux to be written as:

$$N_A = k_1(C_I - mC_{II}) \tag{3.5}$$

where the transfer coefficient, k_1 pertains to the region at the interface and approaches a very large value if there is no resistance, and approaches zero if there is an interfacial resistance. The subscripts I and II refer to phases I and II, respectively. The term "m" in the above equation 3.5 represents the relationship between equilibrium concentrations in phases I and II.

2. General Summary and Evaluation of Mass Transfer Theories

For the purposes of the discussion which deals with solid-liquid mass transfer it seems appropriate to classify the above-mentioned theories as falling in either the film category or the surface renewal group. The concept of an interfacial resistance seems to be controversial at present and is not subject to incorporation in either category. Needless to say, however, more research involving this concept may allow such incorporation.

There is at present insufficient experimental evidence to completely favor the film theory or the surface renewal theory. The mass transfer driving force for both theories is chosen as the difference in the bulk fluid concentration and the concentration at the interface.

In the film theory proposed by Whitman[7] the fundamental assumptions are those of Nernst.[6] These involve the assumptions of a stagnant layer of liquid or a liquid film adjacent to the solid surface. Turbulence may exist elsewhere in the system. These assumptions have in both cases been the starting point for the two-film theory and subsequent mathematical treatment of mass transfer. In penetration[8] or random surface renewal theories[9,10] there is involved the continuous replacement of fresh liquid to the solid surface probably admitted by turbulent eddy motion. Usually the mathematical treatment of mass transfer in the latter case follows a certain sequence of preliminary steps which involves generating mathematical relationships to express the rate of surface renewal, the distribution of eddy lifetimes or frequencies, as well as the molecular diffusivity of this system. For this study, it is more convenient to express the mass transfer coefficient in terms of the following relationships for either the film theories or the surface renewal group:

$$k_1 = D_v/\Delta x_f \quad \text{(Film Theories)} \tag{3.6}$$

$$k_1 = (D_v s)^u \quad \text{(Surface Renewal Theories)} \tag{3.7}$$

where k_l is the mass transfer coefficient, D_v represents the molecular diffusivity, Δx_f represents the film thickness, s = fractional rate of surface renewal, and u represents the value of 0.5. The fundamental difference between the groups appears to be in the relationship of the mass transfer coefficient k to the exponent on the molecular diffusivity. In the former case the mass transfer coefficient is directly related to the molecular diffusivity, and in the latter case the mass transfer coefficient depends upon the square root of the molecular diffusivity.

However, it is noted that while verification of mass transfer data as definitely falling in either group may be possible, the direct verification of either theory for different substances of widely variant physical properties presents difficulty. For example, in the film theory, the film thickness has not yet been directly measured. In the surface renewal theory, the rate of surface renewal remains an experimental problem. Therefore, neither theory may be regarded as entirely acceptable, and direct verification of either theory must be postponed until these experimental obstacles are overcome.

3. Solid-to-Liquid Mass Transfer

Several major contributions have been made in the field of solid-to-liquid mass transfer. The theories which have been developed have attained varying degrees of success in predicting mass transfer data. Garner and Grafton[17] developed equations for the mass transfer from a sphere. Friedlander[18] and Kronig and Brujsten[19] developed equations for heat and mass transfer from cylinders and spheres at low N_{Re}. These authors[19] were not able to predict with accuracy mass transfer rates and coefficients, for example, as did Friedlander[18] with linearized solutions to the Navier-Stokes equations for the boundary layer. Sherwood and Ryan[20] summarize the models previously used to describe turbulent diffusion between phases. More specifically, they compare Hatta's stagnant film model with Danckwerts' (Refs. 9, 10) penetration of a renewable interface model, which itself was a modification of Higbie's model. Sherwood and Ryan propose a third model which utilizes a film and the expression developed by Deissler[21] for the variation of eddy viscosity in the turbulent core Furthermore, the same authors point out that the equation which will predict with accuracy the phenomena of heat and mass transport in turbulent flow must await the exact understanding of the mechanism of turbulence and turbulent transfer processes.

Therefore, in lieu of the inability to express the influence of individual parameters separately, the field of mass, heat and momentum transport has relied upon the correlation of experimental data by variables expressed in dimensionless groups. A recent example of this approach is found in the work of Steele and Geankoplis[22] in their semi-theoretical approach to the problem. They used the J_d factor, $\left(\frac{k_l}{V_s} N_{Sc}^{2/3}\right)$, for mass

transfer (Chilton-Colburn analogy) and correlated their data versus the Reynolds number for the dissolution of spheres of benzoic acid, 2-naphthol, and cinnamic acid into water flowing past the sphere.

4. Mass Transfer and Mechanisms in Liquid Metals

In comparison to the simpler systems such as dissolution into water or some organic liquid, the mass transfer of metals into metals is expected to present a more complex problem as far as mechanism is concerned. It is realized, of course, that a better understanding of the liquid state could help in concept, design, and interpretation of a research problem in this area. Provided a theory of the liquid state was well known and understood, an approach to the mass transfer problem in liquid metals could obviously be theoretical, and could deal with a static system. Another approach in the theory of mass transport, and one in which practical information could result is to utilize a dynamic experimental technique. This means, in essence, to utilize a flowing system. The rate of mass transfer was measured for metal shapes dissolving in mercury at room temperature by Dunn and Bonilla.[3] Sherwood numbers for horizontal cylinders of tin, cadmium, zinc, and lead dissolving by natural convection agreed with Nusselt numbers for heat transfer in nonmetallic liquids at the same Rayleigh numbers (Grashof x Prandtl number). Dissolving of zinc tubes by mercury flowing through them agreed with heat transfer correlations for nonmetal systems at a Reynolds number range between 5×10^2 and 2×10^4. Bonilla did not investigate mass transfer from spheres. Generally, he concluded that mass transfer in liquid metal systems followed the same correlations as presented for other solids and fluids in mass transfer.

The work of Epstein[23] is recalled in connection with a treatment to the mass transfer problem where the iron-sodium system was analyzed. Epstein indicates that in a static, isothermal system, the rate of mass transfer is determined by classical solution theory which involves a solution rate constant. As pointed out by Epstein, the value of this parameter depends upon which of the following two mechanistic steps is rate controlling:

a. The diffusion of solute through the liquid;

b. The transfer of solute through a solid film of some product of chemical reaction at the solid-liquid interface.

Manly[24] mentioned the following possible mechanisms in his corrosion study:

(1) simple solution of metal;

(2) alloying of solid metal constituents with solvent metal;

(3) intergranular diffusion;

(4) reaction of impurities;

(5) temperature gradient induced mass transfer; and

(6) concentration gradient induced mass transfer.

In a dynamic system such as the one employed in the study described in this report (the dissolution of uranium spheres in flowing cadmium), the following probable mechanisms might be suggested as additional ones for consideration:

(7) mechanical attrition (i.e., turbulence effects)

(a) regular mass transfer--no surface pitting

(b) regular mass transfer--high surface pitting;

(8) generation of electromotive couple; and

(9) chemical reaction products adhering to solid phase at interface--i.e., interfacial resistance.

It may be helpful to summarize all of these listed mechanisms to present a clearer picture of the dissolution process. For this discussion the following table has been prepared. Examination of Table I shows the following possibilities as regards individual mechanisms which may occur during dissolution:

(1) A change in temperature of either solute or solvent may induce a temperature gradient which influences the concentration profiles in the vicinity of the solid-liquid interface. If solubility changes with temperature, then the concentration driving force which is taken as the saturated concentration minus the concentration in the bulk liquid becomes a function of temperature of the liquid. The physical properties of the liquid such as density, viscosity, molecular diffusivity, are a function of temperature.

(2) Chemical reactions tend to complicate mass transfer because of the probable formation of chemical reaction products. These products may collect on the solid surface and reduce the mass transfer rate. The chemical reactants may also react at local sites on the solid surface; these local spots may resist mass transfer and as a result dissolution occurs around them until the final result is that these same areas are dissolved out carrying entire chunks of solute crystals with them. After chunks of solute crystals are dug out the surface becomes susceptible to accelerated dissolution. Reactions between chemical reactants at grain boundaries may provide a start for intergranular penetration. This becomes especially important when temperature changes bring about expansion of the reaction products at grain boundaries which tend to open paths for intergranular diffusion of liquid into solid.

TABLE I. Mass Transfer Characteristics

Factor or Source of Proposed Mechanism	Mechanism or Result of Source
1. Temperature	1. Temperature-gradient induced mass transfer. 2. Variation of solubility with temperature. 3. Variation of physical properties of solvent.
2. Chemical Reactions	1. Chemical reaction at interface of solid and liquid causing finite resistance. 2. May occur at local sites thus causing local attack and hence an increase in interfacial area for other mechanisms present. 3. Occurrence at grain boundaries causes possible expansion of solid structure especially at temperature variation making substrate susceptible to porous or intergranular diffusion.
3. Solute Surface Preparation Prior to Exposure to Solvent	1. Acid treated surfaces may lead to partial or initial dissolution. 2. Surface electropolished may also cause some effect on initial dissolution rate. 3. Hardness variation over surface.
4. Solute Characteristics	1. Hardness, and/or chemical affinity for solute to solute molecules or atoms may lead to ease of molecular activation, erosion susceptibility, etc. 2. Crystal orientation at solid surface and at grain boundaries. 3. Grain size, anisotropy effects, impurities, may lead to intergranular penetration, reactions at grain boundaries, etc. 4. Porosity of solid, that is, number of and length of diffusion paths.
5. Solvent Saturation	1. Concentration of solute in solvent affects concentration induced mass transfer. 2. Heterogeneous reactions between phases may cause formation of intermetallics which complicate thermodynamic description. 3. Purity of solvent. 4. Classification of solvent (i.e., metal, fused salt, electrolyte, organic or water, etc.)

(3) The condition of the surface of the solid, for example its relative roughness, may affect the initial mass transfer rate. Furthermore, if the surface of the solid varies in relative hardness dissolution will take place at a faster rate on the softer areas. In general, a metal surface that has been acid cleaned to remove oxide films is rougher than a surface that has been electropolished for the same purposes.

(4) Solute characteristics are important in the mass transfer from solids to solvent media. The relative hardness of different solutes becomes a major factor in affecting the mass transfer rate under conditions of solution rate mass transfer. Solutes with hardness numbers close to that of talc, viz., benzoic acid and cinnamic acid will certainly be attacked to a greater extent than metal solutes by erosion and mechanical attrition. Since the degree of erosion at a solid surface is also a function of the relative velocity between solid and liquid as well as hardness, the effects of erosion are expected to be greatest at the higher pumping rates.

Crystal orientation at boundaries which are exposed to solvent or in regions where solvent may diffuse during dissolution may allow overall dissolution to proceed in a preferred direction or manner. In solutes where the grains are regularly oriented and where intergranular or porous diffusion is present, the rates of attack may be different than under similar circumstances for solutes which possess randomly-oriented structures.

The condition of the individual grains such as variation of grain size which also implies a change in surface area and also certain anisotropic properties may allow preference to one or more of the several dissolution mechanisms as well as allow different rates of attack at individual grains.

(5) The condition and state of the solvent metal may bring about mass transfer under different conditions. The concentration level of the solute in the solvent as already mentioned may affect the mass transfer rate. If the solvent contains impurities or chemical reactants, then intermetallics may form between the various impurities, and the solvent or solute, which tend to complicate the dissolution process. The general chemical nature of the solvent may also play an important role with certain solutes.

The above discussion has dealt with mass transfer and mechanisms which may be applicable to liquid metal systems. Most generally, however, the data presented on metal systems in the literature were from corrosion studies and were obtained as a result of the pressing developmental problems associated with the integrated development of nuclear reactors. Hoffman[25] gives the summary of classified and unclassified literature to 1959 dealing with lithium. The work was concerned with the

containment of lithium in engineering systems. Until recently, there was little information on the kinetic and solubility relationships for metals dissolving in lithium. Ward and Taylor[26] studied the kinetics of dissolution of copper in liquid lead and bismuth and also iron in bismuth. Measuring the solute concentration as a function of time at various temperatures under static and dynamic conditions, they concluded that the net rate of dissolution was determined by the diffusion step. Stevenson and Wolff[27] surmised that the dissolution of copper and nickel in liquid lead is diffusion controlled at lower velocities, but mixed control, i.e., diffusion and solution rate, occurs at the higher velocities. Lommel and Chalmers[28] employing a different technique, concluded that the dissolution of lead in liquid lead-tin alloys was diffusion limited at no stirring rates and at high stirring rates was solution rate limited.

5. Dissolution as a Rate Process

Here, the dissolution process may be considered to be a result of either individual, consecutive, or simultaneous driving forces which provide the potential for mass flux and which is limited or controlled by some resistance such as a film, interfacial resistance, or reaction mechanism. Several rates could be postulated but the most probable and therefore the most fundamental ones may be immediately written for a dynamic isothermal loop such as the one employed in this study. These follow below:

(1) ease of molecular activation at interface;

(2) diffusion of solute molecules through a saturated film or partially saturated film, viz., a Nernst film; and

(3) diffusion of solute molecules through a complete or partial zone of some chemical reaction product at the interface.

Note that Epstein[23] discussed the latter two steps.

In the most general case, it is assumed that all of these postulates are present and that each contributes a certain resistance to mass flux from the solid phase. Apparently, the first mechanism is always present since a necessary amount of energy must be supplied to the solid phase at the interface to activate the diffusing atoms or molecules. The concept of a solute diffusing through a saturated film of solvent located adjacent to the solid at the interface is relatively easy to accept under the conditions of laminar flow. Should the solid phase contain impurities or alloys which react with the solvent, or should intermetallics be formed between solute molecules and the solvent, diffusion of the reaction products to the solid-liquid interface may allow the development of a film which hinders mass transfer. Under conditions of median pumping rates where the level of turbulence is

moderate, these reaction products may completely adhere to the solid surface and a definite resistance to normal mass transfer occurs. As the pumping rate is increased to higher relative velocities, to a Reynolds number range of 5×10^5, the level of turbulence increases and its effect at the solid-liquid interface tends to a maximum as some of this reaction product zone or all of it is carried away by eddy penetration to the solid surface.

From the consideration of dissolution as a rate process and for the purposes of an analytical study simple models may be suggested which help form the foundation for the treatment of experimental data. In terms of the rate steps listed above, the following cases (I-IV) classify typical conditions for dissolution under varying flow rates and temperatures.

Case I Laminar Flow--No Chemical Reaction--The steps which might exist are (1) surface activation of solute followed by (2) the molecular diffusion through the Nernst film.

Case II Laminar Flow--With Chemical Reaction--Here, dissolution from solute into the solvent may occur according to (1) surface activation, (2) diffusion across a surface film formed by possible adherence of chemical reaction products or intermetallics followed by (3) diffusion through a Nernst type liquid film.

Case III Slightly Turbulent Flow--It is postulated that the boundary layer begins to become unstable with some eddy penetration to the solid surface. Therefore, there is possibly a region where mixed control occurs as molecular diffusion and solution rate. This probably manifests itself in the initial stages predominantly as molecular diffusion with a gradual change and preference to solution rate as the relative velocity is increased to fully turbulent flow. The sequence of steps may vary depending upon the presence or absence of chemical reaction products or intermetallics:

(1) No Chemical Reaction Products--In this situation the following may occur:

(a) The solute molecules are activated, and

(b) either diffuse through a boundary layer to the bulk stream, or the solute molecules may be swept from the solid surface by the fluid momentum. A partial boundary layer still exists.

(2) Chemical Reaction Products Present--It is proposed that the following may exist:

(a) The solute molecules are activated, and

(b) must then diffuse across an adhering film of chemical reaction products where step (b) of (1) above may apply.

Case IV Fully Turbulent Flow-- Turbulent conditions and turbulent diffusion through phases constitute the most difficult situation to assign a model for dissolution. The model would have to account for the actual shift of the boundary layer over the sphere and its absence at the very high velocities. Furthermore, if chemical reaction products were present, the mechanical forces resulting from turbulent eddies acting at the solid surface may not allow deposition of chemical reaction products. Mention must also be made of the probable existence of an important mechanism at the higher velocities, commonly called pitting.

Pitting results at specific locations on the solid surface which may be prestressed zones where the solute is more resistant to attack than at other areas; in this situation entire chunks of crystals may be left in initial stages of dissolution as adjacent areas of the solute are dissolved away. Finally, the solute is dissolved around the points of higher relative potential energy and the chunks are eroded away. Pitting may also occur at the low or high relative velocities as a result of cavitation erosion which results from an abnormal pressure distribution over the solid surface. Another reason for pitting may result from nonuniform solute purity. This type of pitting could occur at any velocity range as dissolution progressed. If inclusions resulting from the presence of impurities, or solid state chemical reactions resulting from the reaction between impurities, or impurities and solute, exist in the solid phase, dissolution may occur around them. They are therefore swept away by the fluid momentum as they are loosened leaving depressions or cavities in the solid surface. The final result, in essence, amounts to a pitted solid surface and an increase of solid phase surface area.

6. Semi-empirical Correlations in Mass Transfer

Employing dimensional analysis many engineers have correlated much data for heat and mass transfer. In general, many of these correlations for mass transfer employ the Sherwood number, the Reynolds number, the Schmidt number, and the Grashof number modified for mass transfer. For fluids with Prandtl and Schmidt numbers >1, the counterparts to these numbers in heat transfer are the Nusselt number, the Reynolds number, the Prandtl number, and the Grashof number for heat transfer.

A semi-theoretical approach to mass transfer from spheres has been shown by Steele[22] who employed the classical Chilton-Colburn analogy for mass transfer. It is recalled that the Chilton-Colburn analogy is strictly valid for N_{Pr} and N_{Sc} equal to 1 since it stems from the Reynolds analogy. However, its general use and derivation has been discussed in Chapter III. It will be useful to also test the applicability of this correlation in this study.

a. Correlations from Spheres Using N_{Sh}

Sherwood[29] presents a summary of data on mass transfer to single spheres, but does not compare the results with friction or momentum transfer. The data which were correlated were selected from the following: Froessling[30] on aniline, water, naphthalene, nitrobenzene: Powell[31] on water and ice; Houghton and Radford[32] on water data as correlated as the Sherwood number as ordinate versus the product of the Reynolds' number and Schmidt number to the 2/3 power on a log-log plot. Sherwood states that for these substances, the data for heat and mass transfer appear to be in fair agreement.

Steinberger and Treybal[4] measured the dissolution rates from benzoic acid spheres and employed the functional correlation

$$N_{Sh} = \psi(N_{Re}, N_{Sc}, N_{Gr}). \tag{3.8}$$

They compared their results with those of Mathers[33] for natural convection and with Maisel,[34] Kramers,[35] Garner and Grafton,[17] Garner and Suckling,[36] and Gates and Shanks[37] to show the effect of Grashof and Schmidt moduli. Assuming that the general correlation for mass transfer from spheres to liquids and gases was of the following form

$$N_{Sh} = 2.0 + 0.569(N_{Gr} N_{Sc})^{0.25} + 0.347 N_{Re}^{0.62}(N_{Sc}^{1/2})^{0.62} \tag{3.9}$$

they correlated data of Froessling,[30] Houghton and Radford,[32] Hsu, Sato, and Sage,[38] Maisel and Sherwood,[34] Powell[31] Ranz and Marshall,[73] Garner and Grafton,[17] Garner and Suckling,[36] and Gates and Shanks[37] for mass transfer and found that the data could be correlated over a wide range of number moduli with an average deviation of about 20 percent. All of these data were below a Reynolds number of 10^5.

b. Correlations Using the J_d Factor

The Chilton-Colburn J_d factor for mass transfer is given as

$$J_d = \frac{k_1}{V}(N_{Sc})^{2/3} \tag{3.10}$$

$$J_d = 0.023(N_{Re})^{-0.2} \tag{3.11}$$

for forced convection conditions. For the viscous region, the Leveque[41] equation becomes

$$J_d = 1.61(N_{Re})^{-0.666}(L/D)^{-1/3}. \tag{3.12}$$

Linton and Sherwood[39] on mass transfer inside of tubes made from cinnamic acid, benzoic acid, and 2-naphthol showed that equations 3.11 and 3.12 predicted rates with reasonable agreement with experiments. However, mass transfer on wetted wall columns did not agree too well because of movement of the liquid film.

c. Dissolution from Plates

Using flat plates of stainless steel 304 and liquid lithium, Gill et.al.[40] studied the mass transfer rate and used Von Karmans integral method to analyze the data. They made a heat balance over a flat metal plate using the 1/7 power law for turbulent velocity distribution and arrived at relationships for local and total fluxes:

$$q = 0.0285\ \rho C_p V \theta (\mu/\rho V_0 z)^{0.2} \tag{3.13}$$

$$q = 0.356\ \mu C_p \theta (\rho V L/\mu)^{0.8} \tag{3.14}$$

The assumption is that for a constant ΔC the integral mass flux over the length of the plate varies with $(V_0 L/\mu)^{0.8}$ for an isothermal system if liquid resistance controls. If the transfer process is controlled by solid-phase diffusion, the rate is independent of velocity and directly proportional to the length of the plate.

Dunn and Bonilla[3] as previously stated, studied the mass transfer rates of solid metal shapes dissolving into mercury. Natural convection mass transfer involved the rates of dissolution of cylinders of tin, lead, zinc, and cadmium in mercury. Also, mercury was pumped through zinc tubes and the mass transfer data correlated employing the Sherwood number as a function of the Grashof number for mass transfer and the Schmidt number. They concluded that mass transfer in liquid metals essentially followed mass transfer in other systems and agreed fairly well with heat transfer in nonmetals. They found that the J_d factor for packed beds of metal shot dissolving in Hg could be better correlated when the Schmidt number was raised to the 0.58 exponent.[3]

d. Discussion of Chilton-Colburn Analogy[72]

The classical analogy between heat transfer and pipe friction known as the Reynolds analogy is strictly valid when N_{Pr} and N_{Sc} equal 1. The analogy holds for most gases at ordinary pressures.

Prandtl and Taylor[41] modified the Reynolds analogy for heat transfer by allowing for the mechanism of heat transfer in the laminar, buffer, and turbulent zones and as a result of relating their expression and

the expression for the momentum transfer coefficient f, the following equation results for the relationship between heat and the momentum transport

$$h = \frac{f}{2} C_p V_a \rho \frac{1}{\left(1 - \frac{V_F}{V_a} + \frac{V_F}{V_a} N_{Pr}\right)}. \tag{3.15}$$

It is found that equation 3.15, although a modification and improvement of the Reynolds analogy, for heat transfer still does not predict data well for substances whose N_{Pr} is greatly different from unity.

Colburn in a heat transfer correlation found that the data could be described more completely by replacing the term

$$\left(1 - \frac{V_F}{V_a} + \frac{V_F}{V_a} N_{Pr}\right) \tag{3.16}$$

by the term N_{Pr} raised to the 2/3 power. Upon this substitution, equation 3.15 becomes

$$h = \frac{f}{2} C_p V_a \rho \frac{1}{N_{Pr}^{2/3}}. \tag{3.17}$$

Equation 3.17 may be solved for the momentum transfer coefficient or friction factor f,

$$\frac{f}{2} = \frac{h}{C_p V_a \rho} N_{Pr}^{2/3}. \tag{3.18}$$

The term on the right side of the equality in equation 3.18 is called the Chilton-Colburn J_d factor for heat transfer.

Equations 3.15, 3.16, and 3.17 are based upon the analogies which may be written between heat and momentum transfer. Similar expressions may be developed between mass and momentum transfer as well as the Taylor-Prandtl analog for mass transfer. This allows the Colburn J_d factor for mass transfer to be written with a procedure similar to that described. In this case the mass transfer is characterized by the Schmidt number, N_{Sc}, in the same way that the Prandtl number, N_{Pr}, characterized heat transfer. Therefore, the mass transfer equation similar to equation 3.15 for heat transfer becomes

$$\frac{f}{2} = \frac{k_g M_a P}{V_a \rho}\left(1 - \frac{V_F}{V_a} + \frac{V_F}{V_a} N_{Sc}\right) \tag{3.19}$$

or,

$$\frac{f}{2} = \frac{k_g M_a P}{V_a \rho} (N_{Sc})^{2/3} = J_d. \qquad (3.20)$$

This expression with the Schmidt number to the 2/3 power in equation 3.20 is the Colburn J_d factor for mass transfer. Treybal[41] states that the term

$$\left(1 - \frac{V_F}{V_a} + \frac{V_F}{V_a} N_{Sc}\right) \qquad (3.21)$$

of equation 3.19 may be considered as the result of two contributions (again allowing for the different mechanisms of mass transfer). The first part of equation 3.21, i.e., $\left(1 - \frac{V_F}{V_a}\right)$, may be taken as $\left(1 - \frac{V_F}{V_a}\right) N_{Sc}^0$ and according to Treybal[41] represents the contribution to mass transfer in the turbulent core. The remainder of the term, viz., $\frac{V_F}{V_a} N_{Sc}^1$, represents the laminar film contribution where the importance of D_v or the N_{Sc} to the power of 1 is important. The Colburn modification according to Treybal compromises the two contributions by assigning the N_{Sc} an exponent of 2/3 which is between 0 for the turbulent contribution and 1 for the laminar contribution. The implication of a compromise between the laminar and turbulent contributions which leads to the exponent of 0.666 is questionable for liquid metals. Therefore, the exponent on the Schmidt number for this study may be different than 0.666. Gaffney and Drew[2] found that for the mass transfer from succinic acid spheres in packed beds to water that a plot of aHt versus the Schmidt number showed that the exponent on the Schmidt number was 0.58. They also found that the exponent for gases was 0.666.

IV. STATEMENT OF PROBLEM

A. Introduction

Liquid metals constitute a group of substances which are especially interesting because of their specific physical properties. For example, their relative high thermal conductivities make them an excellent choice for coolants in nuclear reactors when other factors are considered such as their low melting points, and high densities with corresponding low vapor pressures. Thus, they are capable of removing relatively large amounts of heat in relatively small volumes. As a result of this application, quite a voluminous amount of material has been published concerning their heat transfer properties.[42,43] Comparison of the experimental data in liquid metals with the predicted data for heat transfer coefficients of liquid metals showed that the empirical expressions for the Nusselt number N_{Nu} must be modified to account for these discrepancies.

Corrosion problems in these systems are very important since thermal differences in a loop can result in dissolution and deposition at some cold spot giving a "plugged" condition. A study of these problems involves the determination of the mass transfer coefficients and their variation with other prime variables. In aqueous systems where mass transfer data are not available for some specific system, but heat transfer data are available, these coefficients for mass transfer may be predicted from the heat transfer data employing the Chilton-Colburn analogy.[41] Many of the underlying assumptions here are based upon the Reynolds analogy which only holds for values of the N_{Pr} and N_{Sc} equal to 1. It becomes obvious then, that mass transfer data cannot be predicted from empirical equations similar to those given for heat transfer by simply replacing dimensionless groups in heat transfer by their counterparts in mass transfer for the liquid metals since the N_{Pr} is much less than 1 for liquid metals.

For the above reasons, it was decided to study mass transfer in liquid metal systems. A study of mass transfer from a metal sphere in a flowing metal system was selected because this would constitute an extension of similar work by Steele and Geankoplis[22] in aqueous systems. Appreciable differences in the physical properties of metal systems as compared with aqueous systems result in considerable difference in dimensionless groups used to correlate mass transfer data, i.e., Reynolds and Schmidt numbers. This makes possible a better definition of the effects of various parameters on mass transfer. Mass transfer in metal systems was also of interest to the co-sponsoring institution, Argonne National Laboratory, because of its strong interest in the use of metal systems for processing nuclear fuel materials.

The specific problem was considered to consist of two parts: first, a determination of mass transfer data as a function of prime variables

such as velocity and physical properties of the medium, secondly, a comparison of the experimentally determined data with other mass transfer data to test the range of applicability of previous mass transfer correlations which have been proposed for various gases and liquids. It was believed that this problem should yield some knowledge of the generality of mass transfer correlations and should provide some insight into the relative importance of newer mass transfer theories.

B. Problem Statement

1. Scope

It was thought that the investigation of the varying effects of the different mechanisms postulated in mass transfer and the extension of known methods of correlating experimental data could best be accomplished with a dynamic system. Probably, because of the complex phenomena occurring during the transport in liquid metals, the semi-theoretical or empirical approach in the analysis of the data offers a more attractive interpretation of the data.

2. Selection of the Uranium-Cadmium System

The uranium-cadmium system (see Fig. 1) was chosen for this study because of the following considerations:

a. It was desirable to choose a system which would allow the temperature effect on the Schmidt number to be determined. That is, the values of the exponent on the Schmidt number could be determined by varying the temperature of the system which implies a change in the physical properties.

b. Because of the possible formation of intermetallics which tend to complicate the dissolution process, it was considered desirable to select a system based upon its phase diagram where the liquid was in equilibrium with pure solid solute over an extended temperature range. The uranium-cadmium phase diagram shows that no intermetallics are formed above a temperature of ~475°C.

c. The uranium-cadmium phase diagram also shows that above 471°C, the solubility of uranium in cadmium, as a function of temperature, remains fairly constant. This fact provides a possible way of eliminating the variation of solubility with temperature when mass transfer calculations are made based upon the concentration driving force. The driving force for mass transfer is considered to be the difference in the solubility at the saturated condition and the actual concentration of the solute in the liquid.

d. The techniques of chemical analysis of uranium in cadmium were available in the Chemical Engineering Division at Argonne. Sufficient technology dealing with the handling and materials problems of uranium and liquid metals such as cadmium and zinc was also available.

e. The materials of construction of the cadmium-uranium system was considered to be a minor problem, since cadmium does not wet nor leach elements such as Ni, Cr, etc. from the stainless steels. In static corrosion tests at Argonne[44] in a circulating loop, it was found that below 640°C, SS314 resisted corrosion attack by cadmium better than others in the series, either SS316 or SS405.

3. Experimental Approach

Single, solid spheres of uranium are to be placed in a pipe and positioned in the stream by a small support rod from the rear. The spheres will be of 1/2-inch diameter, and the test section, i.e., the conduit, will be 1.5-inch pipe; the flowing fluid will be molten cadmium and will be circulated past the test sphere in a continuously connected closed loop.

4. Variables to Be Studied

The effects of temperature, velocity of flowing fluid, and concentration difference will be observed on the net rate of dissolution.

a. Velocity

The velocity of the flowing molten cadmium will be varied which implies a change in the Reynolds number. In the low velocity range it is possible to establish analytical relationships as in laminar flow. There certainly is a need to investigate the high Reynolds numbers as this will extend previous data and more fully help define the general mass transfer behavior in this regime.

b. Temperature

The temperature was varied from 500 to 600°C in order to vary the physical properties and the Schmidt number of the molten cadmium. The Schmidt number was changed by approximately 60%.

c. Driving Force for Mass Transfer

The concentration of uranium in the molten cadmium will be varied as a fraction of the saturated condition. At saturation the driving force is zero, and no mass flux should be obtained. Others have noticed a transfer of mass.[22]

V. DESCRIPTION OF PROCESS FLOW FOR MASS TRANSFER

The fundamental process employed in the mass transfer from single, solid uranium spheres to molten cadmium employed an arrangement of experimental equipment shown as a line drawing in Fig. 2. Molten cadmium at temperatures between 500 and 600°C was pumped from the pump reservoir at B into a 1.5 inch inside diameter pipe at D, through an orifice at E, around the 1.5 inch pipe into the hydrodynamic entrance length at F and past the uranium sphere at J. After flowing past the uranium sphere at J, the molten cadmium discharged into the surge reservoir at A. The surge reservoir was connected to the pump reservoir by a 4 inch inside diameter pipe which closed the dynamic loop. This created a circuitous path for the molten cadmium. Uranium spheres which were used as test samples were inserted into the experimental position at J for a mass transfer run. The samples were inserted and removed from the experimental position through the sample port shown at C.

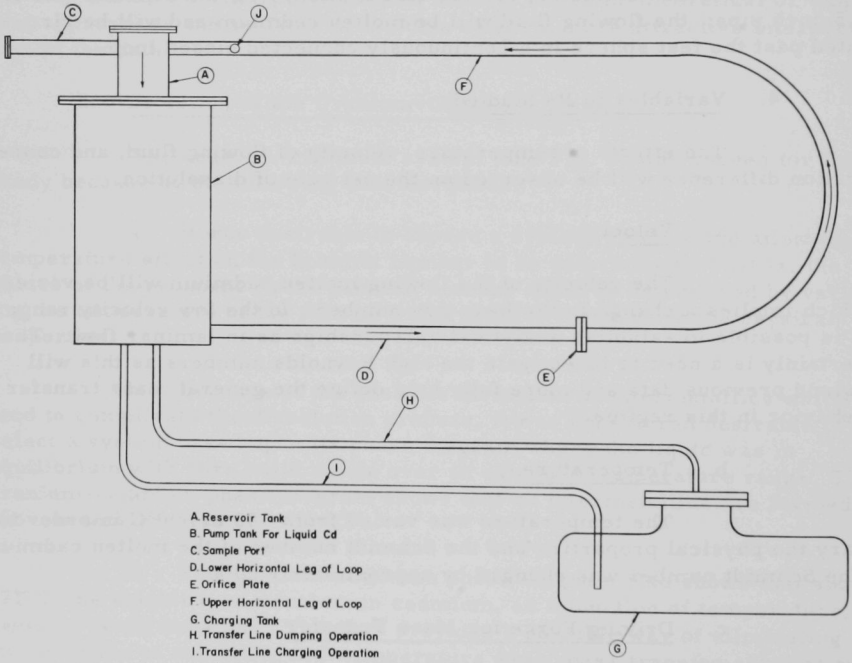

Fig. 2. Process Flow for Mass Transfer Study

The fundamental process variables investigated were the weight loss from the sphere, the velocity of the molten cadmium, the temperature of the molten cadmium, the concentration of the uranium in the molten cadmium, and the time of exposure of the uranium sphere to the molten cadmium. Provisions were provided for recording the RPM of the pump versus the pressure drop across the orifice. The temperature used for the mass transfer correlations was obtained by monitoring the molten cadmium at the dissolving position by using bayonet type immersion thermocouples. Because of the rapid reaction of uranium with oxides, the dynamic loop was kept under argon blanket gas which provided essentially an inert system during the experimental program. As already mentioned in Chapter IV, the range of the variables which were to be investigated stipulated the magnitude of the basic process, and the choice of materials of construction for the dynamic loop. The detailed design and fabrication of experimental equipment brought about by the range of these variables such as the extension of flow rates to a Reynolds number range of 4×10^5 and a temperature range of the system in the vicinity of 500-600°C is discussed in detail in the Appendix, Chapter XV. This discussion includes the specific design considerations including the choice of materials of construction and a detailed account of the techniques of fabrication of the experimental apparatus.

VI. EXPERIMENTAL DEVELOPMENT WORK AND PROCEDURES

A. Introduction

In order to study the mass transfer from uranium spheres into molten cadmium, several preliminary stages of development had to be investigated. These specific areas included (1) the preparation and production of single one-half inch uranium spheres, (2) a study of how to minimize vibrations in the experimental equipment, (3) the specific details of routine analysis such as weighing techniques, methods of removing a cadmium film from the uranium sphere after a mass transfer run, techniques of pre-wetting the uranium samples prior to a mass transfer run, and (4) details of laboratory analysis of the uranium spheres before and after a mass transfer run. This chapter shall discuss the specific techniques concerning this experimental study.

B. Production of Uranium Spheres for Mass Transfer Study

Fabrication of the uranium spheres employed a technique similar to that of lens grinding. A 5/8-inch diameter uranium rod was placed in a dividing head at a 15° angle from the horizontal and a tool bit was mounted in a boring head so that it swept a radius of about 5/16 inches. This was rotated and then brought down about 0.015 inches and held in this position until each cut around the periphery was completed. This step was continued until the higher end of the rod was machined to the center. Then the boring head was locked in its vertical position and the tool bit adjusted in the head to bring the diameter of the sphere to 0.500 inches.

This operation generated about 7/8 of a sphere; the remainder of the sphere was generated in the next operation. The next operation consisted of placing this partial sphere in proper position on a lathe to machine off the stem. The spheres were then tapped and drilled for the stainless steel 304 support rod. Some difficulty was encountered with drilling and threading the sphere since the support rods were 1/16 inch in diameter at the point where they held the sphere. The photograph in Fig. 3 shows the partial completion of the operation described above. The figure shows the sphere at the completion of the initial operation.

C. Production of Randomly Orientated Uranium Spheres and Heat Treatment

1. Introduction

A great deal of consideration was given to the production of uranium spheres for the dissolution study, particularly to the solid phase crystal orientation. It is well known that when spheres are used as test

samples under forced convection conditions, the liquid dissolving medium flows in a rather well established or typical flow pattern past the sphere. In order to retain something close to spherical geometry during a run, it was desirable to take precautions to obtain symmetrical flow separation past the test sphere. Otherwise, should the test sphere begin to dissolve at some zone of its surface at a faster relative rate than the rest of the surface, or in some preferred direction, the flow separation would become distorted from the typically expected pattern. This situation might develop if the spheres were machined from uranium stock material which was rolled, or extruded, with an inherently preferred crystal orientation. Secondly, it was necessary to establish a method of treating the uranium so that the metallurgical history of individual samples was consistent. This provided a partial foundation which was necessary to establish consistent mass transfer data.

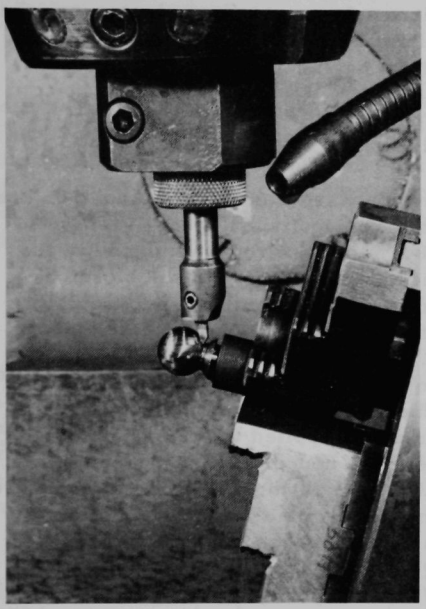

108-4440

Fig. 3. Photograph of Partially Completed Uranium Sphere for Mass Transfer Study

2. Heat Treating Studies

There is evidence that when uranium is cooled from temperatures corresponding to either the beta-phase or gamma phase that subgraining occurs and is accompanied by crystal orientation. This may be attributed to the work of Chiswik and Lloyd.[47] These authors report that uranium specimens that have been annealed at 740°C and thereafter rapidly quenched showed evidence of subgraining and a more regular orientation relative to grains which were separated by high angle boundaries.

a. Method Employed in Heat Treatment of Uranium Spheres

A method was worked out to heat treat the uranium sphere which included encapsulation of the sphere in a vapor tube, under vacuum, heating the sample for 24 hours in the beta range, and finally quenching the sample after its removal from the annealing furnace.

(1) Encapsulation of Uranium Spheres

A method was developed to encapsulate the sphere for subsequent heat treatment. The uranium sphere was first electro-polished for about 45 seconds. After removal from the electro-polishing solution, it was stored under acetone until ready to be encapsulated. The electro-polishing solution consisted of 45% H_2SO_4
45% H_2O
10% Glycol.

A 3/4 inch Vycor tube was selected and closed on one end by a high temperature flame. The electropolished sphere (1/2 inch diameter) including its stainless steel 304 support rod was placed in the Vycor tube and the sphere in this position was adjacent to the closed end. About 8-10 inches from the closed end of the Vycor tube, a necked down section was made by application of a flame, until the diameter of the restricted section was about 1/4 inch. Figure 4 shows the encapsulated sphere prior to heat treatment. The open end was attached to a non-collapsible rubber hose by inserting the Vycor rod to a depth of about 2 inches; high vacuum sealing compound was applied to the Vycor tube prior to attachment to the rubber hose. The noncollapsible rubber hose was attached to a diffusion pump capable of creating 3×10^{-5} mm pressure. Liquid nitrogen freeze valves were employed in the vacuum pump. After about 45 minutes of pumping, the high vacuum gages were checked to see if they were stable. Then by applying a flame to the restricted section of the Vycor tube the encapsulation of the sample by the molten-tube was completed by the unbalance of pressure forces acting on the molten Vycor at the necked down section.

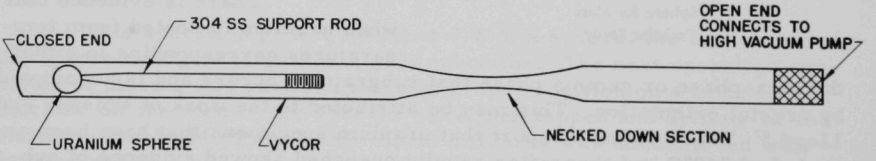

Fig. 4. Encapsulation of Uranium Sphere Prior to Heat Treatment

(2) Annealing Procedure

The Vycor tube was attached to a tantalum wire and lowered into a SS 304 tube which was isolated in a molten lead bath contained in a high temperature furnace. The capsule was immersed in a lead bath, by placing it in a tube. This tube was centered in the lead bath. The temperature at the sample was checked by employing a portable potentiometer with a reference cold junction at 20°C. The temperature at the sample position in the furnace was held at 700° ± 1°C for a period of

24 hours, which was well into the beta range of uranium. The thermocouple was located in the same tube with the sample.

(3) Quenching Uranium Sphere

The uranium sphere was removed from the molten lead bath while still encapsulated and was immersed into water at 20°C. The Vycor protection tube was broken with pliers almost simultaneously after the sample was immersed. Cooling occurred within 25 seconds after immersion. It was subsequently found that the uranium stock could be heat treated prior to the machining operation. This also allowed greater ease in machining the spheres.

b. Control Test for Crystal Orientation (X-Ray Diffraction)

A run was made in the heat treating study to determine the effects of the annealing and quenching procedure for uranium spheres. A 1/2 inch uranium cube was machined from uranium stock and marked on one face with an "E." The stock uranium material consisted of extruded uranium rods whose crystalline orientation was in a preferred direction. The symbol "E" was placed on the plane of the cube which was perpendicular to the direction of extrusion of stock material.

The testing procedure for the annealing and quenching operation consisted of obtaining X-ray diffraction patterns before the heat treatment and subsequent to the treatment. X-ray diffraction patterns were obtained of the face opposite the side E and of the face adjacent to the side E so that representative of each could be analyzed. These separate diffraction patterns represented crystalline orientations in the direction of extrusion of the original stock material. After heat treatment, the same two surfaces were examined for representative X-ray patterns.

Visual comparison of the X-ray diffraction patterns obtained from identical surfaces before and after heat treatment showed that the beta heat treatment introduced considerable random crystal orientation in the test cube. This was further tested by a calculation of the volume fraction $P(\alpha, \beta)$ of material with various orientations compared to a material with a high degree of random orientations. Mueller[48] and others utilized this factor in their study of the preferred orientation in rolled uranium rods. Table II shows the $P(\alpha, \beta)$ values calculated by this method for the transverse and parallel planes before and after heat treatment.

TABLE II. Summary of Diffraction Data for Uranium Control Test for Randomization Techniques

	I					I/I^0				$P(\alpha,\beta)$			
Hkl Plane	A	B	C	D	I^0	A	B	C	D	A	B	C	D
020	40	50	0	0	42	0.95	1.19	0.00	0.00	0.48	0.68	0.00	0.00
110	780	720	700	670	380	2.05	1.89	1.84	1.76	1.03	1.08	1.15	1.04
021	820	835	500	1040	770	1.06	1.08	0.65	1.35	0.53	0.62	0.41	0.79
002	170	465	650	510	254	0.67	1.83	2.56	2.01	0.34	1.05	1.60	1.18
111	630	750	770	765	300	2.10	2.50	2.57	2.55	1.06	1.43	1.61	1.50
022	25	45	45	45	24	1.04	1.88	1.88	1.88	0.52	1.07	1.18	1.11
112	270	520	700	490	303	0.89	1.72	2.31	1.62	0.45	0.98	1.44	0.95
130	50	20	35	35	20	2.50	1.03	1.75	1.75	1.26	0.59	1.09	1.03
131	690	420	460	505	234	2.95	1.79	1.97	2.16	1.48	1.02	1.23	1.27
040	90	30	40	35	37	2.43	0.81	1.08	0.95	1.22	0.46	0.68	0.56
023	50	110	150	150	94	0.53	1.17	1.60	1.60	0.27	0.67	1.00	0.94
200	80	50	60	70	44	1.82	1.14	1.36	1.59	0.91	0.65	0.85	0.94
041	100	30	0	60	20	5.00	1.50	0.00	3.00	2.51	0.86	0.00	1.76
113	35	135	170	95	65	0.54	2.08	2.62	1.46	0.27	1.19	1.64	0.86
132	65	50	60	60	18	3.61	2.78	3.33	3.33	1.81	1.59	2.08	1.96
042	115	90	70	110	50	2.30	1.00	1.40	2.20	1.16	0.57	0.88	1.29
221	340	390	360	380	100	3.40	3.90	3.60	3.90	1.71	2.23	2.25	2.24
133	70	180	220	150	88	0.80	2.05	2.50	1.70	0.40	1.17	1.56	1.00
114	0	90	140	100	51	0.00	1.76	2.75	1.96	0.00	1.01	1.72	1.15
043	50	30	0	0	12	4.17	2.50	0.00	0.00	2.10	1.43	0.00	0.00
150	90	50	35	50	37	2.43	1.35	0.95	1.35	1.22	0.77	0.59	0.79
240	70	45	25	30	30	2.33	1.50	0.83	1.00	1.17	0.86	0.52	0.59
223	60	125	140	100	68	0.88	1.84	2.06	1.47	0.44	1.05	1.29	0.86
241	100	70	50	55	20	5.00	3.54	2.50	2.75	2.51	2.02	1.56	1.62
152	175	125	90	130	71	2.46	1.76	1.27	1.83	1.24	1.01	0.79	1.08
060	30	0	30	0	10	3.00	0.00	3.00	0.00	1.51	0.00	1.88	0.00
061	50	25	0	0	20	2.50	1.25	0.00	0.00	1.26	0.71	0.00	0.00
242	120	125	135	110	83	1.45	1.51	1.63	1.33	0.73	0.86	1.02	0.78
115	40	55	50	65	24	1.67	2.29	2.08	2.71	0.84	1.31	1.30	1.59
062	50	25	0	50	22	2.27	1.14	0.00	2.27	1.14	0.65	0.00	1.34
312	40	75	40	70	36	1.11	2.08	1.11	1.94	0.56	1.19	0.69	1.14
243	35	60	35	45	26	1.35	2.31	1.35	1.73	0.68	1.32	0.84	1.02
135	135	145	125	150	84	1.61	1.73	1.49	1.79	0.81	0.99	0.93	1.05
006	0	0	0	35	25	0.00	0.00	0.00	1.40	0.00	0.00	0.00	0.82
261	170	80	50	55	36	4.72	2.22	1.39	1.53	2.37	1.27	0.87	0.90
244	0	130	125	85	61	0.00	2.13	2.05	1.39	0.00	1.22	1.28	0.82
						1.99*	1.75*	1.60*	1.70*				

*$\left[\frac{1}{N}\sum(I/I^0)\right]$.

c. Equations Used to Calculate $P(\alpha, \beta)$ of Beta Heat Treatment

The measured intensity from a certain crystal plane lying parallel to the cross section of a rod specimen with unknown fiber texture[48] and the corresponding intensity I°_{hkl} from a random specimen are related by the $P(\alpha, \beta)$ of the unknown texture by the equation

$$\frac{I_{hkl}}{I^{\circ}_{hkl}} = \left(\frac{C}{C_0}\right)^{P(\alpha,\beta)} . \qquad (6.1)$$

Therefore an index of 1.0 for the value of $P(\alpha, \beta)$ becomes the ideal limit for the unknown texture to give the random texture. The values C and C_0 depend upon extinction phenomena and the values α and β define the crystal orientation as obtained from the hkl reflecting plane. The assumption is made that C/C_0 is independent of hkl and P is normalized over the entire orientation range according to

$$\frac{1}{4\pi}\left[\int_{\alpha=0}^{\alpha=2\pi}\int_{\beta=0}^{\beta=2\pi} P(\alpha, \beta)\, d\alpha d\beta = 1\right]. \tag{6.2}$$

If discrete orientations are chosen, the ratio C/C_0 is obtained by

$$\frac{C}{C_0} = \frac{1}{n}\sum_{hkl}\frac{I_{hkl}}{I^{\circ}_{hkl}} \tag{6.3}$$

where n is the number of reflections (hkl) used in the summation. Furthermore the value of $P(\alpha, \beta)$ is given by

$$P(\alpha, \beta) = \frac{\left(\frac{I_{hkl}}{I^{\circ}_{hkl}}\right)}{\frac{1}{N}\sum\frac{I_{hkl}}{I^{\circ}_{hkl}}}. \tag{6.4}$$

It is observed from the calculation results shown on Table II (columns A, B, C, and D), that after the heat treatment, there is a tendency for the $P(\alpha, \beta)$ values to approach the ideal limit of 1.0. For example, the following summary in Table III of some specific planes illustrates that a more random like crystalline structure was obtained after the heat treatment of the uranium. Most of the mass transfer runs in this study will be made using randomly orientated uranium spheres. Some runs will be made using nonrandomized spheres to see if there is a significant difference in the overall dissolution rates. However, the main objectives of this study were to obtain good, reproducible mass transfer data for the mass transfer correlations.

TABLE III. Selected Values from Table II for Discussion of Randomization Techniques

	Before		After	
Plane	A	B	C	D
021	0.53	0.41	0.62	0.79
022	0.52	1.07	1.18	1.11
312	0.56	1.14	0.69	1.14
261	2.37	1.27	0.87	0.90
312	0.56	1.19	0.69	1.14

D. Laboratory Study of the Wetting of Uranium with Molten Cadmium

1. Introduction

The establishment of a true interface between the solid phase and the liquid phase at the beginning of a mass transfer run is perhaps the most important single factor in obtaining good mass transfer data. Obviously, some wetting occurs in most instances, but the surface area at the solid boundary must be reasonably representative of the ideal surface area. This is especially true in the analysis of mass flux across phase boundaries which is proportional to the surface area involved. Generally, some oxide or protective film on the solid surface prohibits the complete wetting by liquid metals. Since partial wetting of the surface occurs if a film exists, mass transfer data based upon the amount of mass transferred from the solid phase were not reproducible.

The wetting of metals by liquid metals is accomplished by effectively removing the oxide film to insure a clean interface. Two methods were developed for removing the oxide film prior to wetting. One method consisted of employing some chemical agent which attacked the oxide, dissolving it away. This left a clean solid uranium surface. The other method was a physical one and involved mechanical action on the solid surface. This action caused the oxide film to crack yielding to wetting. Both methods have been employed in this study and shall be discussed.

2. Chemical Wetting

In this method, the oxide film on the uranium surface was first removed by leaving the uranium sphere in a beaker of cold concentrated HNO_3 until a clean uranium surface was observed. The uranium was then washed with cold HNO_3 and acetone. Benzing[49] found that by introducing samples treated in this manner into a zinc melt at 550°C protected by Dow 230 flux (Dow 230 flux consists of 55% KCl, 34% $MgCl_2$, 9% $BaCl_2$, and 2% CaF_2) that wetting of uranium with zinc occurred in less than one minute. It is suspected that a reduction of the uranium oxide on the surface proceeded according to a reaction which formed a uranium zinc intermetallic. It is believed that the oxides are collected in the flux. The uranium samples were protected at the interface from further oxide formation and could be stored until needed for the mass transfer experiments.

It was found, however, that uranium spheres could be wet better by a slight variation of the above procedure. The oxide was removed in this case by first electropolishing the spheres in Baumrucker's solution. Baumrucker's solution consists of 5 Parts C_2H_5OH,
5 Parts Ethylene Glycol, and
8 Parts H_3PO_4.

It was found that electropolishing of the uranium spheres could be accomplished in about 30 seconds, yielding a shiny bright uranium surface. After electropolishing, the surface-cleaned uranium spheres were stored under acetone until they were to be wetted by zinc. These uranium spheres were wet with zinc at 550°C protected by the 230 flux. Wetting was accomplished in less than 20 seconds. After removal from the zinc, the spheres were cooled by water, and the surfaces inspected to see if complete wetting had been accomplished. A picture showing a sphere before and after zinc wetting is shown in Fig. 5. In those cases where the surface was not completely wet with zinc, the surface was cleaned again in the manner described above. A modification of Benzing's[49] procedure was then repeated. A photomicrograph of the uranium-cadmium interface is shown in Fig. 6.

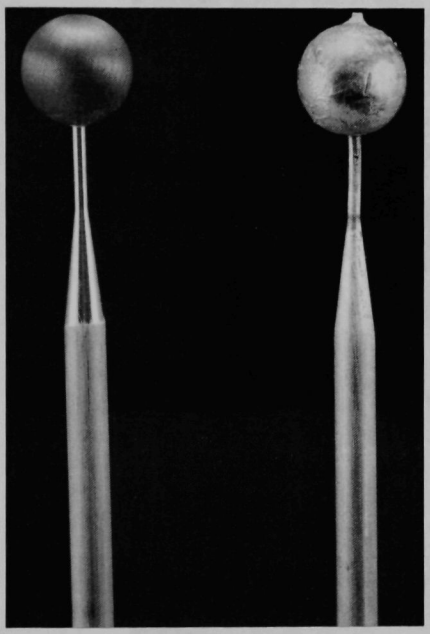

108-5329

Fig. 5. Uranium Sphere Prior to Wetting (Left) Compared to Uranium Sphere after Wetting with Zinc (Right)

3. Physical Wetting

Other methods were investigated which might lead to different wetting techniques. It has been known that the ultrasonic soldering iron could generate a wetted surface in liquid metals by causing cavitation action on the solid surface by the adjacent liquid metal.[62] This breaks up the oxide film to permit wetting of the solid by the liquid.

An ultrasonic generator (Fig. 60, Chapter XV, Appendix) capable of generating ultrasonic energy at a frequency of 20 kc was located in the Reactor Engineering Division of Argonne National Laboratory. It was made available for possible applications to study wetting. This generator was found capable of energizing transducer components which contained either barium titanate or magnetostriction types connected in parallel. The output impedance could be adjusted for a particular load which would not exceed a total resistance sufficient to 2 kw. It was found that a load not to exceed about 25 ohms total resistance at 20 kc would provide sufficient energy to conduct the experiment. It was found that the wetting of uranium by molten cadmium using the ultrasonic technique could be accomplished in one minute. The wetting was complete and uniform at the solid-liquid interface between uranium and cadmium. The comparison

between the results obtained using chemically wetted uranium spheres and ultrasonically wetted spheres in the mass transfer study is discussed in Chapter X. However, the chemical method was the major process used to wet most of the spheres for the mass transfer study. The details of the ultrasonic apparatus and the appropriate discussions are given in Chapter XV in the Appendix.

108-6371 250X

Fig. 6. Photomicrograph of Uranium-Zinc Interface Using Molten Zinc and Dow-230 Molten Salt Flux for Wetting

VII. DISCUSSION OF PHYSICAL PROPERTIES FOR SCHMIDT NUMBER, N_{Sc}

A. Introduction

The correlation of mass transfer data using semi-empirical equations involves the use of the Schmidt number, N_{Sc}. The Schmidt number is formed by dividing the liquid film viscosity by the product of the solution density and the experimental molecular diffusivity. Physically, the Schmidt number represents the ratio of momentum transfer as affected by a velocity gradient to the actual mass transferred by molecular diffusion through the influence of a concentration gradient. Mention has been made elsewhere that this ratio may be changed by varying these physical properties through a change of temperature. It is again recalled that in the uranium-cadmium system, this ratio may be changed by varying the temperature while the driving force for mass transfer remains essentially constant. The Schmidt number for the molten cadmium will be formed by using experimental values of the molecular diffusivity, D_V. Experimental values of the density and viscosity are available and will be used in the calculation.

B. Solution Density for N_{Sc}

The density of a solution of uranium in molten cadmium as a function of temperature was not available. However, at the concentration used, less than 2% error was involved in using the density of the molten cadmium itself. This evaluation is described in the section concerning the error analysis of the overall mass transfer correlations. The density data was taken from Liquid Metals Handbook[42] and is also plotted in Fig. 7.

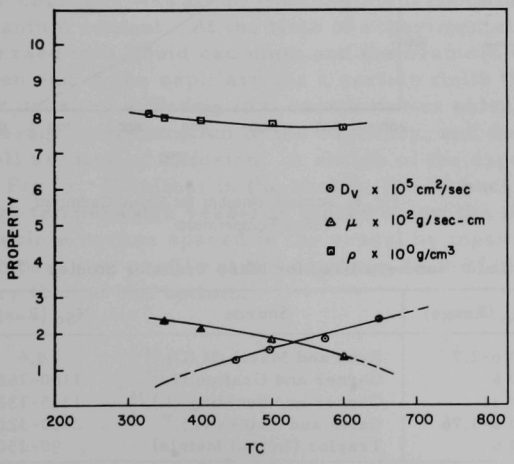

Fig. 7

Physical Properties of Molten Cadmium Versus Temperature

C. Viscosity of Molten Cadmium for N_{Sc}

Source of Experimental Data and Preparation for N_{Sc}

The viscosity data reported below were taken from Liquid Metals Handbook.[42] As explained in the introductory paragraph, the viscosity appears in the numerator of the Schmidt number. Ordinarily, the viscosity is evaluated at the liquid film temperature which is defined as the arithmetic average of the temperature of the bulk liquid and the temperature at the surface of the solid. However, the assumption was made in this study that for liquid metals using the viscosity at the bulk temperature was reasonably close to the average value. The variation of viscosity with temperature is plotted in Fig. 7. The plot of the Schmidt numbers appears in the following Fig. 8. Table V shows the range of Schmidt numbers used for other mass transfer studies.

TABLE IV. Density and Viscosity for Molten Cadmium

T(°C)	Density (gm/cm^3)	Viscosity Poise x 10^2
330	8.01	
350	7.99	2.37
400	7.93	2.16
500	7.82	1.84
600	7.72	1.54

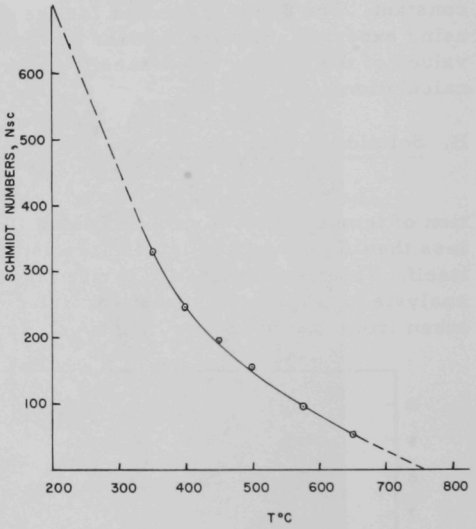

Fig. 8. Schmidt Number for Liquid Cadmium Versus Temperature

TABLE V. Summary of Schmidt Numbers Used for Mass Transfer Studies

Source	N_{Sc} (Range)	Source	N_{Sc} (Range)
Froessling (G),[30]	0.6-2.7	Ranz and Marshall (G),[73]	0.6
Houghton and Radford (G),[32]	0.6	Garner and Grafton (L)[17]	1100-1680
Hsu, Sato and Sage (G),[38]	2.11	Garner and Suckling (L),[36]	1135-1320
Maisel and Sherwood (G),[34]	0.6-1.76	Gates and Shanks (L),[37]	2800-3200
Powell (G),[31]	0.6	Traylor (Liquid Metals)	90-150

(G) Gases.
(L) Liquids.

D. Determination of Diffusivity for Uranium-Cadmium

1. Introduction

Molecular diffusivities for metal solutes diffusing into liquid metal solvents were noticeably absent from the literature. Dunn and Bonilla[3] in their study of liquid metals stated that the molecular diffusivities in liquid metal systems were generally about 2 or 3 times those values predicted by the Stokes-Einstein expression. Parkman[69] in his study of mass transfer in lithium estimated the molecular diffusivity from the Wilke[41] expression used to estimate diffusivities for aqueous and organic liquids. It is apparent that experimental diffusivities should enable one to determine with greater accuracy the empirical expressions and dimensionless groups which depend upon this physical property. The molecular diffusivity for uranium diffusing into cadmium was experimentally determined in a separate program in the Chemical Engineering Division at Argonne by J. C. Hesson.[1]

2. Procedure for Determination of D_v

a. Experimental Technique

The experimental method used in obtaining diffusion coefficients for uranium in cadmium employed the capillary reservoir technique. In this method a capillary was closed at one end and filled with a known concentration of the substance which could diffuse out the open end of the capillary when placed into a suitable liquid metal solution. Usually the liquid metal solution into which the capillary was immersed contained essentially zero concentration of the diffusate. Prior to the diffusion experiment, the capillary was filled with cadmium containing about 1.0% of known uranium content. At the time of experimentation this capillary was immersed into liquid cadmium and the uranium was allowed to diffuse out the open end of the capillary for a certain finite time. The diffusion coefficient for uranium diffusing into cadmium was calculated from initial and final average concentration in the capillary, and the length of the capillary as well as time of diffusion. A sketch of the experimental apparatus is shown in Fig. 9. Note that in the sketch, the furnace is shown at the right and the high temperature vessel is placed below the lower edge of the furnace. The crucible is then spaced in the vessel by means of a spacer such that the temperature profile at the capillary is 1-2° higher at the top of the capillary than at the bottom.

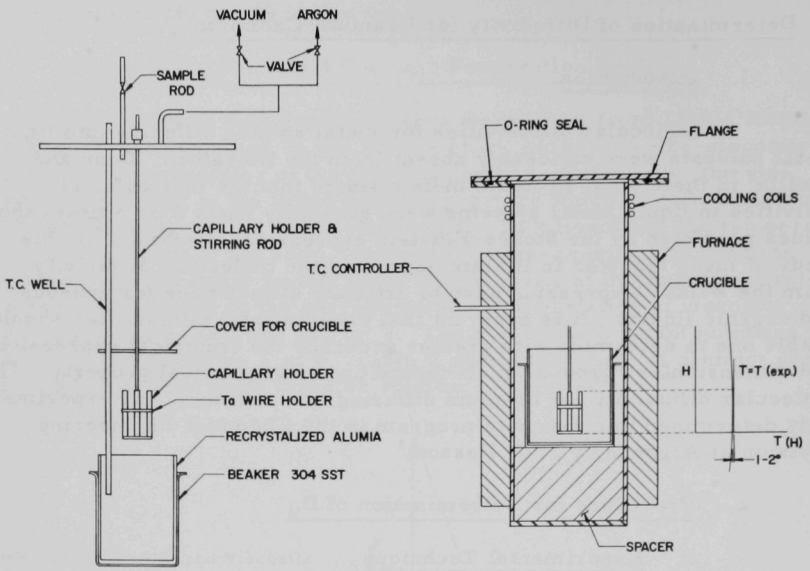

Fig. 9. Apparatus for D_v Determination for Uranium Diffusing in Molten Cadmium

b. Equations Used to Calculate D_v

Diffusion under the conditions described above follows Fick's second law of diffusion. This law states that:

$$C_{(t)} = -D_v \text{ div grad } C \tag{7.1}$$

for arbitrary direction. Neglecting radial diffusion in the capillary and considering diffusion in the longitudinal direction of the capillary allowed the above equation to be written as

$$\frac{\partial C}{\partial t} = D_v \partial^2 C / \partial x^2 \tag{7.2}$$

with the following boundary conditions

$$\frac{\partial C}{\partial x}(x \rightarrow 0) = 0, \quad t \geq 0 \tag{7.3}$$

$$C_1 = 0, \quad t \geq 0 \tag{7.4}$$

$$C_{(x)} = C_0, \quad 0 \leq x \geq 1, \quad t = 0 \tag{7.5}$$

$$C_{(x,t)} = 0, \quad \text{elsewhere} \tag{7.6}$$

The solution to Fick's second law with the given initial and boundary conditions is given by Churchill[1] and after integration becomes,

$$\frac{C}{C_0} = \frac{8}{\pi^2} \sum_{n=1}^{\infty} \left(\frac{1}{2n-1}\right)^2 \exp-\left(\frac{2n-1}{2}\right)^2 \left(\frac{\pi}{l}\right)^2 D_v t \tag{7.7}$$

where C and C_0 are the initial and final amounts of U in the capillary after and before diffusion, respectively. It is also shown that if the term $\left(\frac{\pi^2}{8} \frac{C}{C_0}\right)$ is less than about 0.7 the series in the above equation can be cut off after n = 1 with the introduction of very little error. Alternate expressions which will approximate the solution of Fick's second law may be collected. Figure 10 shows the semi-infinite solution as equation 7.9 compared to the equation of Grace and Derge[74] which appears as equation 7.8 to follow.

$$\frac{C_0 - C_a}{C_0 - C_s} = \frac{2}{l}\left(\frac{D_v t}{\pi}\right)^{1/2} \tag{7.8}$$

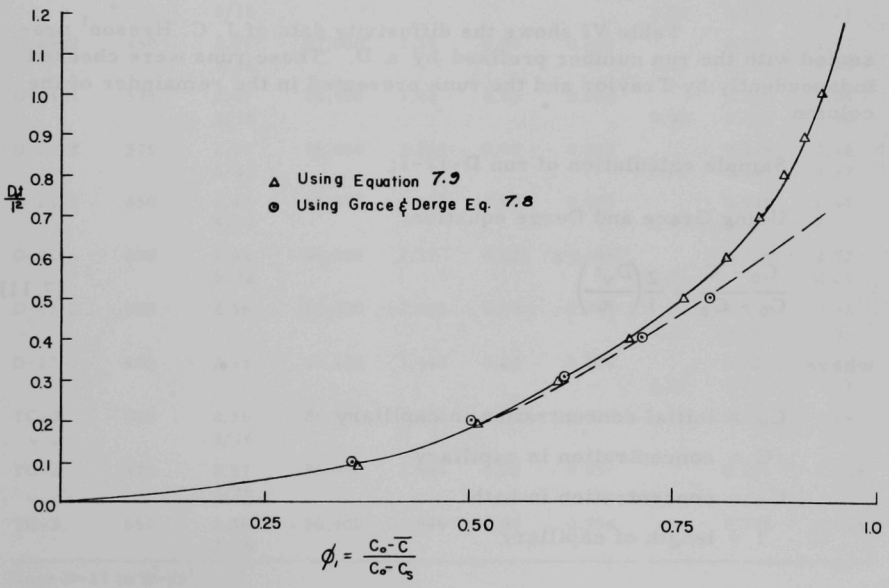

Fig. 10. Plot of $D_v t/l^2$ Versus $\phi_1 = \frac{C_0 - \overline{C}}{C_0 - C_s}$

where C_0 represents the initial concentration in the capillary, C_a represents the average concentration and C_s represents the concentration in the bath where the capillary is immersed.

The semi-infinite solution to Fick's second law with the concentration in the bath not equal to zero may be written as

$$\frac{C - C_0}{C_a - C_0} = 1 - \frac{8}{\pi^2}\left[\sum_{n=1}^{\infty}\left(\frac{1}{2n-1}\right)^2 \exp-\left(\frac{2n-1}{2}\right)^2\left(\frac{\pi}{l}\right)^2 D_v t\right] \tag{7.9}$$

where C and C_0 are the initial and final amounts of uranium in the capillary after and before diffusion, respectively, and C_a is equal to the bath concentration. This equation may be written as

$$\frac{C - C_0}{C_a - C_0} = 1 - \frac{8}{\pi^2}\left[\frac{1}{1}e^{-\frac{D_v t\pi^2}{4\,l^2}} + \frac{1}{9}e^{-\frac{D_v 9\pi^2 t}{4\,l^2}} + \frac{1}{25}e^{-\frac{25 D_v t\pi^2}{4\,l^2}} + \ldots)\right] \tag{7.10}$$

3. Sample Calculation of Experimental Data

a. Sample Calculation of Run D-17-1

Table VI shows the diffusivity data of J. C. Hesson[1] presented with the run number prefixed by a D. These runs were checked independently by Traylor and the runs presented in the remainder of the column.

Sample calculation of run D-17-1:

Using Grace and Derge equation,

$$\frac{C_0 - C}{C_0 - C_s} = \frac{2}{l}\left(\frac{D_v t}{\pi}\right)^{1/2} \tag{7.11}$$

where

C_0 = initial concentration in capillary

C = concentration in capillary

C_s = concentration in bath

l = length of capillary

For D-17-1: $C_0 = 1.455$

$C_s = 0.00$

$C_a = 0.706$

$l = 2.55$ cm

$$\frac{C_0 - C_a}{C_0 - C_s} = \frac{1.445 - 0.706}{1.445 - 0.0} = \frac{0.739}{1.445} = 0.5114$$

$$\frac{(C_0 - C_a)^2}{C_0 - C_s} = 0.26152$$

$$D = \frac{(0.26152)(3.14)(2.55)^2}{(86{,}400) \times 4} = 1.55^{(10^{-5})} \frac{cm^2}{sec} \qquad (7.12)$$

TABLE VI. Summary of Experimental Diffusivity Data for Uranium-Cadmium System

Run	Temp, °C	L, cm OD, in.	Time, sec	Uranium Percent C_0	C_s	C	C_1	Computed Values D_t/l^2	$D \times 10^5$
D-25-1	450	2.41	86,400	1.358	0.00	0.685		0.193	1.30
		3/16					1.10	0.180	1.21
D-24-2	450	2.47	87,000	1.37	0.00	0.685		0.195	1.37
		3/16					1.13	0.175	1.23
D-24-1	575	2.47	86,400	1.42	0.00	0.603		0.260	1.84
		3/16					0.96	0.255	1.80
D-23-2	575	2.44	86,400	1.365	0.00	0.503		0.315	2.18
		5/32					0.86	0.285	1.97
D-23-1	650	2.45	86,400	1.365	0.00	0.472		0.345	2.44
		5/32					0.79	0.320	2.23
D-22	650	2.44	86,400	1.37	0.023	0.483		0.335	2.32
		5/32					0.79		2.21
D-17-2	500	2.56	86,400	1.455	0.00	0.743		0.190	1.44
							1.12	0.205	1.56
D-17-1	500	2.55	86,400	1.445	0.00	0.706		0.205	1.56
							1.09	0.210	1.57
TC-1	500	2.56	86,400	1.502	0.018	0.710		0.22	1.66
		3/16							
TC-2	575	2.57	86,000	1.986	0.00	0.833		0.256	1.958
		3/16							
TC-3	650	2.56	86,400	1.986	0.00	0.754		0.315	2.398
		3/16							

Runs D-17 to D-25[1]
Run TC 1-3 (Traylor)

The above equation was used to calculate D_v using independent data which were obtained by Traylor in Run TC-1 with the average concentration, C_a, replaced by the weighted average

$$C_{Wa} = \frac{0.0202 \times 10^2}{2.8582} = 0.710\%$$

From Run TC-1:
Wt of Capillary Section

	Capillary Section				
	No. 1	No. 2	No. 3	No. 4	Σ
U + C_d	0.6328	0.6067	0.9337	0.685	2.858
U Alone	0.0020	0.0041	0.0078	0.0063	0.0202
% U	0.320	0.675	0.835	0.920	0.710

$C_0 = 1.502\%$

$C_{Wa} = 0.710\%$

$C_s = 0.018\%$

$\frac{C_0 - C_{Wa}}{C_0 - C_{Wa}} = 1.502$

$l = 2.56$ cm

$$D_v = \frac{(1.010 \times 2.54)^2 (0.22)}{86{,}400} = 1.66\ (10^{-5})$$

b. Sample Calculation of TC-1 Using Equation 7.13

A sample calculation will be shown using the following equation to calculate D_v using finite length of diffusion

$$\frac{C_0 - C}{C_0 - C_s} = 1 - \frac{8}{\pi^2} \sum_{n=1}^{n=\infty} \frac{1}{n^2} \left[\sin\left(\frac{n\pi}{2}\right) \right]^2 e^{-\frac{Dn^2\pi^2 t}{4 l^2}} \qquad (7.13)$$

Figure 11 shows a plot of the above equation as ϕ_1 and ϕ_2 versus $D_v \times 10^5$, where

$$\phi_1 = \frac{C_0 - C}{C_0 - C_s}, \quad \text{and} \quad \phi_2 = 1 - \frac{8}{\pi^2} \sum_{n=1}^{n=\infty} \frac{1}{n^2} \left[\sin\left(\frac{n\pi}{2}\right) \right]^2 e^{-\frac{D_v n^2 \pi^2 t}{(2l^2)}} \qquad (7.14)$$

Knowing the initial concentration C_0, the average concentration $\bar{C}$, and the bath concentration C_s, $D_v \times 10^5$ may be read from the graph which follows as Fig. 11.

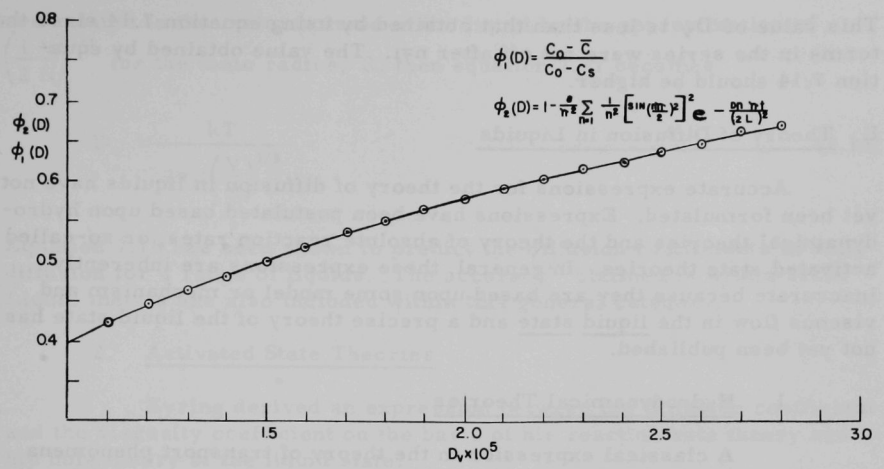

Fig. 11. Plot of Semi-infinite Solution to Fick's Second Law Versus $D_v \times 10^5$

The detailed calculation follows. For TC-1

$C_0 = 1.502\%$ $\quad t = 86{,}400$ sec

$C_{Wa} = 0.710\%$

$C_s = 0.018\%$

$l = 2.56$ cm

$$\phi_1 = \frac{C_0 - C_{Wa}}{C_0 - C_s} = \frac{1.502 - 0.710}{1.502 - 0.018} = \frac{0.792}{1.484} = 0.5336$$

$D_v \times 10^5 = 1.729$ $\quad D_v = 1.729\ (10^{-5})$ cm^2/sec

An alternate calculation may be obtained using this equation and Fig. 10. In Fig. 10 the term $\frac{D_v t}{l^2}$ is plotted versus $\frac{C_0 - C_{Wa}}{C_0 - C_s}$. The procedure consists of obtaining the ratio $\frac{C_0 - C}{C_0 - C_s}$ and reading a corresponding value of $\frac{D_v t}{l^2}$ from Fig. 10. The molecular diffusivity $D_v \times 10^5$ is obtained by calculation using the length of capillary and time of diffusion. From TC-1, $\frac{C_0 - C}{C_0 - C_s} = 0.5336$

$$\frac{Dt}{l^2} = 0.22; \quad D_v = \frac{0.22(6.579)}{86{,}400} = 1.665 \times 10^{-5}$$

This value of D_V is less than that obtained by using equation 7.14 since the terms in the series were cut off after n=1. The value obtained by equation 7.14 should be higher.

E. Theory of Diffusion in Liquids

Accurate expressions for the theory of diffusion in liquids have not yet been formulated. Expressions have been postulated based upon hydrodynamical theories and the theory of absolute reaction rates, or so-called activated state theories. In general, these expressions are inherently inaccurate because they are based upon some model or mechanism and viscous flow in the liquid state and a precise theory of the liquid state has not yet been published.

1. Hydrodynamical Theories

A classical expression in the theory of transport phenomena results from the consideration of a Brownian motion of a particle of radius R in some solvent medium whose viscosity is μ

$$D = Kt/6\pi R\mu \tag{7.15}$$

Equation 7.15 is called the Stokes-Einstein expression, and k equals Boltzmann constant, where T equals the absolute temperature. Equation 7.15 relates the self diffusion coefficient D to the viscosity, μ, coefficient of the liquid.

Sutherland[52] modified the Stokes-Einstein expression to the following form for the diffusion coefficient:

$$D = \frac{kT}{6R} \cdot \frac{1 + 3\mu/R}{1 + 2\mu/R} \tag{7.16}$$

In equation 7.16 the term μ, represents the coefficient of sliding friction between the particle and the medium. For large particles, the coefficient μ is taken as infinity and in this case equation 7.16 reduces to equation 7.15 or the Stokes-Einstein expression. For the case of self diffusion where the radius of the diffusing particle is approximately the same as that of the medium of viscosity μ, equation 7.16 reduces to

$$D = \frac{kT}{4\pi R\mu} \tag{7.17}$$

Applications of equations 7.15 and 7.17 involve the assignment of values to R at a given temperature and viscosity and then calculating the diffusivity D_V. If the assumption can be made that self-diffusion exists (molecules are all similar) and the molecules of radius R (or ionic radii)

are related to the molar volume of the liquid by the approximation of $\left(\frac{1}{2}\frac{V}{N}\right)^{1/3}$ for the ionic radius, R, then equation 7.17 becomes

$$D_v = \frac{kT}{2\pi\mu\left(\frac{V}{N}\right)^{1/3}} \tag{7.18}$$

Equation 7.18 has been shown to predict the diffusion coefficients in self diffusion for a range of liquids. The accuracy[55] claimed is within ±12%. Liquid metals are also included within this general category.

2. Activated State Theories

Eyring derived an expression between the diffusion coefficient and the viscosity coefficient on the basis of his reaction rate theory and his hole theory of the liquid state.

$$D = \frac{d_1 kT}{d_2 d_3 \mu} \tag{7.19}$$

In equation 7.19 d_3 represents the interatomic distance in the direction of diffusion and d_1 and d_2 are the interatomic distances perpendicular to d_3. In the case of spherical particles in a medium with a high degree of local order, the approximation

$d_1 = d_2 = d_3$ may be made.

The mean jump distance d_1 of a particle into an adjacent hole does not necessarily equal the interatomic distance, but approximates this distance. Assuming that the four distances are equal, equation 7.19 reduces to

$$d = kT/d\mu \tag{7.20}$$

If it is further assumed that d is about equal to the molecular volume for N molecules, i.e. $d = (V/N)^{1/3}$, then

$$D = \frac{kT}{\mu} \cdot (N/V)^{1/3} \tag{7.21}$$

Equation 7.21 is used as the Eyring approximation for the self diffusion coefficient.

In a recent article by Carlson, Eyring, and Ree[54] concerning the thermodynamic and transport properties of molten metals in which the self diffusion coefficient of sodium is shown to agree with the experimental data for the same coefficient, the following equation is suggested to calculate the data:

$$D = \frac{kT}{\alpha\mu} \cdot (N/V)^{1/3} \qquad (7.22)$$

The term α represents the effective number of neighbors of a molecule lying in the same plane. This value is approximately equal to six for close packed structures. The same equation is used to calculate the self diffusion coefficient for Hg which also agrees with the experimental data as shown in the article.

3. Other Expressions Sometimes Used to Calculate D_V

The following equations were collected from various sources to predict D_V, the molecular diffusivity for comparison with experimental data:

(a) Stokes-Einstein[53]

$$D_V = \frac{kT}{6\pi\mu} \qquad (7.15)$$

k = Boltzmann's Constant
T = Absolute Temperature
μ = Viscosity
R = Radius of diffusing species

(b) Eyring Equation[56]

$$D = \frac{kT}{\mu(V/N)^{1/3}} \qquad (7.21)$$

k = Boltzmann's Constant
(V/N) = Estimate for R

(c) Carlson, Eyring-Ree Equation[54]

$$D = \frac{kT}{\alpha(V/N)_{ij}\mu} \qquad (7.22)$$

α = about 6
$(V/N)_{ij} = X_1(V/N)_i + X_j(V/N)_j$

(d) Li-Chang Equation[55]

$$D = \frac{kT}{\mu(2\pi)(V/N)^{1/3}} \qquad (7.23)$$

The above equations were also used to predict D_V data for the uranium-cadmium system in order to make a comparison with the experimental data. The plot of the experimental data and the molecular diffusivities predicted by using the above equations is shown in the following graph as Fig. 12. The summary of data is given in Table VII.

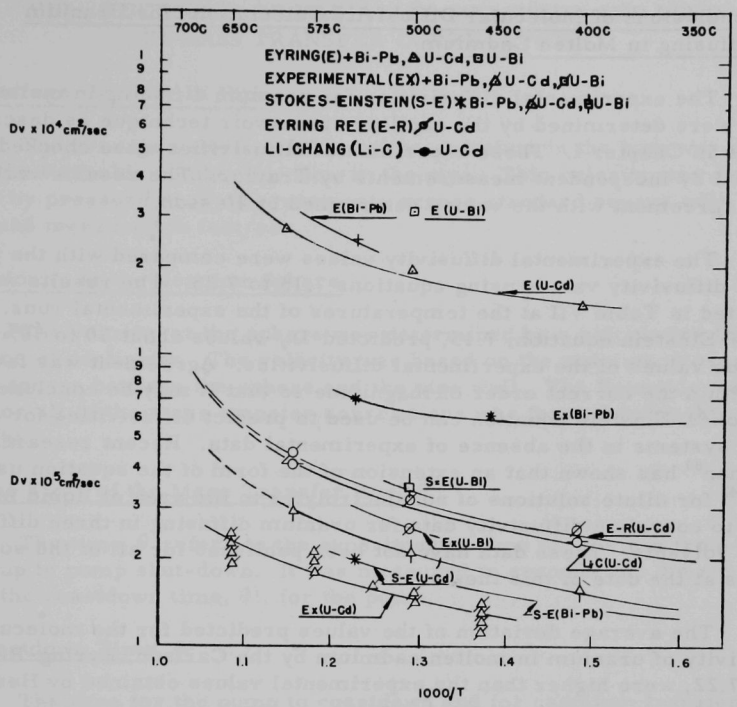

Fig. 12. Experimental Data for Molecular Diffusivities in Molten Metals

TABLE VII. Diffusivity Data for Uranium-Cadmium, Uranium-Bismuth, and Lead-Bismuth as Predicted by Various Equations

Temp T(°C)	System U-Cd	Molecular Diffusivities Calculated by: Stokes-Einstein[53] $D_V \times 10^5$	Eyring[56] $D_V \times 10^5$	Eyring-Ree[54] $D_V \times 10^5$	Li-Chang[55] $D_V \times 10^5$	Bird[55] $D_V \times 10^5$	Experimental $D_V \times 10\%$
330		1.295	12.164	2.03	1.969	1.943	1.0
350		1.355	12.696	2.12	2.072	2.033	1.125
400		1.606	15.011	2.505	2.454	2.409	1.87
500		2.165	20.197	3.35	3.273	3.248	1.44-1.623
600		2.922	27.064	4.52	4.507	4.383	1.75
	Bi-Pb						
540		1.99	2.5×10^4				
518							6.6
431							5.4
	U-Bi						
330		2.21					
350		2.33					
400		2.7					
500		3.52	3.31×10^4				
600		4.53					

F. Conclusions of Molecular Diffusivity Calculations for Uranium Diffusing in Molten Cadmium

The experimental diffusivities for uranium diffusing in molten cadmium were determined by the capillary reservoir technique as described earlier in Chapter I. These experimental diffusivities were checked and verified by independent measurements by Traylor. The results were in close agreement with the values determined by Hesson.[1]

The experimental diffusivity values were compared with the predicted diffusivity values using equations 7.15 to 7.23. The results were tabulated in Table VII at the temperatures of the experimental runs. The Stokes-Einstein equation, 7.15, predicted D_v values about 30 to 50% higher than the values of the experimental diffusivities. Agreement was favorable and within the correct order of magnitude so that it may be concluded that the Stokes-Einstein equation can be used to predict diffusivities for liquid metal systems in the absence of experimental data. Recent research by Hootman[80] has shown that an extension of the form of the equation used by Wilke[41] for dilute solutions of nonelectrolytes to the area of liquid metals tends to correlate diffusivity data for uranium diffusing in three different metal solvents. These data have not been published for all of the solvent metals at the date of this thesis.

The average deviation of the values predicted for the molecular diffusivity of uranium in molten cadmium by the Carlson, Eyring-Ree equation, 7.22, were higher than the experimental values obtained by Hesson.[1]

The average deviation of the values predicted for the molecular diffusivity of uranium in molten cadmium by the Bird equation[55] were 100% to 200% higher than the experimental values. The Eyring equation predicted values for D_v larger than the experimental values by a factor of 10 to 20. The predicted values by the Li-Chang equation were 100% to 200% higher than the experimental values.[55] As mentioned above, the Stokes-Einstein equation predicted values in closest agreement with the experimental data.

The probable reasons that the experimental molecular diffusivities were lower than the values predicted by equations 7.15 to 7.23 may be attributed to the factors resulting from the chemical nature of the system. The actual error results from the uncertainty in the exact value to use for the effective radius of the diffusing uranium. Thus, the chemical factors such as association of the diffusing ion with solvent ions or a complex formation may hinder the diffusing ion and partially account for the differences mentioned above.

VIII. DISCUSSION OF VARIABLES MEASURED AND USED IN MASS TRANSFER CORRELATIONS

A. Average Velocity in Pipe

The average velocity of the molten cadmium in the loop was used to form the Reynolds number for flow in the pipe. This velocity was determined by pressure drop measurements across standard square edge orifices and measured in feet/sec.

B. Velocity at the Uranium Sphere

The velocity at the sphere was determined by a calculation from the equation of continuity. The velocity was based on the uranium cross section at the sphere between the sphere and the pipe wall. The Reynolds number used for all of the mass transfer correlations was formed using this velocity.

C. The Time of the Mass Transfer Run, θ

The time θ refers to the experimental time for the run from pump start-up to pump shut-down. It was measured in seconds and did not include the coastdown time, θ', for the pump.

D. Coastdown Time, θ'

The time for the pump to coastdown and for cadmium transient flow past the sphere after the motor was shut off for the pump was designated as θ'. This time was also measured in seconds.

E. Mass Transfer Coefficient, k_1

The mass transfer coefficient was derived from the measurements made on the weight loss from the sphere, the length of the run, θ, the area of the sphere, A_S, and the concentration driving force, ΔC.

F. The Experimental Temperature, T_e

The experimental temperature, T_e, was taken as the actual temperature of the molten cadmium at the sphere during a mass transfer run. The physical properties were all evaluated at the experimental temperature to determine the Schmidt number, N_{Sc}.

G. Concentration of the Dissolved Uranium in Cadmium

The concentration of the dissolved uranium in the molten cadmium was recorded by the chemical analysis of the liquid samples taken from the

dynamic loop. The concentration is expressed in grams/cc of solution. Usually the concentration was zero for most of the mass transfer runs, unless the effect of variation of the concentration driving force was desired.

H. The Saturated Concentration, C_s

The solubility of the dissolved uranium in the molten cadmium at saturation was used to determine the driving force. Usually the driving force was taken as the saturation concentration, C_s, minus the concentration of the dissolved uranium in the molten cadmium of the loop. This amounted to $C_s - C_l$ and with C_l equal to zero the driving force was C_s. This value for the driving force, C_s, was used for the majority of the mass transfer runs.

I. The Sphere Diameter, d_s

The characteristic dimension to use in the Reynolds number for all correlations was the diameter of the sphere, d_s, obtained by averaging micrometer measurements made on the sphere diameter before and after the runs.

J. The Activity or Effective Uranium Concentration

The effective concentration of the dissolved uranium in the molten cadmium, or the activity, a_l, was obtained by data taken using the atomic fraction of uranium in molten cadmium, the activity coefficient, γl, and the thermodynamic cell measurements.

K. The Physical Properties of the Molten Cadmium

The physical properties are discussed in Chapter VII. The Schmidt number was evaluated from the values of the physical properties at the experimental temperatures of the mass transfer runs. Usually the values of the physical properties at 500°C were used since this was the temperature of the majority of the mass transfer runs.

L. Surface Area of the Sphere

The surface area of the sphere is used in the basic mass transfer equation to evaluate J_d by calculation of the mass transfer coefficient, k_l. The nominal diameter of the sphere was used to calculate the nominal area, A_n. The arithmetic diameter d_s was used to calculate the arithmetic surface area, A_s, at the sphere for the mass transfer correlations, and for the Reynolds number at the sphere, $N_{Re,s}$. The actual difference in the arithmetic surface area and the nominal surface area amounts to about 1%.

M. The Mass Transfer, J_d Factor

The mass transfer J_d factor used in the correlations of this report was based upon the Schmidt number raised to the 2/3 exponent. This was designated in Tables XIX, and XX as $J_d(N_{Sc}^{0.666})$. The J'_d factor used in the correction for temperature was based upon the Schmidt number raised to the 0.58 exponent. The corrections for surface area change, and coastdown time, θ', were made and applied to J_d. The differences have been discussed in the sample calculations which appear in Chapter XVII. Except where specifically stated all of the J_d correlations were based upon the Schmidt number raised to the 2/3 exponent.

N. Tables of Mass Transfer Data

All of the mass transfer data have been tabulated in tables which appear in the Appendix, Chapter XVI.

IX. CALCULATION OF MASS TRANSFER DATA

A. Equations Used to Calculate Mass Transfer Data

The following discussion shall include: the calculation of the mass transfer coefficient k_l; the evaluation of the Schmidt and Reynolds moduli; and the determination of the J_d factor. Expressions shall be presented which depend upon variables which relate the mass flux from the test sample, the length of sample exposure, the flow rate of the molten cadmium, and the physical properties of the system.

1. Mass Transfer Equations Necessary to Evaluate k_l and J_d

a. Calculation of the Mass Transfer Coefficient, k_l

The weight loss is given by the following equation

$$\Delta w = k_l A_s \theta (C_s - C_l) \tag{9.1}$$

where N_A represents the mass flux, A_s equals the surface area of sphere and θ equals the time of exposure of the solute to the solvent, and $(C_s - C_l)$ equals the concentration driving force. The concentration driving force for this study was taken as the difference in solubility of the solute in the solvent and the concentration of solute in the bulk stream. The previous equation can be solved for the mass transfer coefficient

$$k_l = \frac{\Delta w}{A_s \theta (C_s - C_l)}. \tag{9.2}$$

Usually the concentration in the bulk stream C_l is about zero, unless the effect of the concentration driving force on the mass flux is desired. For convenience, the above equation may be written as follows:

$$k_l = \frac{\Delta w}{A_s \theta \Delta C_i}. \tag{9.3}$$

In equation 9.3 the ΔC_i represents $(C_s - C_l)$. If C_l is zero, then the driving force is a maximum and may be represented as ΔC_{max}. In the situation where C_l becomes equal to $0.25\ C_s$, $0.50\ C_s$, $0.75\ C_s$, and $0.90\ C_s$, the driving force becomes, respectively, $0.75 \Delta C_{max}$, $0.50\ \Delta C_{max}$, $0.25\ \Delta C_{max}$, and $0.10 \Delta C_{max}$.

b. Calculation of the Mass Transfer Coefficient for Forced Connection, k_l/V_s

The mass transfer coefficient as shown in equation 9.3 will vary depending upon the velocity. It is advantageous to obtain the ratio of

the mass transfer coefficient to the velocity for the J_d factor versus Reynolds number correlation. The ratio k_1/V_s is written as

$$k_1/V_s = \frac{(w_1 - w_2)\, d_p^2 - d_s^2}{(\pi d_s^2)\, \theta(V_s)\, d_p^2(C_s - C_1)} \tag{9.4}$$

where

d_p = pipe diameter, cm,

d_s = sphere diameter, cm,

θ = time of dissolution, sec,

V_a = average flow rate, cm/sec,

V_s = velocity of molten cadmium at sample,

$w_1 - w_2$ = sphere weight loss at V_s and θ,

and

$C_s - C_1$ = concentration driving force.

The velocities at the sphere for the J_d correlation were obtained from the equation of continuity using the average velocity in the pipe, the area of the loop pipe and the minimum flow area at the sphere. This allowed the velocity at the sphere to be written as

$$V_s = V_a\left(\frac{d_p^2}{d_p^2 - d_s^2}\right). \tag{9.5}$$

It is realized, however, that the average velocity over the sphere is more complicated than that obtained in equation 9.5 by correcting the average pipe velocity by the ratio of free flow area to minimum area for flow at the sphere. The actual velocity over the sphere is a complex function of the boundary layer formation, drag and pressure effects; however, the correlations of the mass transfer data in this report were based upon the velocity obtained at the sphere by using equation 9.5. The Reynolds number was evaluated using V_s.

2. Calculation of J_d Factor for Spheres

The mass transfer J_d factor is defined as

$$J_d = (k_1/V_s)(N_{Sc})^b. \tag{9.6}$$

The group symbolized by N_{Sc} is called the Schmidt number. It represents the ratio of fluid properties which shows the rate of transfer of momentum under the influence of a velocity gradient and the rate of mass transfer by

molecular diffusion under the influence of a concentration gradient. The Schmidt number as previously shown is evaluated from the physical properties of the fluid, viz., viscosity, μ, density ρ, and the molecular diffusivity D_v of the experiment. The exponent b in the above equation is taken to be 0.666 unless otherwise stated.

The sample calculations for k_l, k_l/V_s, J_d, and the detailed error analysis are given in the Appendix, Chapter XVII.

B. Analysis of Possible Errors in J_d Mass Transfer Data Resulting from Transient Flow in Loop

1. Introduction

The employment of a centrifugal pump for pumping the molten metal past the sphere in the dynamic loop created a small problem as regards the start-up and coast-down periods relative to the steady flow rate. It was customary to measure the experimental time from the instant that the motor which drives the pump was turned on until the instant that the motor was shut off. However, a finite time was involved in pumping a slug of molten cadmium from the pump reservoir to the uranium sphere during the start-up period. Also after the motor was shut off molten cadmium still flowed past the sphere at an unsteady flow rate which depended upon its rate of decay as affected through inertial resistance and conventional pressure drop across the loop. In fact analysis of the rate of decay is even more complicated than simple pressure drop calculations indicate from the Bernoulli equation since the molten cadmium must flow past the impeller and is damped by the drag resistance associated with the pump shaft and shaft connections to the driving unit.

2. Principles and Theory

It is recalled that the flow rate of the molten cadmium was measured by an electromagnetic flowmeter and based upon the principle of its operation, the generated emf is proportional to the average velocity of the molten cadmium as determined by flow through an orifice. According to this principle, the emf generated as the liquid metal flows through the magnetic field of the magnets positioned on the low horizontal leg of the loop is expressed as

$$E = K B L V. \tag{9.7}$$

For properly mounted magnets and at any given temperature, B (magnetic flux) is constant for the loop pipe. K is a constant which depends upon the geometry of the duct, the electrical resistances of the duct and flowing metal and the geometry of the magnetic field. K is usually considered constant at any given temperature and location.

If E_i and V_i are the emf and velocity at time t_i and E_{ss}, V_{ss} are the emf and corresponding velocity at steady flow then for the same magnet and given temperature and allowing for the constant K, B, L the ratios of E_i to E_{ss} and V_i to V_{ss} are essentially equivalent according to 9.7.

Having established the above equation and the assumption upon which it was based, it is desirable to obtain the emf (transient emf) during the start-up and shutdown periods. It was found that an ordinary emf chart recorder should indicate the magnitude but could not yield a fast enough chart speed to record the transient growth and decay of the flow rate.

3. Experimental Equipment

It was found that by using a Heiland Visicorder and DC amplifier that growth and decay curves could be obtained during start-up and shut-down of the dynamic loop. The set-up for the experimental measurements is shown schematically in Fig. 13.

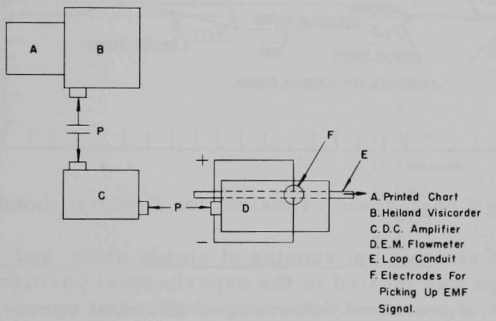

Fig. 13. Experimental Apparatus for Measuring Flow Transients in Dynamic Loop

A motor switching circuit starts and stops the motor drive unit for the molten metal pump. According to equation 9.7, after pumping begins an emf is generated proportional to the velocity of the flowing metal. (The lower horizontal leg of the loop pipe where the EM flowmeter is located is always filled with molten metal to maintain wetting of the walls, etc.) The generated emf at D is then fed to a DC amplifier which amplifies the signal at C and the amplified signal is picked up by the Visicorder at B. A printed chart at A shows the transient pattern as affected by the specific chart speed. The Visicorder used in these experiments could give chart speeds of 5 to 25 inches per minute.

4. Experimental Procedure

a. Start-up Operation. The dynamic loop was allowed to reach an experimental temperature of 500°C and the magnet temperature was periodically checked to insure that its temperature remained constant. At various speed ratios using the Vari-speed drive the pump was simultaneously started with the Visicorder. It was found that the start-up time

required to reach a steady flow rate was negligible compared to the longer coastdown periods. Corrections were not made for the start-up time to reach steady flow rate.

b. Shut-down Operation. After the start-up transient was recorded and the loop allowed to operate at steady flow for some 10 seconds, the pump was stopped by cutting power to the motor drive unit. The decay curves for the unsteady flow patterns versus time after shut-down were obtained and a typical transient is shown in Fig. 14.

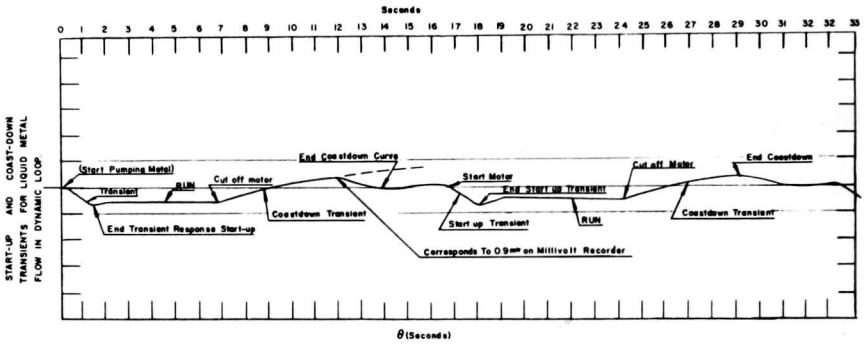

Fig. 14. Typical Trace Showing Coast-down Transient for Dynamic Loop

In each cycle of starting up, running at steady state, and shutting down, the dummy sphere was located in the experimental position in the loop. At least five cycles of transient data were obtained at seven different pumping speeds. Also data were taken at both chart speeds. Figure 14, which is a typical trace of transient data for the dynamic loop, indicates the following:

a. start-up transient,

b. steady flow,

c. coast-down transient, and

d. total times to start-up and coast-down.

5. Discussion and Analysis of Transient Data

It is assumed that the flow ratios are related to the electromotive forces generated at the magnet by the flowing cadmium. If V_{ss} and E_{ss} represent the steady flow velocity and corresponding emf, respectively, and V_i and E_i represent the flow rate and corresponding emf at same time after the power is shut off to the pump, then the ratios V_i/V_{ss} and E_i/E_{ss}

are essentially equivalent. These ratios represent the fraction of the experimental velocity for a regular mass transfer run vs time after the power is cut to the pump.

It is desirable to obtain basic information regarding this coast-down transient as dissolution occurs at a rate dependent upon the time rate of change of velocity after power is cut to the pump. Actually, the measured weight from the sphere during the time the pump runs must be corrected to account for the amount dissolved off in the coast-down in the loop.

The correction that is applied amounts to obtaining a factor which represents the effective mass transferred by some average effective velocity during the coast-down time. The transient data is recorded from a typical visicorder trace and is shown in the following table for a speed of 2150 rpm. The speed setting on the varispeed motor corresponded to an index of 7 on the motor.

TABLE VIII. Table of Transient Data for Coast-Down

t_i	$E_{ss} \times 10$	E_i
0	9 mv	1.0
1		0.94
2		0.79
3		0.60
4		0.372
5		0.165
6		0.082
7		0.025
7.5		0.0

The average flow rate is obtained by a graphical integration which amounts to obtaining the time average of the transient from the time the pump is shut off until the flow stops completely. The following equation 9.8 represents this average where $\bar{\epsilon}$ represents the average fraction of the experimental velocity for the coast-down period for the mass transfer run.

$$\bar{\epsilon} = \frac{V_i}{V_{ss}} = \frac{\int_{\theta=0}^{\theta=\theta} \epsilon(\theta)\, d\theta}{\int_{\theta=\theta}^{\theta=\theta} d\theta} = \frac{\sum_{\theta=0}^{\theta=\theta} \epsilon_i(\theta)\, \Delta\theta_n}{\sum_{\theta_i(\theta)}^{\theta_n(\theta)} \Delta\theta_n}. \tag{9.8}$$

When $\bar{\epsilon}$ is found the average velocity at the sphere for the decay period is obtained by recalling

$$\frac{\bar{E}_i}{E_{ss}} = \frac{\bar{V}_i}{V_{ss}} = \bar{\epsilon}; \qquad \bar{V} = \bar{\epsilon} V_{ss} \tag{9.9}$$

where V_{ss} represents the experimental velocity at the instant before the pump is cut off and $\bar{V}$ represents the average velocity determined by this graphical integration.

A typical graphical integration is summarized in the following table for a speed of 2140 rpm.

Interval over θ	Area over Interval
0.0 to 1.0	0.925
1.0 to 2.0	0.885
2.0 to 3.0	0.720
3.0 to 4.0	0.495
4.0 to 5.0	0.320
5.0 to 6.0	0.100
6.0 to 7.5	0.0375

$$\Sigma\theta_i = 7.5, \quad \Sigma A_i = \Sigma\epsilon_i, \quad (\theta)\,\Delta\theta = 2.812$$

$$\overline{\epsilon} = \frac{2.812}{7.5} = 0.374, \quad \overline{V} = 0.374\,(V_{ss})$$

The total time to coast-down at each speed is plotted in Fig. 15 as a function of the velocity. Figures 16 and 17 show the fraction of steady flow for different speeds plotted versus the decay times θ' after power is cut to the pump. Data for graphical integrations may be taken from these plots to obtain the average flow rate.

The procedure used to obtain the average mass transferred amounts to using the apparent k_1/V_s obtained from the conventional calculation based on an average sphere diameter to calculate the amount transferred in time θ. This allows a new and a better estimate of k_1/V_s to be obtained after correcting for coast-down. The effective mass transferred, $\Delta w'$, becomes

$$\Delta w' = \left(\frac{k_1}{V_s}\right) \times A_s \times \Delta C \times \theta' \times \overline{\epsilon} \times V_{ss} \qquad (9.10)$$

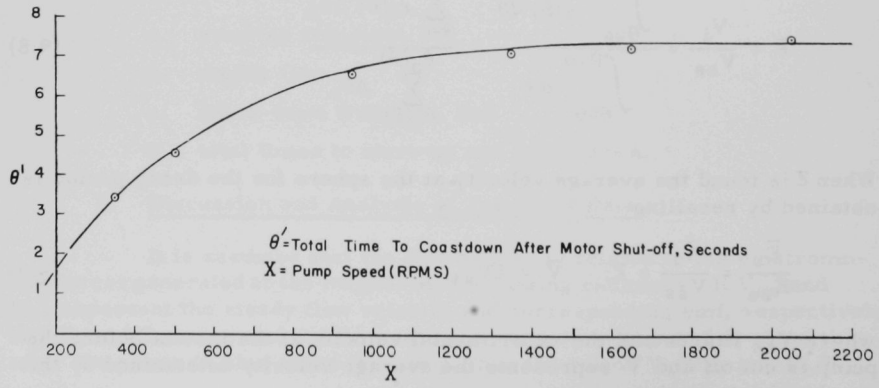

Fig. 15. Total Time for Molten Cadmium to Coast-down Versus Speed after Power Is Cut to Pump

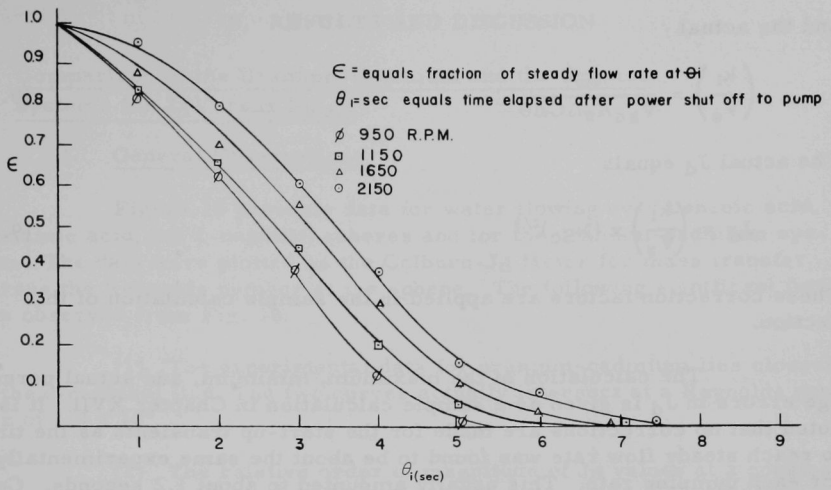

Fig. 16. Fraction of Experimental Flow Rate Versus Time after Power Is Cut Off to Molten Metal Pump at High Speeds

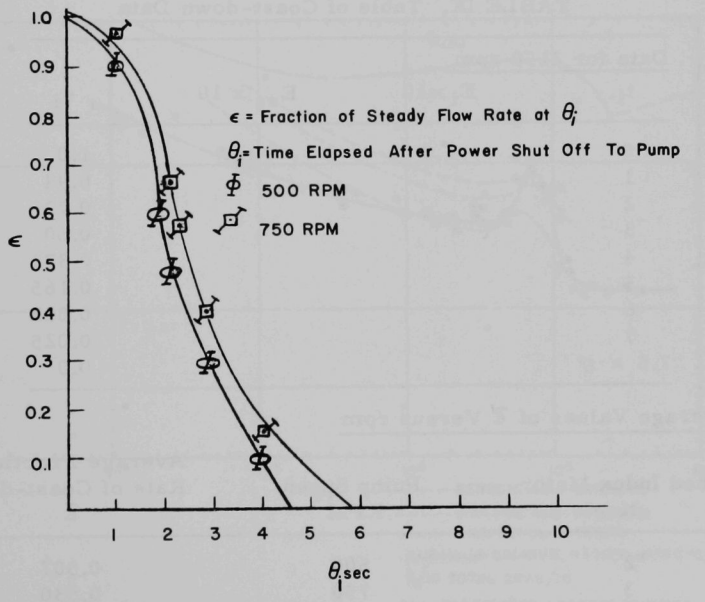

Fig. 17. Fraction of Experimental Flow Rate Versus Time after Power Is Cut Off to Molten Metal Pump at Low Speeds

and the actual

$$\left(\frac{k_l}{V_s}\right) = \frac{\Delta w'}{V_{ss} A_s \Delta C \Delta \theta}. \tag{9.11}$$

The actual J_d equals

$$J_d = \left(\frac{k_l}{V_s}\right) \times (N_{Sc})^{2/3} \tag{9.12}$$

These correction factors are applied in the sample calculation of this section.

The calculation of the maximum, minimum, and actual percentage errors in J_d is given as a sample calculation in Chapter XVII. It is noted that no corrections are made for the start-up transients as the time to reach steady flow rate was found to be about the same experimentally for each pumping rate. This usually amounted to about 1.2 seconds. Coast-down corrections were only made for runs less than 3 minutes duration (1, 2, and 3 minutes).

TABLE IX. Table of Coast-down Data

Data for 2150 rpm

t_i	$E_i \times 10$	$E_{ss} \times 10$	ϵ_i
0	1.0	9 mv	1.0
1			0.94
2			0.79
3			0.60
4			0.372
5			0.165
6			0.082
7			0.025
7.5 = θ'			0.0

Average Values of $\bar{\epsilon}$ Versus rpm

Speed Index Motor N	Pump Speed RPM	Average Fractional Rate of Coast-down $\bar{\epsilon}$
2	500	0.507
3	750	0.530
4	950	0.384
5	1350	0.436
6	1650	0.463
7	2150	0.374

X. RESULTS AND DISCUSSION

A. Comparison of the Uranium-Cadmium and the Organic Systems for J_d Versus $N_{Re,s}$

1. General Observations

Figure 18 presents data for water flowing over benzoic acid, cinnamic acid, and 2-naphthol spheres and for the uranium-cadmium system. The data were plotted as the Colburn-J_d factor for mass transfer versus the Reynolds number at the sphere. The following significant facts are observed from Fig. 18:

(1) The experimental data for uranium-cadmium lies closest to the 2-naphthol line. The two curves actually intersect at a Reynolds number of 1.0×10^4.

(2) The relative order of magnitude of J_d values at a constant Reynolds number appears congruent to the relative hardness of the different

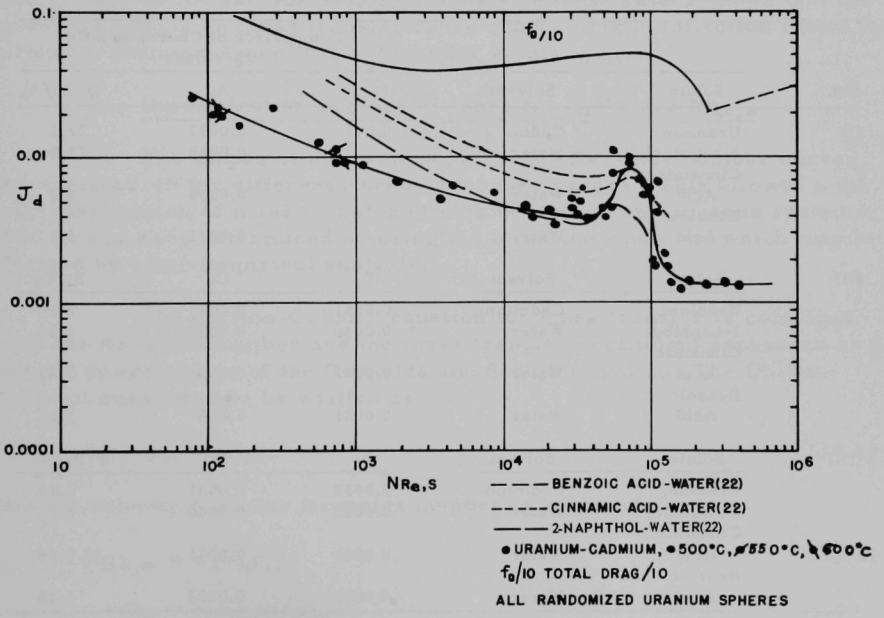

Fig. 18. J_d Versus $N_{Re,s}$ for Different Organic Solutes Dissolving in Water and for the Uranium-Cadmium System

solutes, i.e., the softest solute has the highest J_d value. Steele and Geankoplis[22] also observed this fact.

(3) The J_d factor curves for all solutes have a characteristic rise and fall in the vinicity of 100,000 Reynolds number. The rise in the uranium-cadmium curve starts at a J_d value lower than that of the 2-naphthol curve and rises in a similar manner to the total drag curve.

(4) The slopes of the curves at the lower velocities were not the same but were steeper for the organic solutes.

(5) Experimental data were not presented for the organic solutes below 500. It is extended down to 100 for the uranium-cadmium system. Data were also presented for the uranium-cadmium system extending as far up as 5×10^5.

The total drag coefficient was also plotted versus the Reynolds number in order to show the general similarities between momentum and mass transfer for the uranium-cadmium system. The J_d points are summarized in Table X in order to compare the mass transfer curves to the

TABLE X. J_d Values at Reynolds Numbers of 3.5×10^4 and 7×10^4

	System		Comparison of Characteristic J_d Values		
Set	Solute	Solvent	$f_d/10$	A_i	$f_d/10/A_i$
(I)	Uranium	Cadmium	0.045	0.0037	12.1
	2-naphthol	Water		0.0038	11.8
	Cinnamic Acid	Water		0.0055	8.2
	Benzoic Acid	Water		0.0071	6.3
(II)	Solute	Solvent	B_i	C_i	B_i/C_i
	Uranium	Cadmium	0.0081	0.003	2.69
	2-naphthol	Water	0.0046	0.0034	1.36
	Cinnamic Acid	Water	0.0071	0.005	1.43
	Benzoic Acid	Water	0.0081	0.006	1.35
(III)	Solute	Solvent	A_i	B_i	B_i/A_i
	Uranium	Cadmium	0.0037	0.0081	2.19
	2-naphthol	Water	0.0038	0.0046	1.21
	Cinnamic Acid	Water	0.0055	0.0071	1.29
	Benzoic Acid	Water	0.0071	0.0082	1.15

The A_i values were taken at a Reynolds number of 3.5×10^4.
The B_i and C_i values are all taken at a Reynolds number of 7×10^4.

total drag coefficient in the vicinity of 100,000 Re,s. Here both drag and mass transfer curves show a decided increase in the magnitude of the drag coefficient and the values of J_d. The change is more prominent for the uranium-cadmium system than for the organic solutes. These are the only mass transfer studies made at a velocity beyond the hump.

Table X shows the comparison of characteristic J_d values for the different solutes. The values are chosen from Fig. 18 at $N_{Re,s}$ of 3.5×10^4 and 7×10^4. Comparison of data in set II presented essential information. The C_i values were obtained by extrapolation of the various J_d versus Reynolds number curves through the hump. The B_i values correspond to peak J_d values at the hump. The ratios B_i/C_i are taken to show that the pressure effects on mass transfer for uranium-cadmium are about 2 times that of the other solutes. These ratios are as follows: uranium-cadmium, 2.69; 2 naphthol-water, 1.35; cinnamic acid-water, 1.43; and benzoic acid-water, 1.35.

In data set III, the A_i values correspond to a position in the J_d versus Reynolds curves prior to the abnormal rise. These values are all taken at $N_{Re,s}$ of 3.5×10^4. All of the J_d versus $N_{Re,s}$ curves for the various solutes show the same inflection point at this Reynolds number. A comparison of the various peak J_d values with these values shows that the pressure effects on mass transfer cause characteristic inflection ratios for uranium-cadmium twice that of the other solutes.

2. Determination of Slope of Lines for J_d Versus $N_{Re,s}$

The slopes of the various J_d versus Reynolds number curves were compared for different Reynolds number ranges. This allowed a direct comparison of mass transfer effects in organic and aqueous systems. The slopes were determined by using the following equations which may be derived by semi-empirical analysis.

The Chilton-Colburn equation for mass transfer is combined with the Reynolds number and the mass transfer coefficient expressed as a simple power series of the Reynolds and Schmidt moduli. The Chilton-Colburn equation may be written as

$$J_d = k_1/V_s(N_{Sc})^x \tag{10.1}$$

and the velocity from the Reynolds number is substituted in

$$N_{Re,s} = d_s V_s \rho/\mu, \tag{10.2}$$

$$V_s = N_{Re,s}\mu/\rho d_s. \tag{10.3}$$

This substitution yields the following equations:

$$J_d = \frac{k_1}{N_{Re,s}\mu/\rho d_s} (N_{Sc})^x = \frac{k_1 \rho d_s}{N_{Re,s}\mu} \left(\frac{\mu}{\rho D_V}\right)^x \tag{10.4}$$

$$J_d = \frac{k_1 d_s}{N_{Re,s}} \frac{\mu^{x-1}\rho^{1-x}}{D_v^x} = \phi\left(\frac{1}{N_{Re,s}}\right) \phi'(\mu, \rho, D_v). \tag{10.5}$$

Equation 10.5 would indicate that as $N_{Re,s}$ approaches zero the J_d factor becomes infinite. However, k_1 is not a constant but is a function of velocity. Thus, an independent equation must be obtained which expresses k_1 as a function of velocity at the low Reynolds number range. One familiar expression results from the empirical equation as follows between the Sherwood number and the Reynolds and Schmidt numbers.

$$N_{Sh} = C_1 N_{Re,s}{}^a N_{Sc}{}^b. \tag{10.6}$$

Equation 10.6 is substituted in equation 10.5 to yield

$$J_d = \frac{\left[\frac{C_1 D_V N_{Re,s}{}^a N_{Sc}{}^b}{d_s}\right]\left[\frac{\mu}{\rho D_v}\right]^x}{N_{Re,s}\mu/\rho d_s}. \tag{10.7}$$

Equation 10.7 simplifies to

$$J_d = C_1 D_v^{1-x} \mu^{x-1} \rho^{1-x} N_{Re,s}{}^{a-1} N_{Sc}{}^b. \tag{10.8}$$

This states that J_d is proportional to the Reynolds number to the (a - 1) power, or

$$J_d \propto \phi(N_{Re,s})^{a-1} \phi'(\mu, \rho, D_v) \tag{10.9}$$

Equation 10.9 is written as log J_d = log constant + log ϕ' + (a - 1)

$$(\log N_{Re,s}) \text{ or } \log J_d = \text{constant} + (a - 1) \log N_{Re,s} \tag{10.10}$$

for a specific temperature since ϕ' remains constant. The term (a - 1) represents the slope of the J_d curve for the specific Reynolds range. Table XI summarizes the measured slopes from Fig. 18 of the various J_d curves over the Reynolds number range from 10^2 to 5×10^5.

TABLE XI. Slope of J_d and k_l Versus $N_{Re,s}$ for Laminar Flow

Reference	System: Solute	System: Solvent	N_{Re}: Lower Limit	N_{Re}: Upper Limit	Slope of J_d (a - 1)	Slope of k_l (a)
	Uranium	Cadmium	10^2	10^3	-0.424	+0.575
			10^3	2×10^4	-0.267	+0.732
			2×10^5	10^6	0 (approx.)	1.0 (approx.)
(22)	2-naphthol	Water	5×10^2	3×10^3	-0.649	+0.350
			3×10^3	3×10^4	-0.363	+0.636
(22)	Cinnamic Acid	Water	6×10^2	3×10^3	-0.649	+0.351
			3×10^3	2×10^4	-0.424	+0.575
(22)	Benzoic Acid	Water	7×10^2	3×10^3	-0.509	+0.490
			6×10^3	2×10^4	-0.338	+0.661

3. The Variation of k_l with Velocity

Most generalized correlations of experimental mass transfer data for spheres predict that the mass transfer coefficient varies with velocity raised to the 0.5 power for laminar flow. Table XII summarizes the results of other investigators as well as the experimental data obtained in this study for cadmium flow over spheres of uranium. Steinberger and Treybal[4] state that the results of several investigators show that the variation of the exponent of the Reynolds number varies from 0.35 to 0.6. However, included within this range are the mass transfer data from liquid drops and pellets in packed beds and liquids in wetted wall columns. This encompasses, therefore, liquid-liquid and liquid-gas mass transfer. For solid to liquid mass transfer, Table XII shows that the exponent of the

TABLE XII. Data for Variation of k_l with V_s for Laminar Flow between 100 and 1000 $N_{Re,s}$

Reference	Solute Solvent	Geometry	Exponent on V_s
(17)	Benzoic Acid Water	Spheres	0.5
(4)	Benzoic Acid Water	Spheres	0.62
(22)	Benzoic Acid Water	Spheres	0.490
(22)	Cinnamic Acid Water	Spheres	0.351
(22)	2-naphthol Water	Spheres	0.350
	Uranium Cadmium	Spheres	0.575

velocity varies in a similar manner to that observed by Steinberger and Treybal.[4] Independent investigators obtained a value of 0.5 to 0.6 for the variation of k_l with velocity for the exponent on the velocity using benzoic acid spheres.[17,22] For solid-liquid transfer with spheres Table XII indicates a variation of 0.35 to 0.62 which is the same as Steinberger and Treybal.[4] The value of 0.575 for laminar flow for the uranium-cadmium system tends to indicate that liquid metal mass transfer data may be correlated by similar expressions used for aqueous systems. This would tend to confirm the applicability of the Chilton-Colburn equation for liquid metal mass transfer.

From Table XI showing the slopes of the various J_d lines, it is observed that the slopes change as the Reynolds number range for the specific slope increases. The first slope may be assigned to the region of laminar flow where it is generally assumed that laminar mass transfer occurs in the boundary layer. The next Reynolds number range where the slope increases may indicate the probable effects of turbulent action at the solid surface with some eddies penetrating directly to the solid surface. It is noted that the first data for solid spheres for Reynolds numbers above 1.5×10^5 are those of this report. The mass transfer equations obtained in a conventional manner empirically tend to indicate that in the high velocity range the mass transfer coefficient varies with velocity raised to approximately an exponent of 1.0. Table XIII summarizes some of the work which supports this fact.

TABLE XIII. Variations of k_l with Velocity at High Reynolds Numbers

Reference	Solute	Solvent or Gas	Geometry	Exponent on V_s
(39)	Benzoic Acid	Water	Pipes	0.83
	Cinnamic Acid	Water		
	2-naphthol	Water		
(63)	2-naphthol	Air	Wetted Column	0.83
	Uranium	Cadmium	Spheres	1.0 (approx.)

It is noted that all of the dimensional equations including the Chilton-Colburn equation tend to confirm the fact that the mass transfer coefficient is a function of velocity raised to the 0.83 exponent. The values of 1.0 for uranium spheres is questionable in the Reynolds number range from 3×10^5 to 5×10^5 since a sufficient number of data points were not obtained to accurately position the slope of the J_d versus Reynolds number curve. If the slope is flat, the exponent on V_s at the highest velocity is

about 1.0 since the slope of the J_d line, evaluated as (a - 1), is zero. The observed slope is essentially consistent with that expected since it has the correct order of magnitude.

4. Qualitative Discussion of the Relationship of Total Drag Curve to J_d at 10^5 Reynolds Number (The Hump Region)

It may be observed from Fig. 18 that there is a characteristic increase in the mass transfer J_d factor in the vicinity of 10^5 Reynolds number. This increase in J_d is common to all of the J_d versus Reynolds number curves.

The total drag of single spheres results from drag and pressure effects over the sphere. Both peaks occur at the same Reynolds numbers but the peak for the drag curve is much broader. There are no skin friction data for spheres in the hump region and it is skin friction data which should be compared to J_d and not total drag. Nevertheless, one can obtain a qualitative physical analogy concerning what happens by observing the total drag curve. In front of the sphere and along the leading edge as the Reynolds number increases, the velocity increases due to decreasing flow area. The pressure on the forward half of the sphere decreases and then increases to the rear. The particles in the viscous layer reach a point along the surface from the leading edge of the sphere where an adverse pressure gradient is encountered such that separation occurs and eddy motion results at the rear of the sphere. This is generally designated as the wake area.

The effect of the shift of the point of separation with Reynolds number from the forward portion of the sphere to the rear of the sphere is observed by the rise and subsequent decrease in the total drag curve at Reynolds numbers of 10^5 corresponding to highly turbulent flow.

Either artificial roughening of the sphere or natural roughening due to mass transfer of the spherical surface along the leading edge can introduce turbulence into the boundary layer. This causes eddy motion and a "tripping action" of the boundary which is discussed in detail in a later section of this chapter. The "tripping action" contributes significantly to the hump in the J_d versus Reynolds number curve. The form drag and pressure effects as discussed in detail above contribute to the natural occurrence of the phenomena.

Many investigators have shown that at high flow rates, turbulent eddies penetrate directly to the solid surface. The penetration of eddies directly to the solid surface combined with the recirculation of the molten cadmium behind the sphere by turbulent eddy motion are the chief reasons for the increase in J_d factors at a Reynolds number of 10^5. The greater increase in J_d factors for the uranium-cadmium system as compared to organic-water systems is probably attributed to the factors outlined in the previously discussed paragraphs.

B. Discussion of Temperature Effect upon J_d Versus $N_{Re,s}$

1. Correction of N_{Sc} for Change of Temperature

The mass transfer J_d factor may be written as

$$J_d = \frac{k_1}{V_s} (N_{Sc})^b. \qquad (10.11)$$

Most investigators have used this basic definition to correlate their mass transfer data. Generally, the exponent, b, on the Schmidt number has been taken to be 0.666. (A discussion has been presented in Chapter III of this report concerning the origin of the exponent.) Some doubt existed concerning the validity of the number 0.666 for correlating liquid metal mass transfer data. There were two reasons to support the argument:

(a) Most investigators in heat transfer studies with liquid metals found that conventional expressions used in heat transfer did not correlate their data. In a high temperature system the possibilities of somewhat similar discrepancies between conventional mass transfer correlations and liquid metal mass transfer data might be expected.

(b) The values of the physical properties used for forming the Schmidt number are different for liquid metals than for aqueous and organic systems. Thus a variation in temperature on J_d may not be accounted for by using a value of 0.666 for the exponent on the Schmidt number. This exponent and its probable value has been discussed in Chapter III. Therefore, it was advantageous to test the experimental mass transfer data for the uranium-cadmium system.

2. Determination of b Using the J_d Factor Plot

A method to determine the exponent on the Schmidt number may be obtained by taking the definition of the J_d factor and plotting log $(1/k_1/V_s)$ versus log N_{Sc} at a constant $N_{Re,s}$. The experimental data were plotted according to this method and appear in Fig. 19. The change in the boundary layer thickness is again detected since the slopes are not comparable at the separate Reynolds number ranges. The following values were obtained at each Reynolds number for the variation of the Schmidt number.

$N_{Re,s}$	Exponent
115	0.60
735	0.58

An average of the values was 0.59. It should be noted, however, that the range of the Schmidt numbers covered was 60%. Hence, the slopes from Fig. 21 are only approximate.

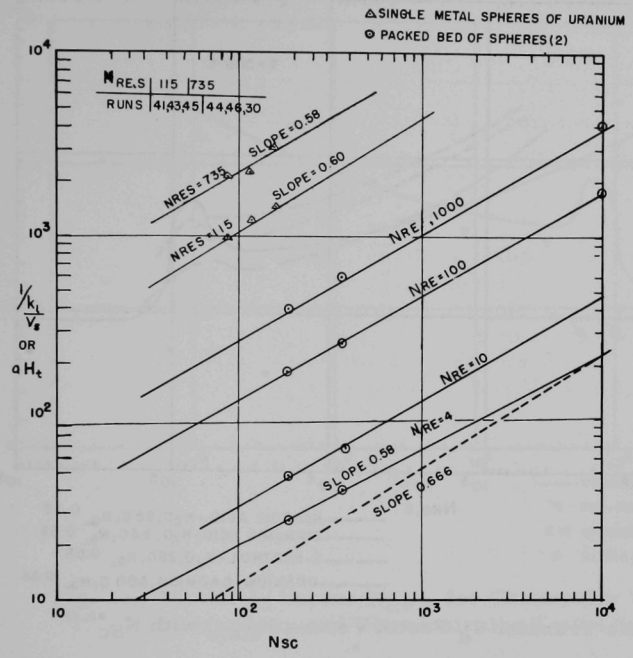

Fig. 19

Plot of $1/k_l/V_s$ or aH_t Versus N_{Sc}

A check of the literature to see if other investigators had correlated data with values close to 0.59 for the Schmidt number exponent revealed that this value possessed the correct order of magnitude. Gaffney and Drew[2] studied mass transfer from an unsaturated acetone-succinic acid solution using a packed bed of succinic acid pellets. They found that the exponent on the Schmidt number was 0.58. These values are sufficiently close enough to confirm the original doubt concerning the conventionally used 0.666. The experimental mass transfer data for uranium-cadmium will be correlated using a value of 0.58 for the exponent on the Schmidt number. The Gaffney-Drew data for packed beds also appear on the $(1/k_l/V_s)$ versus N_{Sc} plot shown in Fig. 19. These data are plotted as aH_t versus N_{Sc}.

3. Discussion of J_d versus $N_{Re,s}$ with $N_{Sc}^{0.58}$

The experimental mass transfer data for the uranium-cadmium system were plotted and corrected by using the 0.58 exponent on the Schmidt number. Figure 20 shows this graph as well as mass transfer data for water flow over benzoic acid, cinnamic acid, and 2-naphthol spheres. The value of 0.58 on the Schmidt number tends to correlate the experimental uranium-cadmium data so that at the Reynolds numbers of 4×10^3 and 1×10^5 the 2-naphthol and the uranium-cadmium curves coincide. The data for cinnamic acid and benzoic acid were not brought any closer to the uranium-cadmium curve using the 0.58 value.

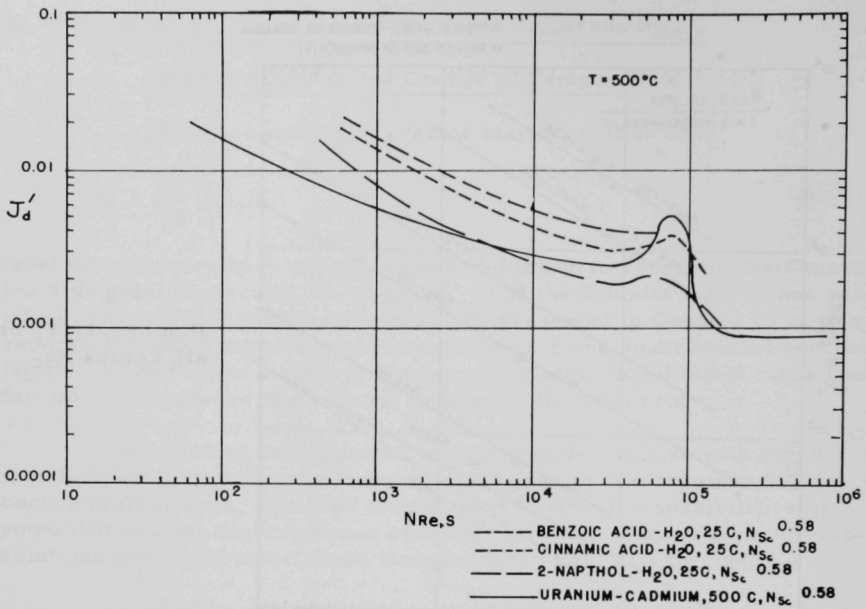

Fig. 20. Mass Transfer J_d' Factor Versus $N_{Re,s}$ with $N_{Sc}^{0.58}$

C. Discussion of the Effects of Metallurgical Treatment and Methods of Wetting upon Mass Transfer

1. The Heat Treatment of Uranium and Its Effect on the Mass Transfer Coefficient (Chemically Wetted)

The heat treatment of uranium which amounts to the alpha to beta phase transformation through an annealing and quenching process tends to produce a randomized grain orientation as well as more uniformly sized grains. The effects of mass transfer on spheres produced from this type of structure as compared to that on spheres produced from structures with preferred grain orientation may be observed in Fig. 21. The mass transfer from nonrandomized uranium spheres is not as great as that from the randomized spheres. This may be seen by comparing J_d values for the two structures. There are two reasons for the noted higher J_d values for the randomized spheres. Both are a result of the heat treating process. The randomized spheres have structures possessing smaller grains and grains which are rather regularly orientated. For the same time of exposure and at the same velocity of the molten cadmium, the surface area between phases is somewhat larger for the randomized sphere.

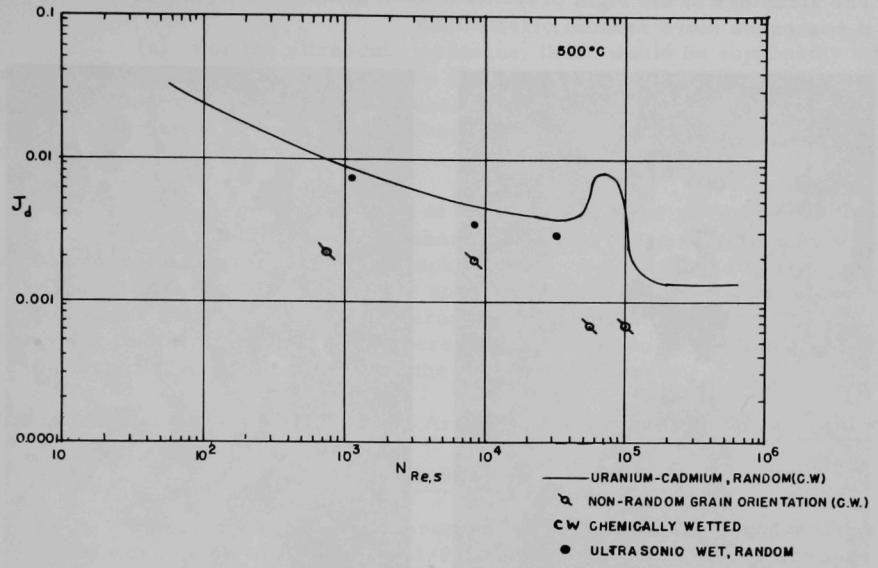

Fig. 21. Plot of J_d Versus $N_{Re,s}$ for Chemically Wetted, Random, Nonrandom, and Ultrasonically Wetted Spheres

This enhances mass transfer since the rate of dissolution is proportional to the exposed surface area between phases. The regular orientation would tend to produce an interface upon dissolution whose production in surface area per unit time would be greater because of uniform attack at the interface.

That the above logic as well as the experimental facts for uranium-cadmium presented in Fig. 21 are well based may be supported by the work of Stevenson and Wolff.[27] They found for the Cu-Nickel alloy that the fine grain structure was attacked to a greater extent than the coarse structure.

From Fig. 21, it is observed that the fine structure (randomized spheres) was attacked about 2 to 5 times as much as the coarse (nonrandomized) structure. Stevenson and Wolff[27] make no quantative comparison between the relative differences in dissolution between the coarse and fine structure and their respective grain sizes. The photomicrographs shown in Fig. 22 show a test uranium sample before and after heat treatment. It is observed from Fig. 22 that the sample after heat treatment possesses a finer structure as sub-graining appears. The photomicrograph shows the structure of uranium before the heat treatment at the left. The structure at the right shows the effects of the heat treatment.

The structure at the right presents a finer grain size and it appears that it possesses more random orientations.

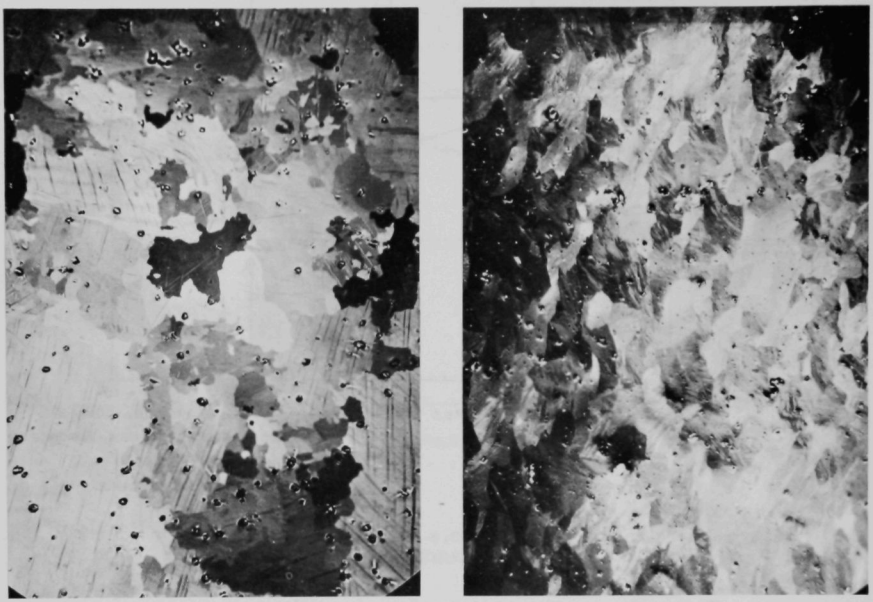

Fig. 22. Photomicrograph of Uranium before and after Heat Treatment Showing Random and Nonrandom Structures

Most of the runs in the mass transfer study of the uranium-cadmium system were made using randomized spheres. The data were found to be reproducible over the Reynolds number range from 10^2 to 4×10^5 as shown in Fig. 21. The runs with the nonrandomized spheres indeed showed that the uranium was attacked in a slightly preferred direction.

2. The Effect of Ultrasonics upon the Mass Transfer Coefficient and Comparison with Chemical Wetting Methods (Randomized Spheres)

Most of the runs for the J_d versus Reynolds curve were obtained by employing uranium spheres which were wet by the chemical method discussed in Chapter XV. It was expected that a uranium sphere which was wetted by using the ultrasonic apparatus might yield J_d values with a slightly different value relative to those obtained using spheres wet with the chemical method. It was postulated that the ultrasonic treatment might produce two fundamental effects. These were as follows:

(a) For the ultrasonic technique, there would be supposedly no reaction film at the interface between the solid uranium and the cadmium phase for the prewet sphere. Whereas, the possibility existed of some intermetallic formation between the uranium solid phase and the molten zinc in the chemical wetting procedure.

(b) The probable effect of ultrasonic surface waves on the solid uranium surface could cause some changes in solid phase structure as well as possibly an initial dissolution attack. Figure 21 shows the differences resulting from using chemically wet spheres and ultrasonically wet spheres. The J_d curve for the dissolution of uranium in cadmium is about 10 to 25% lower for the ultrasonically wet spheres as compared to the chemically wetted spheres. This is almost within the experimental error.

D. Discussion of Change of Surface Area between Phases for Mass Transfer

1. Using Different Diameter Spheres

In order to obtain the variation of surface area with mass transfer, runs were made with 1/2 inch, 3/8 inch, and 1/4 inch spheres at separate Reynolds numbers chosen over the entire Reynolds number range. Five runs were made with 3/8 and 1/4 inch spheres at five separate Reynolds numbers. The data appear plotted in Fig. 23.

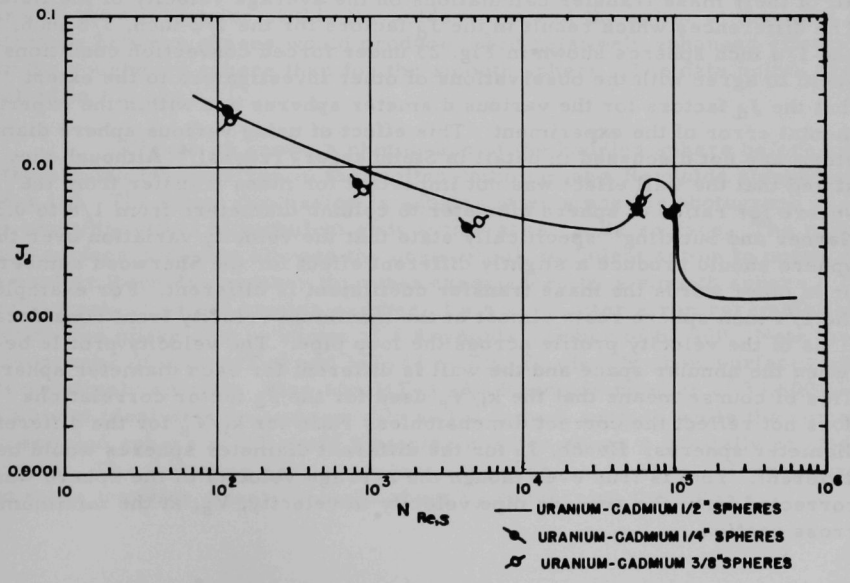

Fig. 23. Plot of J_d Versus $N_{Re,s}$ for Different Diameter Spheres

The deviation of the J_d factors for the 3/8 inch and 1/4 inch spheres from the J_d factors for 1/2 inch spheres is presented in Table XIV.

TABLE XIV. Comparison of J_d for 3/8 inch and 1/4 inch Spheres to J_d for 1/2 inch Spheres Versus $N_{Re,s}$

Run No.	110	111	112	113	114	115	116	117	118	119
J_d (1/2 inch)	.022	.0097	.0054	.0066	.0045	.023	.0057	.0096	.0053	.0072
J_d (3/8 inch)	.0207	.00713	.00431	.00597	.00532	-	-	-	-	-
% J_d (3/8 inch)	6	27	20	9	17	-	-	-	-	-
J_d (1/4 inch)	-	-	-	-	-	.021	.00387	.00739	.00514	.00477
% J_d (1/4 inch)	-	-	-	-	-	8.6	32	23	3	34
$N_{Re,s}$	124	903	5,160	61,100	104,000	114	4,330	906	57,900	95,600

The J_d data for various diameters does vary but little from the expected experimental error. The analysis of the experimental error in J_d is about 15%. If it is assumed that the same error could be involved in each J_d factor for the various diameter spheres then the results are to be expected. Garner and Suckling[36] in their study of the dissolution from benzoic acid and adipic acid spheres to water indicated that above N_{Re} of 100 that their correlation using the Sherwood number N_{Sh} showed that the mass transfer data for 3/8 inch, 1/2 inch, 5/8 inch, and 3/4 inch spheres were correlated by a single curve. These authors[36] indicate that the variation of the velocity over the surface of the sphere may be important. They based all of their mass transfer calculations on the average velocity of the fluid. The differences which result in the J_d factors for the 1/2 inch, 3/8 inch, and 1/4 inch spheres shown in Fig. 23 under forced convection conditions seem to agree with the observations of other investigators to the extent that the J_d factors for the various diameter spheres are within the experimental error of the experiment. This effect of using various sphere diameters was not discussed in detail in Steinberger-Treybal.[4] Although they stated that the wall effect was not important for mass transfer from the sphere for ratios of sphere diameter to column diameters from 1/8 to 0.3. Garner and Suckling[36] specifically state that the velocity variation over the sphere should produce a slightly different effect for the Sherwood number or in other words the mass transfer coefficient is different. For example, the 1/4 inch sphere rests almost at the maximum velocity from considerations of the velocity profile across the loop pipe. The velocity profile between the annular space and the wall is different for each diameter sphere. This of course means that the k_l/V_s used for the J_d factor correlations does not reflect the correct dimensionless ratio for k_l/V_s for the different diameter spheres. Hence, J_d for the different diameter spheres would be different. This is true even though the average velocity of the sphere was corrected from the average pipe velocity to velocity, V_s, at the minimum cross section.

The J_d values were calculated using the linear mean diameter before and after a run. However, using a true mean diameter by integration of the basic differential equation gave values of this value within 1% of the linear mean diameter. Hence use of the linear mean diameter was sufficiently accurate for the J_d calculations. The linear mean diameter was obtained by averaging micrometer measurements on the sphere diameter before and after a run. The mean diameter was used to calculate the mean surface area of the sphere A_s.

2. Using Artificially Roughened or Smooth Spheres

Roughened spheres were generated by a knurling process on the surface. The spheres were knurled in such a way that the weight loss of the sphere before and after knurling was negligible. The knurling process created a surface whose radial distance between tips and valleys amounted to about 1/64 of an inch with a uniformly roughened surface. Runs were made at separate Reynolds numbers of 330 and 8800 and the J_d values only for random spheres were compared with the previously obtained J_d values for nonroughened surfaces. The difference between J_d values at a Reynolds number of 330 was negligible for the roughened and smooth spheres. This was expected since it was postulated that diffusion through the laminar boundary layer was the controlling mechanism at this Reynolds number. The J_d value for the roughened sphere at a Reynolds number of 8.8×10^3 was somewhat higher than the corresponding J_d value for a smooth surface. This was also expected since it was noticed that some turbulent penetration through the film begins at this Reynolds range and the action at the solid interface between phases would produce more relatively enhanced effects for the roughened sphere than for the smooth sphere. The data points are plotted in Fig. 24.

Figure 25 shows a photograph of the knurled sphere before and after a mass transfer run in the molten cadmium at a Reynolds number of 8.8×10^3. The above discussion is substantiated since the photograph shows the probable effect of turbulent eddy action at the solid surface. The roughened surface probably allowed the onset of full turbulent action to occur at an earlier Reynolds number than that experienced by a smooth sphere. The knurled sphere at a Reynolds number of 8.8×10^3 after a run resembles very closely the pitted sphere shown at a Reynolds number of 62,900. Note that photographs of runs MT-4 and MT-34 of Fig. 26 clearly show surfaces which are relatively smooth. Also run MT-4 at a Reynolds number of 34,800 shows an almost ideal aerodynamic profile and a smooth surface while the run with the knurled sphere at 8.8×10^3 Reynolds number shows a partially eroded surface. The following section includes the discussion of turbulence, drag, and mass transfer effects brought about by roughening the sphere.

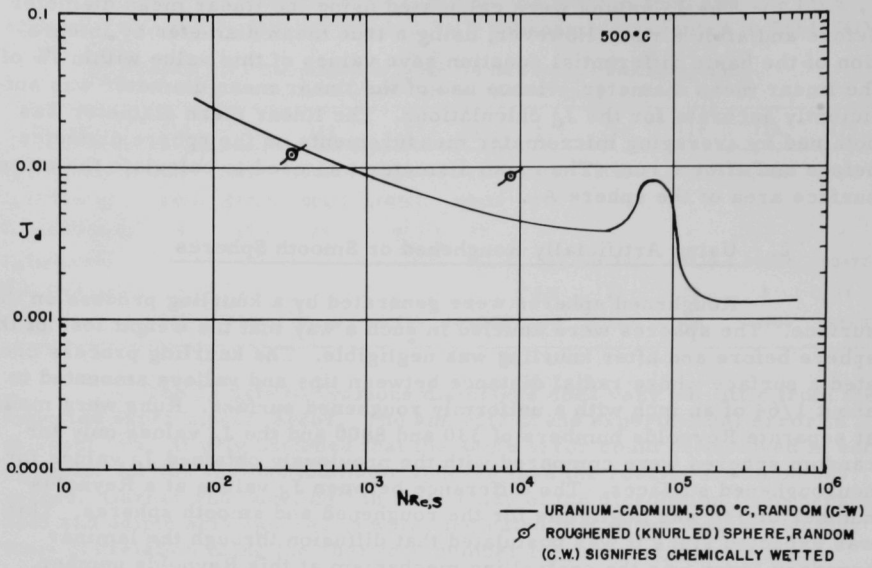

Fig. 24. Plot of J_d versus $N_{Re,s}$ for Roughened Spheres Showing Relationship to Smooth Spheres

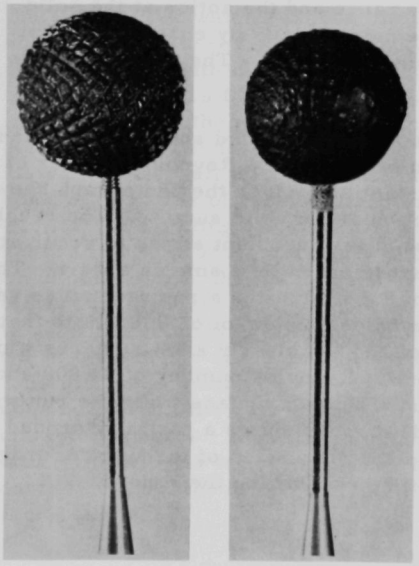

Fig. 25

Photograph Showing Knurled Sphere before (left), and after (right) a Run

108-6225

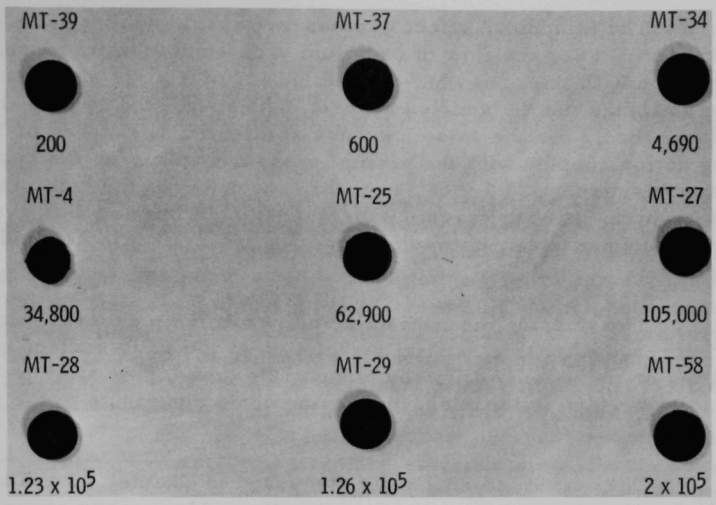

Fig. 26. Photograph Showing Flow over Spheres at Different Reynolds Numbers

3. Discussion of the J_d Versus Reynolds Number Curve at the Hump Region

It was mentioned in the previous section and may be observed from Fig. 24 that the J_d factor for the roughened sphere was higher at a Reynolds number of 8.8×10^3 than the J_d factor for a smooth sphere. This probably results from the effects brought about by the introduction of turbulence in the forward portion of the roughened sphere at a lower Reynolds number than should be expected for turbulence occurring normally over a smooth sphere. Thus turbulent eddies penetrate directly to the surface of the solid sphere creating an additional exchange of mass in addition to that expected at this Reynolds number by laminar diffusion, or slightly turbulent mass transfer. Figure 25 shows the roughened sphere after a mass transfer run and the obvious weight losses in the forward and rear regions of the surface. The relative effect of turbulent action on the roughened sphere may be seen by observing the run MT-4 at a Reynolds number of 3.48×10^4 for a smooth sphere in Fig. 26. The smooth and roughened spheres were heat treated and it was known that grain orientations and grain sizes for the spheres were similar.

The roughened sphere induces a "tripping" action into the boundary layer and hence turbulence into the forward portion of the sphere.[78] Therefore, the mass transfer results tend to confirm the relative effects of fluid flow action over the smooth and roughened surfaces.

The "tripping" effect was observed in the vicinity of 8.8×10^3 Reynolds number for the flow of cadmium over smooth uranium spheres. In connection with this, runs MT-25 and MT-27 of Fig. 26 show the same surface attack as for the knurled sphere. The roughened sphere shows the same J_d as the J_d for the smooth sphere at a Reynolds number of 330. This tripping action coupled with the normal pressure drag over the sphere at this Reynolds number (8.8×10^3) probably accounts for the hump in the J_d versus Reynolds number curve. With meager skin friction data available, the qualitative similarity between form drag and J_d at this Reynolds range is apparent.

The tripping mechanism could result from several sources. The occurrence of pitting, partial dissolution at the solid surface around impurities or inclusions, diffusion along grain boundaries after local attack at the solid surface is initiated, or erosion could contribute to the tripping action.

These mechanisms were discussed in Chapter III and tabulated in Table I. They become important in this Reynolds number range (4×10^5 to 5×10^5) since turbulent eddies penetrate directly to the solid surface. They probably are not as important at the low Reynolds number range where mass diffusion through the laminar boundary layer controls.

Experimental evidence obtained in this study showed that pitting and erosion effects occur at the Reynolds number corresponding to the region of the hump ($N_{Re,s}$ 8×10^4). The spheres were more pitted and eroded and the weight losses were greater at this Reynolds number range.

It is believed that the experimental evidence obtained by the dissolution from uranium spheres in the Reynolds number range from 5×10^4 to 1.5×10^5 presents the first evidence of the tripping mechanism in mass transfer and its effect on the boundary layer.

E. Discussion of the Experimental Data for the Uranium-Cadmium System and Comparison with the Transfer Coefficient for Momentum

It has been stated earlier in this report that in the absence of experimental data on mass transfer for a specific system that the mass transfer coefficients would be predicted from heat transfer data by application of the general Chilton-Colburn analogy. This analogy states

$$J_h = \frac{h}{\rho C_p V_s}\left(\frac{C_p \mu}{k}\right)^{2/3} = \frac{k_l}{V_s}\left(\frac{\mu}{\rho D_v}\right)^{2/3}. \qquad (10.12)$$

The right hand side equals J_d which is the Chilton-Colburn J_d factor for mass transfer. This analogy has found wide application in aqueous and organic systems. It seemed appropriate to test the limited form of the analogy, viz., equation 10.13.

$$J_d = \frac{k_1}{V_s}\left(\frac{\mu}{\rho D_v}\right)^{2/3} = f/2 \qquad (10.13)$$

where f is the skin friction factor for the momentum transfer across the sphere.

In order to establish if the analogy equation 10.13 is correct for liquid metals, the skin friction factor f/2 of organic systems for spheres and rotating cylinders from Tables XV and XVI were plotted in Fig. 27 and compared with the J_d for the uranium-cadmium system. The skin friction factor data for spheres were limited to a Reynolds number range from 100 to 1000 and at one point of 1.56×10^5. At a Reynolds number of 100 to 1000 the f/2 for organics is 2 to 3 times greater than the J_d for the uranium-cadmium system and at 1.5×10^5 the f/2 is approximately 3 times the J_d line. However, in the region of the hump form drag accounts for the major increase in J_d. Hence, it would not be expected that the skin friction and J_d analogy would hold in this region.

TABLE XV. Skin Friction Factor Data for Rotating Cylinders (Read from graph, reference 20)

$N_{Re,s}$	f/2
2×10^2	0.030
1×10^3	0.011
1×10^4	0.0046
1×10^5	0.0027
1×10^6	0.0017

At a Reynolds number of 1000 the skin friction f/2 of organic systems for spheres is in reasonable agreement with J_d for cinnamic acid and 2-naphthol. Extrapolation of the cinnamic and benzoic acid J_d lines to a Reynolds number of 1.56×10^5 shows a close agreement of f/2 and J_d for spheres.

Hence, Fig. 27 shows that the analogy between J_d for liquid metals and f/2 for organic liquids was not confirmed. However, skin friction data for liquid metals are not available and such data when available may show a closer relationship between J_d and f/2.

Data for skin friction f/2 for rotating cylinders[20] or organic liquids in Fig. 27 show a reasonably close agreement with J_d for uranium-cadmium. Sherwood[20] using experimental data shows a close agreement between skin friction, mass transfer, and heat transfer for the rotating cylinders over a very wide Reynolds number range.

TABLE XVI. Skin Friction Data over a Sphere (Read from graph, reference 76)

$N_{Re,s}$	f/2
50	0.14
100	0.083
300	0.041
500	0.030
700	0.025
1,000	0.0205
157,000[77]	0.0045

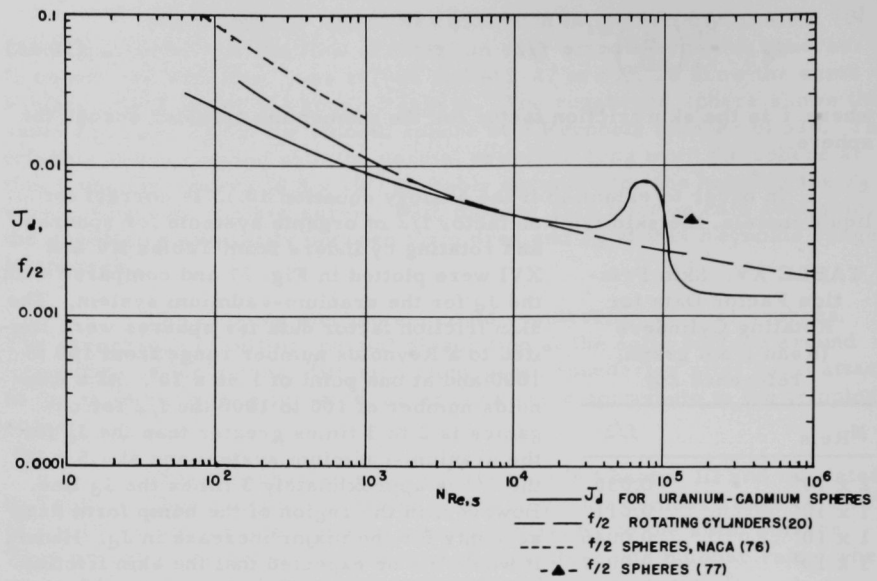

Fig. 27. J_d Versus $N_{Re,s}$ for Uranium-Cadmium and Friction Factor for Cylinders and Spheres

Since it was concluded that at the region of the hump in the J_d curve at a Reynolds number of 10^5 the abnormal increase in J_d results from form drag, the extrapolation of the skin friction curve through a Reynolds range of 4×10^4 to 1.5×10^5 seems plausible.

F. Discussion of the Dependence of Mass Flux upon the Concentration Driving Force for Mass Transfer

1. Introduction

The basic mass transfer equation may be written as

$$\Delta w = k_1 A_s \theta \Delta C. \tag{10.14}$$

A rearrangement of the above equation allows the mass flux N_A to be written as a function of the concentration driving force

$$N_A = \frac{\Delta w}{A_s \theta} = k_1(\Delta C). \tag{10.15}$$

It was observed by Steele and Geankoplis[22] in their investigation of the mass transfer from benzoic acid, cinnamic acid and 2-naphthol spheres that where

mass flux was plotted versus the concentration driving force that a finite mass flux appeared at supposedly saturated conditions. Saturated conditions refer to 100 percent solute concentration in the solvent or dissolving medium. These investigators[22] stated that the reason for a finite flux being observed when theory indicates a zero flux might be associated with the differences in dissolution and deposition rates from and to the sphere, or from physical attrition and turbulence effects resulting from the flow of solvent past the sphere. However, they[22] plotted the mass flux versus the concentration driving force with the Reynolds numbers held constant for each system and found the same effect at a zero concentration driving force.

However, it has been mentioned that the true driving force for mass transfer is not the ordinarily used concentration difference but should be replaced by the effective driving force, or by an activity driving force. The correction of the experimental mass transfer data for this effective driving force should reduce the mass flux to a value close to zero on a plot of mass flux versus activity driving force.

The activity data for the uranium-cadmium system were obtained from the work of Johnson and Martin.[81] The atom fraction of uranium in cadmium solution was plotted versus the logarithm of the activity in Fig. 28. Using values of C_1 which were chosen for the mass transfer

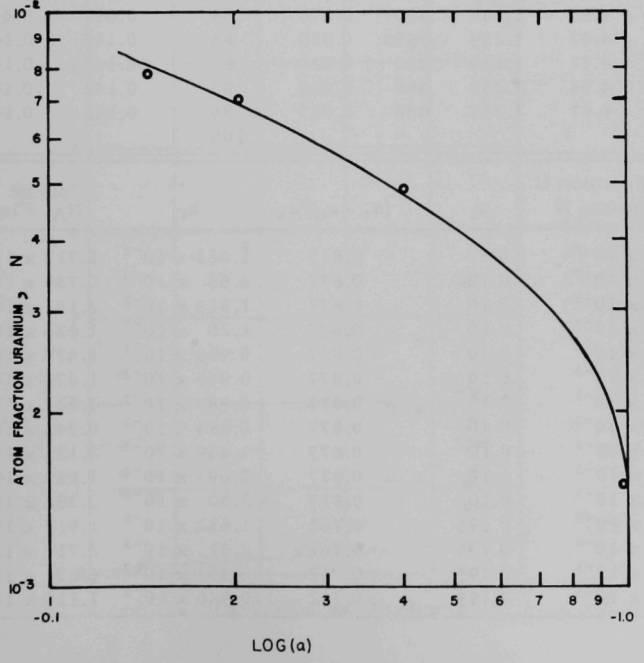

Fig. 28
Atom Fraction of Uranium, N, Versus Log Activity, Log(a)

runs. Figure 28 was used to read an activity value. Table XVII was partially constructed by using these activity data. Equations 10.23 and 10.17 were used to calculate the driving force data tabulated.

TABLE XVII. Activity and Concentration Data Versus k_1 for Flux Analysis

Run No.	Δw	A_s	d_s	θ	ΔC g/cc	C_1 % of C_s	C_1 g/cc	$\Delta C/C_s$
89	0.4056	4.93	1.253	480	0.163	2.5	0.004	0.977
90	0.1765	4.97	1.259	480	0.163	2.5	0.004	0.977
91	0.5748	4.94	1.255	540	0.163	2.5	0.004	0.977
92	0.4844	4.92	1.250	540	0.163	2.5	0.004	0.977
93	0.3550	5.01	1.265	480	0.153	8.1	0.014	0.916
94	0.3448	4.95	1.255	480	0.153	8.1	0.014	0.916
95	0.4074	4.95	1.255	540	0.153	8.1	0.014	0.916
96	0.1990	4.95	1.255	540	0.153	8.1	0.014	0.916
98	0.5053	4.93	1.252	480	0.147	12.2	0.020	0.882
99	0.2736	4.96	1.259	540	0.147	12.2	0.020	0.882
100	0.8708	4.93	1.255	540	0.147	12.2	0.020	0.882
102	0.4506	4.94	1.255	480	0.117	29.9	0.050	0.703
103	0.6420	4.99	1.260	480	0.117	29.9	0.050	0.703
104	1.4869	4.96	1.259	480	0.117	29.9	0.050	0.703
105	0.2636	4.96	1.257	480	0.117	29.9	0.050	0.703
107	1.0230	4.93	1.252	540	0.070	58	0.097	0.417
108	0.2928	4.95	1.255	600	0.070	58	0.097	0.417
109	0.7910	4.87	1.249	480	0.070	58	0.097	0.417
130	0.3148	4.97	1.259	540	0.025	85	0.142	0.149
131	0.3613	4.97	1.259	480	0.025	85	0.142	0.149
132	0.5597	4.95	1.255	480	0.025	85	0.142	0.149
133	0.2316	4.97	1.259	480	0.025	85	0.142	0.149
						100		

Run No.	Atomic Fraction U in Cadmium, N	a_1	$(a_s - a_1)/a_s$	k_1	N_A, Flux
89	0.254×10^{-3}	0.10	0.877	1.053×10^{-3}	1.715×10^{-4}
90	0.254×10^{-3}	0.10	0.877	4.55×10^{-4}	0.739×10^{-4}
91	0.254×10^{-3}	0.10	0.877	1.315×10^{-3}	2.15×10^{-4}
92	0.254×10^{-3}	0.10	0.877	1.20×10^{-3}	1.825×10^{-4}
93	0.82×10^{-3}	0.10	0.877	0.966×10^{-3}	1.475×10^{-4}
94	0.82×10^{-3}	0.10	0.877	0.949×10^{-3}	1.474×10^{-4}
95	0.82×10^{-3}	0.10	0.877	0.989×10^{-3}	1.511×10^{-4}
96	0.82×10^{-3}	0.10	0.877	0.484×10^{-3}	0.743×10^{-4}
98	1.23×10^{-3}	0.10	0.877	1.449×10^{-3}	2.13×10^{-4}
99	1.23×10^{-3}	0.10	0.877	0.693×10^{-3}	1.019×10^{-4}
100	1.23×10^{-3}	0.10	0.877	2.30×10^{-3}	3.38×10^{-4}
102	3.07×10^{-3}	0.195	0.762	1.632×10^{-3}	1.91×10^{-4}
103	3.07×10^{-3}	0.195	0.762	2.31×10^{-3}	2.71×10^{-4}
104	3.07×10^{-3}	0.195	0.762	5.36×10^{-3}	6.27×10^{-4}
105	3.07×10^{-3}	0.195	0.762	0.946×10^{-3}	1.110×10^{-4}

TABLE XVII (Contd.)

Run No.	Atomic Fraction U in Cadmium, N	a_1	$(a_s - a_1)/a_s$	k_1	N_A, Flux
107	5.91×10^{-3}	0.521	0.361	5.47×10^{-3}	3.83×10^{-4}
108	5.91×10^{-3}	0.521	0.361	1.375×10^{-3}	0.987×10^{-4}
109	5.91×10^{-3}	0.521	0.361	4.84×10^{-3}	3.39×10^{-4}
130	8.67×10^{-3}	0.748	0.080	4.67×10^{-3}	1.175×10^{-4}
131	8.67×10^{-3}	0.748	0.080	6.06×10^{-3}	1.515×10^{-4}
132	8.67×10^{-3}	0.748	0.080	9.41×10^{-3}	2.35×10^{-4}
133	8.67×10^{-3}	0.748	0.080	3.87×10^{-3}	0.966×10^{-4}
	10.2×10^{-3}	$0.813(a_s)$			

2. Principles and Definition of Activity Driving Force and Concentration Driving Force

The mass flux from the sphere was plotted in Fig. 29 versus the fraction of the maximum concentration driving force which was varied

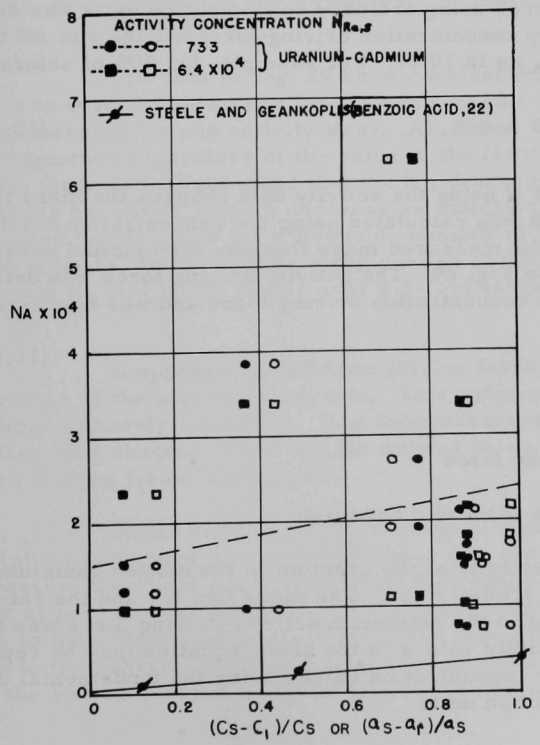

Fig. 29

Mass Flux, N_A, Versus Fraction of Maximum Concentration and Activity Driving Force

for the different mass transfer runs. The actual concentration driving force for mass transfer was varied by adding uranium to the molten cadmium in different measured amounts (by weight). The concentration driving force was thus varied as the addition of the uranium changed the bulk stream concentration of dissolved uranium in cadmium. Usually the concentration in the cadmium was about zero which allowed the maximum driving force to be written as

$$\Delta C_{max} = (C_s - C_1) = (C_s - 0) = C_s. \tag{10.16}$$

This was the maximum driving force based upon concentration units. If C_1 was greater than zero, by adding uranium to the cadmium, the driving force was

$$\frac{\Delta C}{C_s} = \frac{(C_s - C_1)}{C_s}. \tag{10.17}$$

The plot in Fig. 29 shows the mass flux, N_A calculated using experimental data plotted versus the fraction of the maximum driving force. The fraction of the maximum driving force using ordinary concentration units was defined as the ratio of the ordinary concentration driving force for the run ΔC to the maximum driving force C_s as in 10.17. For example, for 90% of saturation,

$$\frac{(C_s - 0.10\ C_s)}{C_s} \times 100 = 90\%. \tag{10.18}$$

In order to see if using the activity data changes the mass flux at zero driving force which was calculated using the concentration driving force and equation 10.15, the measured mass flux was also plotted versus the activity driving force in Fig. 29. The activity driving force was defined in a manner similar to the concentration driving force and was expressed as

$$\Delta a = (a_s - a_1) \tag{10.19}$$

where

Δa = activity driving force

a_s = activity at the saturated condition

and a_1 corresponds to the activity of the uranium in the molten cadmium used for the specific mass transfer run. The mass flux N_A and the ratio of the activity driving force to the maximum activity driving force was also plotted in Fig. 29. The activity values in the above equation may be replaced by their relationship to the concentration values using the fundamental definition of activity in atom fraction units

$$a = \gamma C. \tag{10.20}$$

The activity of the liquid was taken from the actual experimentally measured values of activity versus concentration for uranium dissolved in cadmium as plotted in Fig. 28. This allows the activity driving force to be written as

$$\Delta a = (a_s - a_l) = C_s\gamma_s - C_l\gamma_l. \tag{10.21}$$

The above equation may be rearranged to yield

$$\Delta a = C_s\gamma_s\left(1 - \frac{C_l\gamma_l}{C_s\gamma_s}\right) \tag{10.22}$$

and the ratio of $\Delta a/a_s$ becomes

$$\Delta a/a_s = \frac{C_s\gamma_s\left(1 - \frac{C_l\gamma_l}{C_s\gamma_s}\right)}{C_s\gamma_s}. \tag{10.23}$$

3. Discussion and Comparison of Mass Fluxes at Zero Driving Force

The data in Fig. 29 show considerable scatter and it is not possible to draw definite lines for the two separate Reynolds numbers or for the concentration and activity lines. All fluxes seem to be of the same order of magnitude regardless of the value of the fractional driving force. However, there is a slight trend that the N_A decreases as the fractional ΔC decreases but not as large a decrease as indicated by equation 10.15. It should be noted that the data for a Reynolds number of 6.4×10^4 are in the hump region (Fig. 18) and are in the steep portion of the slope. This is probably why the flux N_A in Fig. 29 varies over a 3-fold range and obscures the true trend in Fig. 29.

It appears that at zero driving force a finite flux is obtained regardless of the scatter of the data. This value of N_A at zero driving force is approximately 1.5×10^{-4}. It is apparent from Fig. 29 that using activities rather than concentrations for the driving force that a similar value of N_A at zero driving force is obtained.

Steele and Geankoplis[22] using benzoic acid (Fig. 29) also obtained a finite flux at zero driving force which was about 1/10 the value given above. However, they[22] did not have activity data available. They state that the finite flux at zero driving force may result from physical attrition from the sphere due to the differences in dissolution and deposition rates of the solute from and to the sphere. Another interpretation could be that the crystals deposited on the sphere surface would be less dense and would tend to grow at activated

sites. Whereas, dissolution rates would depend upon other factors such as surface activation, itself a function of hardness, and lattice energy and the hydrodynamical conditions at the sphere.

There are definite fluxes at zero driving forces whereas equations 10.14 and 10.15 indicate the flux should be zero at this condition. The probable reasons for the finite flux at zero driving force result mainly from physical phenomena which are not reflected by the fundamental equations 10.14 and 10.15 used to calculate the flux from the sphere. These factors are primarily a result of hydrodynamical conditions which exist at the sphere under forced convection conditions. The hydrodynamical conditions of either laminar or turbulent flow allow an exchange of energy and mass to occur at the solid surface. This means true thermodynamic equilibrium is not reached at saturation. The flow in the wake of the sphere would by eddy motion attack the surface irregardless of the value of ΔC. However, radial diffusion exists with crystals isolated in saturated solutions by mass movement from the crystal to the solution and from the solution to the crystal or other isolated areas. The principle may be stated that mass is conserved for the entire uranium-cadmium solution in the loop including the walls of tanks, pipes, and vessels. The argument of the conservation of mass based upon individual flux rates from and to the uranium sphere is doubtful under the saturated condition of uranium in molten cadmium. This would be true under the conditions of forced convection.

The factors listed in Table I of Chapter III become very important in highly turbulent flow in a high temperature system. These have been discussed elsewhere as to their probable action as a result of turbulence and dissolution. Turbulence exists in a forced convection system even though the driving force for mass transfer is zero.

It was shown that neither the activity driving force, which should hold if true thermodynamic equilibrium existed, nor the physical attrition from the sphere, since uranium was harder than the organic solutes, could account for the finite fluxes at zero driving force. The reasons for the finite flux at zero driving force cannot, therefore, be attributed to these factors of activity nor hardness of solute. The other suggested source could result from the pitting and erosion at the sphere at the high velocities. However, it is doubtful if these mechanisms exist at the low velocities where the concentration was varied at a Reynolds number of 733. It may be concluded that also other factors besides the ones mentioned by Steele and Geankoplis[22] or those discussed in this report may cause this finite mass flux at zero driving force.

XI. CONCLUSIONS

A. General Summary of Results

The original objectives of the mass transfer study in the uranium-cadmium system were to determine the effects of such variables as velocity, temperature, and concentration driving force on the mass transfer of single, solid uranium spheres to the molten cadmium. The experimental program developed to the extent that the possibility of exploring other variables resulted as a consequence of the experimental techniques needed to obtain essential information from the test samples. For example, the techniques of wetting brought about the possibility of determining the effect of ultrasonics on mass transfer in liquid metals. Fabrication techniques obtained in producing uranium spheres allowed the effects of surface area variation to be investigated.

Generally, the main objectives of the study were accomplished as regards the effects of velocity and temperature on the mass transfer coefficient. The variation of velocity over a large Reynolds number range (10^2 to 5×10^5) allowed the correlations of the mass transfer data to be more accurately established than previously possible by using a high density solvent, i.e., a liquid metal. It was observed that the velocity effect upon mass transfer in liquid metals was similar to that found by previous investigators in other systems.[3,4,22] Other investigators did not investigate a sufficiently high enough Reynolds number range to obtain its effect on the mass transfer coefficient. Sufficient information was obtained by varying the temperature of the system to allow the exponent on the Schmidt number to be determined. The exponent on the Schmidt number was found to be approximately 0.60 instead of the conventionally used 0.666 in the Chilton-Colburn J_d factor equation. The value of 0.58 was chosen after the Gaffney and Drew correlation.[2] However, most of the data were correlated with the 0.666 exponent in order to test the Colburn analogy and draw conclusions of the comparison of liquid metal data with the data for other systems.

B. Detailed Conclusions

The analysis of the slopes of the J_d versus Reynolds number lines yielded conclusive information for comparison of the mass transfer from uranium spheres to cadmium with the mass transfer in aqueous and organic systems. The slopes of 0.35 to 0.6 for organics in the low Reynolds range less than 3×10^3 compared favorably with the slope of 0.575 for the uranium cadmium system. Most previous investigators found that the mass transfer coefficient varied with the Reynolds number to the 0.5 power in the laminar region. The increases in the slopes of the J_d or k_l lines as the Reynolds number increased were also similar for the uranium-cadmium and the organic systems. The increase in the slopes as the Reynolds number increases may be interpreted to indicate the shift from laminar diffusion to turbulent diffusion. This is logical since the thickness of the laminar layer decreases with the increase in the Reynolds number and turbulent flow with

some eddy penetration to the solid surface occurs. The slope of the J_d versus Reynolds number curve in the highest Reynolds number range above 10^5 was not determined with any precisness since the slope of the curve could be either flat or slightly negative. The order of magnitude of 1 for the exponent on V_s if the curve was flat compared favorably with the value of 0.83 obtained by most investigators.[39,63,4] The effect of diameter of the various spheres showed little effect on the mass transfer coefficient for the 1/2 inch and 3/8 inch spheres. The J_d values for 3/8 inch and 1/4 inch spheres were different but were within experimental error for the J_d correlation of the 1/2 inch spheres.

The variation of the concentration driving force for mass transfer indicated that there was a finite mass flux at zero driving force. Steele and Geankoplis[22] also found the same effect for benzoic acid. The activity driving force plot did not change the mass fluxes at zero driving force to any significant extent. These mass fluxes for the above comparison were calculated based upon actual experimental measurements of weight loss from the sphere. It was concluded that the reasons for the finite flux rates at zero driving force were the results of factors not measured and resulting from pitting and erosion, mechanical effects of the molten cadmium on the solid uranium under forced flow conditions, and absence of thermodynamic equilibrium at saturation. Steele and Geankoplis[22] attempted to explain the finite flux in terms of differences in dissolution and crystallization at the solid surface. They did not attempt to determine the effect of activity driving force on the flux since the activity data were not available. Neither their work nor the present work gave conclusive evidence of the reasons for the finite flux rate at zero driving force.

The effects of using chemically wetted spheres and physically wetted or ultrasonically wetted spheres were small. The J_d values for ultrasonically wet spheres were slightly lower than for chemically wet spheres but this difference was almost within the experimental error.

The uranium that was heat treated yielded randomized orientations and relatively smaller grain sizes. The J_d values were 2 to 5 times higher at the same Reynolds number for the randomized spheres as opposed to the J_d for the nonrandomized spheres. The differences in J_d for the different types of spheres were attributed to the differences in dissolution for the different grain structures brought about by the heat treatment of the uranium. The smaller grains would offer more surface area.

The variation of the temperature of the molten cadmium changed the Schmidt number for molten cadmium by about 2 fold. This allowed the exponent to be determined on the Schmidt number for molten cadmium by a plot of $1/k_1/V_s$ versus the Schmidt number at a constant Reynolds number. The exponent was found to be 0.60 at a Reynolds number of 115 and 0.58 at a Reynolds number of 735. This was in the order of magnitude of

the exponent suggested by Bonilla,[3] 0.58 for liquid metal mass transfer in a packed bed of lead shot dissolving in mercury and also the value of 0.58 obtained by Gaffney and Drew.[2]

The skin friction, f/2, for spheres in organic liquids from Reynolds numbers of 10^2 to 10^3 and at a separate Reynolds number of 1.56×10^5 was 2 to 3 times greater than the J_d for uranium-cadmium. However, the skin friction and J_d for spheres in organic systems seemed to show reasonable agreement.

The roughened sphere provided very essential information for the qualitative comparison of the "tripping mechanism" to the early onset of turbulence and turbulent mass transfer. The greater value of J_d at a Reynolds number of 8.8×10^3 showed that the increase of J_d in the region of the hump could result from a "tripping mechanism." The "tripping mechanism" for the originally smooth sphere would result from the occurrence of pitting, erosion, partial dissolution, and the dissolution around inclusions in the surface of the solid. The "tripping" phenomena was explained in Chapter X of this report.

The uranium-cadmium mass transfer study presented fundamental information as regards the nature of the mass transfer coefficient under forced convection conditions. Prior to this work, the study of mass transfer had been limited for liquid metal systems. Most of the work which had been done was concerned with the heat transfer coefficient for liquid metals flowing over tubes, plates, or over tube banks for nuclear reactor applications. As mentioned earlier, corrosion and mass transfer create complex problems in the coolant paths of reactors and a knowledge of the mass transfer equations which are needed for design and of the mass transfer coefficient provides very essential information for design engineers and scientists. For example, the employment of conventional mass transfer equations for liquid metal systems was somewhat questionable since other investigators[42,43] had found that heat transfer equations had to be modified for liquid metals to account for the low Prandtl numbers ($N_{Pr} \ll 1$) encountered.

The fundamental mass transfer data for the variation of the mass transfer coefficient with velocity from low to very high Reynolds numbers of 100 to 5×10^5 provided for the first time evidence that conventional mass equations could be used for liquid metal systems over a large Reynolds range. Using the uranium-cadmium system as a reference, the mass transfer data for other liquid metal systems may be estimated in this Reynolds number range.

XII. RECOMMENDATIONS FOR FURTHER WORK

A. Introduction

This chapter includes the possible areas of research which can be explored with the dynamic loop. The following major study areas shall be discussed:

(1) the extension of mass transfer studies with the dynamic loop;

(2) the possibilities of a separate heat, and a combined heat and mass transfer study. The essential ideas and probable variables which should be studied will be discussed. Further experimentation in the areas of mass and heat transfer with the uranium cadmium system would seem naturally appropriate for the next stage of experimentation since the experimental equipment for the study should be available.

B. The Extension of Mass Transfer Studies with the Dynamic Loop

1. The Mass Transfer over Geometrical Arrays of Spheres

A natural extension of the mass transfer from single solid uranium spheres to molten cadmium would be to use clusters of spheres for the test sample. Most probably 3/8 inch and 1/4 inch spheres could be assembled on a mounting rod resembling triangular, cubical or rectangular, and cylindrical or rectilinear geometry. The triangular geometry could be arranged in two separate planes for test runs and would involve three or more spheres. The cubical array could be assembled from 4 spheres and mounted similar to the triangular array. The cylindrical array could be placed longitudinal with the flow with two or more spheres positioned immediately behind each other, or the position might be changed to crossflow with the array set crossways to the flowing metal.

The average J_d for each array could be correlated versus the Reynolds number. A separate parametric curve could result for each geometrical array. Other qualitative observations could be made with the effects of fluid flow on the test samples being investigated. Furthermore, local mass transfer coefficients could be taken over each sphere of the array; this might provide some insight into the mechanisms of pitting and erosion. Other variables might include the pitch between spheres and the difference between the local coefficients for different diameter spheres. Other variables might include the variation of uranium concentration in the cadmium and temperature of the system. The time of the experiment would have to be limited since the uranium would dissolve rapidly in the cadmium at the high flow rates.

2. The Mass Transfer over Cylinders and Plates for Liquid Metal Systems

Some work has been conducted in heat transfer for molten metals flowing over tubes and tube banks. It would be advantageous to investigate the mass transfer from single uranium cylinders as well as geometrical arrays of cylinders to flowing cadmium streams. The cylinders could be positioned crossways and longitudinal to the flowing cadmium as before. The data could be taken and treated as described above.

Plates provide an interesting geometry for a mass transfer study since they afford the possibility of a boundary layer study as regards mass transfer in liquid metals. The study of a laminar boundary layer had received considerable attention in aqueous and organic systems. Little work has been done for the mass transfer boundary layer in laminar flow for liquid metals. The experimental equipment, however, provides a means of investigating highly turbulent flow and the turbulent boundary layer. In laminar flow or turbulent flow, the universal velocity profile of Nikuradse could be assumed to apply as well as the conventional equations of motion derived for a flat plate. For turbulent flow with the uranium-cadmium system there is the further possibility with plates that the effect of high mass fluxes on the mass transfer coefficient could be detected. A study with plates would be theoretical and might include measurements of the velocity profile in the dynamic loop and over the plate. This experimental profile could be compared with the profiles calculated from solving the boundary layer equations over the plate. Such a study might show the similarity or the differences between theoretical predictions and experimental measurements for liquid metal systems. This might enable engineers to predict data for other liquid metal systems.

3. Liquid Metal Mass Transfer in a Packed Bed

a. Packed Bed of Spheres

The mass transfer from a packed bed of 3/8 inch and 1/4 inch uranium spheres or cylinders could provide practical information for engineers. The semi-empirical equations could again be applied to correlate the data. The Colburn equation for a packed bed of metal spheres could be modified to account for bed porosity and tested to determine the value of the exponent on the Schmidt number. The variables to be studied would include mass flux, bed length, geometry of packing, temperature of the system, and velocity of the molten cadmium, and pressure drop across the bed. The mass flux could be correlated as a function of the Reynolds numbers for each condition listed above. The pressure drop could be determined experimentally over packed beds of spheres which would not dissolve in the molten metal for each of the variables listed such as packing, diameter of pellet in the bed. The pressure drop obtained under these conditions could be compared with the pressure drop from beds of dissolving spheres.

b. Frequency Response Measurements in Packed Beds

The effects of disturbing the concentration profile of the flowing metal entering the bed to that leaving the bed by the mixing effects in the bed could be investigated. The equations of continuity and motion could be formulated to account for the percentage voids in the bed, with the introduction of a mixing diffusion coefficient D_1. The effects of velocity and pressure drop in the bed upon D_1 could be determined. A radioactive tracer could be used to detect the solute concentration in the flowing metal. A count rate meter could be employed at the inlet and exit or moved along the longitudinal axis of the bed to measure the concentration profile.

C. Proposed Recommendations Based upon This Study

1. Interface Study of Concentration Profile

An important contribution could be made to the mass transfer theory if the concentration profile could be obtained in the immediate vicinity of the solid uranium-cadmium interface. Using a research tool such as the electron microprobe analyzer, the point concentration values of the cadmium which had diffused in and along the individual grain boundaries at the interface could be obtained. The possibilities of chemical reactions between solute and solvent for any general system could be established by a similar investigation. The local or point concentration values could be compared with the reported equilibrium values of the phase diagram to see if true thermodynamic equilibrium was approached.

2. Study of Individual Mass Fluxes from and to the Sphere

It was assumed based upon this study that neither the activity data nor physical attrition could account for the finite flux at zero driving force. However, an investigation was not made of the individual fluxes from and to the sphere. The flux rate may be considered as composed of the difference between the individual flux which diffuses from the solid surface and that which returns to the surface.

It is recommended that the individual fluxes be studied in a similar mass transfer experiment under flowing conditions retaining similar geometry and boundary conditions. In such a study employing liquid metals, the individual fluxes would be obtained using a radioactive tracer to isolate the one of the two fluxes. Radioactive uranium could be added to the cadmium and the analysis of the normal uranium sphere after a mass transfer run would indicate a reverse flux. Conversely, if desired the uranium sphere could be made radioactive and the cadmium analyzed for this.

This would help determine if the individual flux rates are different and also their value at zero driving force. At zero driving force, the individual differences could be compared with the extrapolated values of Steele and Geankoplis[22] and those of this work.

XIII. ACKNOWLEDGMENTS

The writer should like to express his appreciation for the opportunity to conduct full time research on an off-campus thesis appointment at the Argonne National Laboratory, Argonne, Illinois. The scope and magnitude of the problem was of such a nature that its successful completion could only be accomplished where sufficient technology, interest, and funds for experimental equipment were available. The experiences and association of the writer with the highly trained professional and scientific staff, and the availability of research equipment, tools, and techniques in the various laboratories certainly contributed to the success of the dissertation.

The writer expresses special acknowledgment and appreciation to the following individuals for their kindly guidance and assistance during the experimental program: Robert Lux of Central Shops, Argonne, for his kind assistance in the coordination of the equipment fabrication; S. V. Smith and Bernard Fortier of Central Shops for their patience and assistance in generating the uranium spheres for the experimental program; Lowell Lloyd and Lubomir Nowicki of the Metallurgy Division, Argonne, for their assistance in the heat treating studies with the uranium spheres; Ed Sowa of the Reactor Engineering Division, Argonne, for providing the ultrasonic equipment needed in the experimental program; Bill Strickland and Harry Smith of the Drafting Section, Chemical Engineering Division, for their help in the mechanical design of the detailed components of the dynamic loop; Dr. David Miller of The International Institute, Argonne, for his consultation; John Hepperly, who assisted the author in the experimental program; all the members of the Semi-Works High Temperature Group of the Chemical Engineering Division for their helpful criticism and guidance; special acknowledgment to Dr. R. D. Pierce and Dr. Leslie Burris, who assisted and consulted with the author during the experimental program.

Finally, I should like to express personal appreciation to my University advisers, Dr. C. J. Geankoplis and Dr. C. E. Dryden, for their initial direction, planning, and criticism of the research problem and their acceptance of the results of this study.

XIV. BIBLIOGRAPHY

1. Hesson, J. C., Rogers, G., ANL-6477, p. 69 (December 1961).
2. Gaffney, B. J., Drew, T. B., Ind. Eng. Chem. 42, 1120 (1950).
3. Dunn, W. E., Bonilla, C. E., Ferstenberg, C. A., A. I. Ch. E. Journal, 2, 184 (1956).
4. Steinberger, Treybal, A. I. Ch. E. Journal, 6, 227 (1960).
5. Johnson, I., Feder, H., Trans. Am. Inst. Mining Met. Engr., 224, 468 (1962).
6. Nornst, Z., Physikal. Chem., 35, 283 (1900).
7. Whitman, W. G., Chem. Met. Eng., 29, 146 (1923).
8. Higbie, R., Trans. Amer. Inst. Chem. Engr., 31, 365 (1935).
9. Danckwerts, P. V., Ind. Engr. Chem., 43, 1460 (1951).
10. Danckwerts, P. V., Kennedy, A. M., Trans. Inst. Chem. Engrs., London, 32, 549 (1954).
11. Hanratty, T. J., A. I. Ch. E. Journal, 2, 359 (1956).
12. Harriott, P., Chem. Engr. Sci., 17, 149 (1962).
13. Tung, L. H., Drickamer, H. G., J. Chem. Phys., 20, 6 (1952).
14. Emmert, R. E., Pigford, R. L., Chem. Engr. Prog., 50, 87 (1954).
15. Davies, J., Phy. and Colloid Chem., 54, 185 (1950).
16. Scott, E. J., Drickamer, H. G., J. Chem. Phys., 19, 1075 (1951).
17. Garner, F. H., Grafton, R. W., Proc. Roy. Soc. A., 224, 64 (1954).
18. Friedlander, S. K., A. I. Ch. E. Journal, 3, 43 (1957).
19. Kronig, R., Bruijsten, J., Applied Sci. Research, A2, 439 (1949-1951).
20. Sherwood, T. K., Ryan, J. M., Chem. Engr. Sci., 11, 81 (1959).
21. Deissler, R. G., NACA 1210, 69 (1955).
22. Steele, L. R., Geankoplis, C. J., A. I. Ch. E. Journal, 178 (1959).
23. Epstein, L. F., Chem. Engr. Prog. Symp. Series 53, No. 20, 67 (1957).
24. Manly, W. D., ORNL-2055 (1956).
25. Hoffman, E. E., Janseh, D. H., "Lithium Symposium Analytical Proceedings and High Temperature Corrosion," ORNL-CF-57-10-6, (January 1958).
26. Ward, A. G., Taylor, J. W., J. Inst. Metals 85., No. 4 145-152 (1956).
27. Stevenson, D. A., Wolff, J., Trans. Met. Soc., A.I.M.E., 221, 279 (1961).

28. Lommel, J. M., Chalmers, B., Trans. Met. Soc., A.I.M.E., 215, 499 (1959).

29. Sherwood, T. K., and Pigford, R. L., "Absorption and Extraction," McGraw-Hill Book, Co., Inc., New York, 74 (1952).

30. Froessling, N., Gerlands, B., Geophysics 32, 170 (1938).

31. Powell, R. W., Proc. Brit. Assoc. Refrig. 36, 61 (1939-40).

32. Houghton, H. G., Radford, W. H., Mass. Inst. Technol. and Woods Hole Oceanographic Inst., Meterol., 6, No. 3 (Oct. 1938).

33. Mathers, W. G., Madden, A. J., Piret, E. L., Ind. Engr. Chem., 49, 961 (1957).

34. Maisel, D. S., Sherwood, T. K., Chem. Engr. Prog. 46, 131 (1950).

35. Kramers, H. A., Physica, 12, 61 (1946).

36. Garner, F. H., Suckling, R. D., A. I. Ch. E. Journal, 4, 114 (1958).

37. Gates, R. P., Shanks, R. S. M., Thesis, Mass. Inst. Technol., Cambridge (1949).

38. Hsu, N. T., Sato, K., Sage, B. H., Ind. Engr. Chem., 46, 870 (1954).

39. Linton, W. H., Sherwood, T. K., Chem. Engr. Progr., 46, 258 (1950).

40. Gill, W. N., Vanek, R. P., Jelinck, R. V., Grove, C. S., Jr., A. I. Ch. E. Journal, 6, 139 (1960).

41. Treybal, R. E., "Mass Transfer Operations," McGraw-Hill Book Co., Inc., New York (1955).

42. Lyon, R. N., "Liquid Metals Handbook," 2nd ed., U.S. Gov. Printing Office, Washington, 1952.

43. Lubarsky, B., Kaufman, S. J., NACA-TN-3336 (1955).

44. DeKany, John P., Lavendel, H. W., Burris, L. Jr., "Studies of Corrosion by Molten Zinc and Cadmium Systems," ANL-6243 (1960).

45. Tuve, G. L., Sprinkel, R. E., "Orifice Discharge Coefficients for Viscous Liquids," Instrs., 6, 201 (1933); 8, 202 (1935).

46. Affel, R. G., Burger, G. H., Pidgeon, R. E., ORNL-2792, 27 (1950).

47. Chiswik, H. H., and Lloyd, L. T., ANL-5777 (Nov. 1959).

48. Mueller, M. H., AECD-4208 (May 1954).

49. Benzing, David, University of Detroit, private communication.

50. Pierce, R. D., "Stability of Cadmium-Magnesium-Uranium Solutions for Reduction Equipment," ANL-6145 (March 1960).

51. Adams, M. D., "Effects of Stainless Steel Constituents on Uranium Behavior in Liquid Cadmium," ANL-6101, pp. 45-48 (Dec. 1959).

52. Sutherland, W., Phil. Mag., 9, 781 (1905).

53. Moelwyn-Hughes, E. A., "Kinetics of Reactions in Solution," (2d ed.), Clarendon Press, Oxford, pp. 365-367 (1957).

54. Carlson, C. M., Eyring, H., Ree, Taikyue, Proc. National Acad. Sci. (U.S.), 46, No. 5, 649 (May 1960).

55. Drew, T. B., "Advances in Chemical Engineering," McGraw-Hill Book Co., Inc., New York, 2, 196 (1960).

56. Glasstone, Samuel, "Textbook of Physical Chemistry," (2d ed.), D. Van Nostrand Co., New York, (1946).

57. Oldenburger, Rufus, "Mathematical Engineering Analysis," Macmillan Co., New York, (1950).

58. Den Hartog, J. P., "Mechanical Vibrations," (4th ed.), Mc-Graw-Hill Book Co., Inc., New York (1956).

59. Hansen, H. M., Chenea, Paul F., "Mechanics of Vibration," John Wiley and Sons, Inc., New York (1952).

60. Thomson, W. T., "Mechanical Vibrations," (2d ed.), Prentice-Hall, Inc., Englewood Cliffs, N. J. (1953).

61. Timoshenko, S., "Vibration Problems in Engineering," (1st ed.), D. Van Nostrand Co., Inc., Princeton, N. J., (1928).

62. Rostoker, W., "Embrittlement by Liquid Metals," Reinhold Publishers Corp., New York, p. 21 (1960).

63. Gilliland, E. R., Sherwood, T. K., Ind. Engr. Chem., 26, 516 (1934).

64. Johnstone, H. F., Pigford, R. L., Chapin, J. H., Trans. Am. Inst. Chem. Engrs., 37, 25 (1941).

65. Larsen, R. P., Anal. Chem., 31, 545 (1959).

66. Francois, C. A., Anal. Chem., 30, 50 (1958).

67. Maeck, W. J., Booman, Glenn L., Elliott, Maxine C., Rein, James E., Anal. Chem., 31, 1139 (1959).

68. Lommel, J. M., Chalmers, B., Trans. Am. Inst. Mining Met.Engrs., 215, 499 (1959).

69. Parkman, M. F., AD 259-882, SRI Project 1745 (1960).

70. Craighead, C. M., Cawthorne, E. W., Jaffee, R. I., Trans. Amer. Instr. Min. Met.Engr., 203, 81 (1955).

71. Foust, A. S., Wenzel, L. A., Clump, C. W., Maus, L., Anderson, L. B., "Principles of Unit Operations," John Wiley and Sons, New York (1960).

72. Perry, J. H., "Chemical Engineers' Handbook," (3rd ed.), McGraw-Hill Book Co., Inc., New York Section 8, (1950).

73. Sherwood and Reed, "Absorption and Extraction," McGraw-Hill Book Co., Inc., New York (1952).

74. Grace and Derge, "Diffusion in Sn and Sn-Pb Alloys," Trans. A.I.M.E. Journal of Metals (1955).

75. Perry, J. H., "Chemical Engineers' Handbook," (3rd ed.), McGraw-Hill Book Co., Inc., New York Section 8, (1950).

76. Tang, Y. S., Duncan, J. M., Schweyer, H. E., "Heat and Momentum Transfer between a Spherical Particle and Air Streams," NACA-TN-2867, University of Florida (March 1953).

77. Knudsen, J. B., Katz, D. L., "Fluid Dynamics and Heat Transfer," McGraw-Hill Book Co., Inc., New York, p. 315 (1958).

78. Shapiro, Ascher H., "The Fluid Mechanics of Drag," Doubleday and Company, Inc., Garden City, New York (1961).

79. Linton, M., Sutherland, K. L., Chem. Engr. Sci., 112, 214 (1959).

80. Hootman, Harry, Argonne National Laboratory, private communciation (1962).

81. Martin, A., and Johnson, I., "Chemical Engineering Division Summary Report," ANL-6068, 78 (1959).

82. Toor, H. L., Marchello, J. M., A. I. Ch. E. Journal, 4, 97 (1958).

83. Sherwood, T. K., Ind. Engr. Chem., 42, 2077 (1950).

XV. APPENDIX: EQUIPMENT FOR MASS TRANSFER STUDY OF URANIUM IN MOLTEN CADMIUM

A. Equipment Requirements

The major equipment requirements were (1) the achievement of sufficient velocities of cadmium to enable investigations of mass transfer rates at Reynolds numbers of 100 to 100,000, (2) the production of a typical flow pattern past a sphere, and (3) the ability to change operating temperatures sufficiently to effect as large a change as practical in the Schmidt number. Because this was an extension of other work by Geankoplis and Steele,[22] the diameter of the sphere for this mass transfer study was made the same as in their work, i.e., one-half inch. The 1.5 inch ID pipe used by Geankoplis and Steele was also employed in this study, thus keeping the same geometry. This enables direct comparison of the experimental results of the two systems which have widely different physical properties.

The design of specific loop components evolved from technical and practical considerations of the above requirements. The choice of the specific system, i.e., uranium-cadmium, the extension of Reynolds numbers to a magnitude of 10^5, and the experimental study which was to be conducted in the vicinity of 500°C helped firm up the general process design stipulations such as the following:

a. motor and drive assembly for pumping cadmium at high flow rates;

b. detection device or system to determine the velocity of the molten cadmium;

c. design of significant length to overcome hydrodynamic entrance effects;

d. choice and location of heating circuits for the dynamic loop;

e. size and general location of tanks, loop conduit, and sampling system; and

f. sufficient instrumentation to facilitate necessary operation and to conduct precise experimentation for the objectives of the mass transfer study including:
   (1) valves for penumatic and liquid operation,
   (2) thermocouples,
   (3) heating units, controllers and variacs,
   (4) liquid level instrumentation,
   (5) temperature and flow recorders,
   (6) vacuum and inert gas instrumentation.

B. Overall Function of Loop and Process Description

A schematic diagram of the dynamic loop for mass transfer studies is shown in Fig. 2 of Chapter V, and a photograph of the bare uninsulated loop in Fig. 30. Clearly shown in both the photograph and line drawing are the location of the major components: (1) the loop proper, (2) pump and its reservoir tank, (3) charge tank, and (4) the reservoir or surge vessel. Another major component, the sample port or sample introduction and withdrawal mechanism cannot be seen in this photograph.

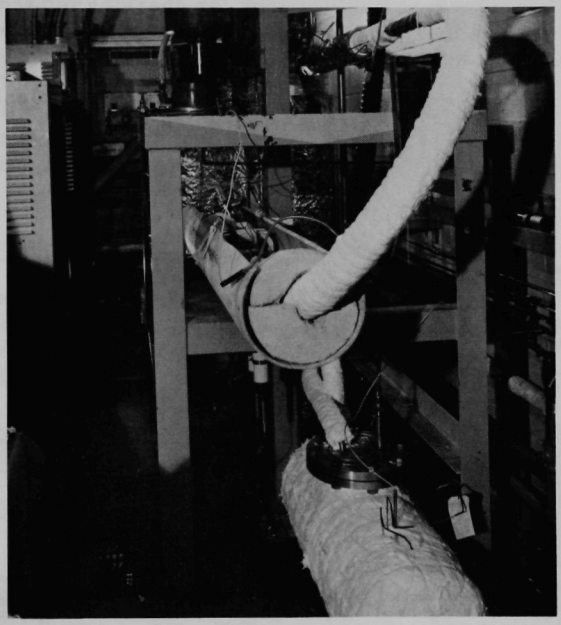

108-5061

Fig. 30. Dynamic Loop for Mass Transfer Studies near Completion

Figure 31 is a detailed schematic layout of the loop and its auxiliary components. A description of the major components and their functions in the loop system are as follows:

1) Loop--1.5-inch, Schedule 80 SS-304 pipe which functions as a conduit for the molten cadmium;

2) Pump--5 HP mechanical pump of the centrifugal type manufactured by the Ruthman Machinery Co. which was vertically mounted in the pump reservoir;

3) Pump tank--a 16-inch diameter SS 304 tank for housing the pump and containing an adequate supply of cadmium for maintenance of the required flows;

4) Surge reservoir--a 6-inch SS tank for receiving the discharging cadmium and for providing an adequate volume for gas disengagement before return of the cadmium to the pump tank;

5) Sample port--a pipe attached to the reservoir tank for insertion and removal of uranium spheres;

6) Charge tank--a 52-liter tank for charging molten cadmium by pressure into the experimental system and into which the contents of the system could be drained; and

7) Auxiliary items--heater circuits, argon gas blanketing and vacuum systems, and thermocouple locations.

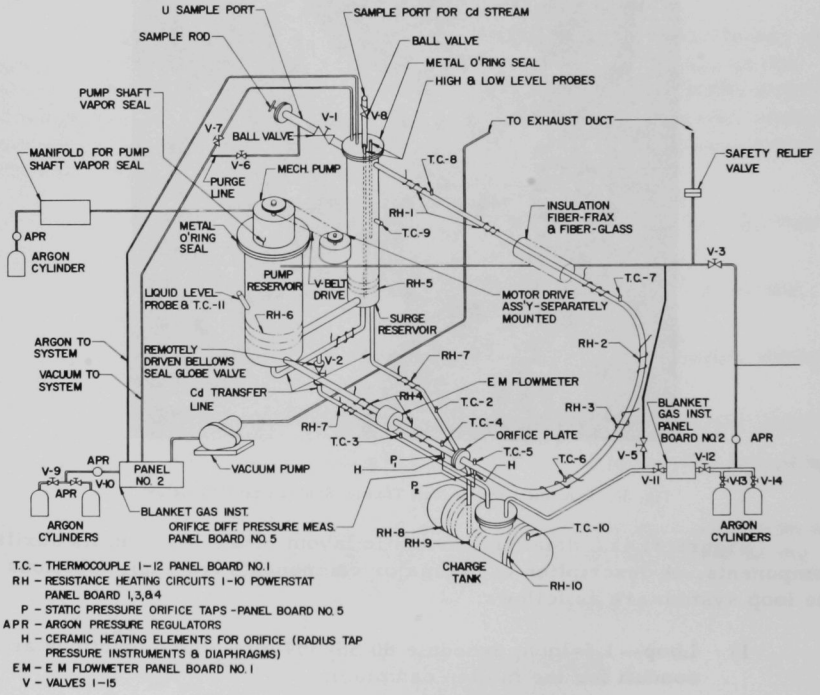

Fig. 31. Isometric Drawing of Dynamic Loop for Mass Transfer Studies

The loop was connected to the reservoir tank and pump tank. Cadmium was pumped from the pump tank through the loop and was returned to the pump tank by a 4-inch pipe which completed the connection between the two tanks. The motor drive assembly was separately mounted on a mounting plate supported by braces which extended to the solid concrete floor of the laboratory area.

Solid cadmium ingots were initially loaded in the charging vessel through its top flange. The cadmium was then melted by using heating circuits RH-8, RH-9, and RH-10, which were all rated at 6.5 kW capacity. The molten cadmium in the charging tank was then forced upwards through a transfer line into the surge reservoir by high pressure argon through valves V-11, V-12 and valves V-13 or V-14 depending upon which cylinder was used for this operation. The other cylinder which was not used for this operation was a sphere and allowed the cylinder charging procedure to occur without shutdown or without dumping the molten cadmium from the experimental system into the charging tank.

C. Discussion of Equipment and Service Requirements

In this section the discussion will include (1) the problems involved in the design of the dynamic loop, (2) major process items and loop components, (3) purchased equipment for the loop, (4) installation modifications, (5) and the instrumentation required for successful operation.

1. Problems Involved in Design of Dynamic Loop and Process Stipulations

a. Selection of Materials of Construction for Cadmium

A primary concern in considering a design of any container system involves the selection of materials of construction which will endure and resist corrosion attack, normal thermal cycling, and ease of fabrication.

Mild and 400 steels are not corroded significantly by cadmium up to 600°C.[44] Type 300 series stainless steels also offer good corrosion resistance, but leaching of nickel is possible from the 300 series steels.[44] However, Pierce and Adams[50,51] found that nickel leaching was nil up to temperatures of 600°C. It is necessary to use a stainless steel to avoid air oxidation to the exterior of the equipment at about 600°C. Therefore, Type 304 was chosen as the container material for the molten cadmium. All component parts such as the baffles and impeller drive assembly, orifice plates, metallic "O" rings for vapor seals at the flanges and ball valves were constructed of SS 304. Whenever welds were necessary, low carbon content welding rods of stainless 304 were used.

b. Special Seals for High Temperature Operation

Because of the high temperatures involved in this study, it was necessary to design the sealing flanges so that the molten cadmium and its vapors could be retained within the loop with essentially no leakage to the environment. Also, the sealing flanges had to be designed so as to withstand the system pressure at the operating temperatures. Metallic "O" rings fabricated from stainless steel 304 were used at all flanges exposed to molten cadmium. The vapor seal at the charging vessel was critical since the pressures used in charging the molten cadmium into the system were of the magnitude of 50 psig. This, too, was a stainless steel "O" ring, but extra precautions were taken in order to insure obtaining a leak-tight joint. Neoprene "O" rings were used in flanges which were at ambient or near ambient temperatures.

Because cadmium generally does not wet stainless steel, the opening of flanges could be accomplished with little difficulty. Wetting of stainless steel 304 with cadmium vapors presented no major problems.

2. Major Process Equipment Items

a. Charging Vessel

It was necessary to provide a means of charging molten cadmium to the experimental portion of the loop from a vessel in which solid cadmium ingots were initially melted. A decision to place the charging vessel at the lowest point of the experimental system allowed this vessel to function in a dual manner. It could be used for the initial charging operation and secondly, it served as a dump tank. In the event of an emergency situation in the loop above the charging vessel, the bellows sealed globe valve in the proper transfer line could be opened; this allowed the molten cadmium to drain to its initial position in the charging vessel. In the experimental stages of the program the bellows-seal globe valve failed. It was replaced by a section of straight pipe which was water-cooled such that it functioned as a freeze valve. On melting the contents of the freeze valve, the loop could be dumped, as before through the bellows valve, into the sump tank. This freeze valve functioned very satisfactorily throughout the duration of the work. It proved more reliable than the bellows valve, but had the disadvantage that the loop could not be dumped as quickly as through the bellows valve because of the delay occasioned by the necessity of melting the contents.

Design considerations included the following: (1) placing the charging vessel on casters to allow for thermal expansion in the transfer lines, (2) the design of a special flange and seal to allow for high pressure argon used in the charging operation at the charge tank, and (3) the introduction of a liquid metal level probe through the sealing flange to allow measurements of liquid level to be taken. These may be seen in Figs. 32, 34, and 41.

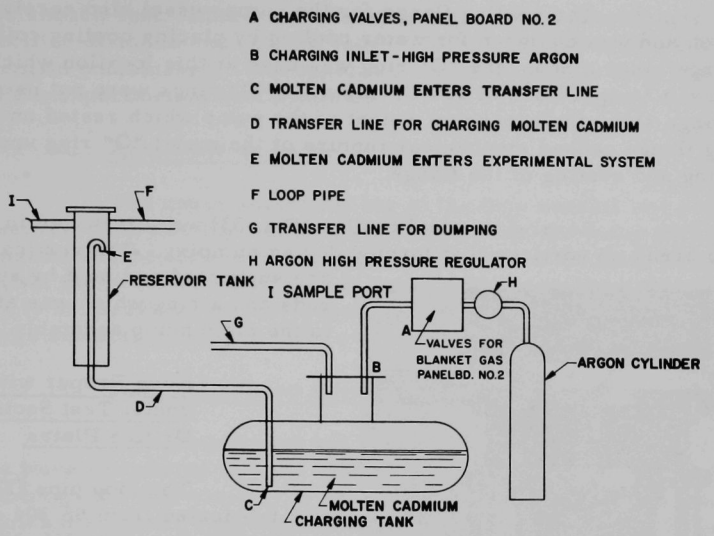

Fig. 32. Charging Process for Molten Cadmium

The charging vessel was designed using the well-known principle of operation of the acid-egg pump and is shown in Fig. 32. High pressure argon was allowed to flow through an argon pressure regulator into the charge tank. The high argon pressure forced molten cadmium upwards through the charging transfer line into the receiver tank as shown. The high pressure flange was designed according to conventional ASME boiler code and a stainless steel 304 metallic "O" ring was used for the seal at the flange. By operating valves at the panelboard, gas is allowed to enter at B and molten cadmium leaves at C flowing through the transfer line at D and finally exits at E. During charging (refer to Fig. 30) the bellows-sealed glove valve, V-2 (a freeze valve as described above) and vent valve V-5 were closed. Conversely, the dumping operation (refer to Fig. 31) consisted of opening V-2 and the vent valve at V-5 to allow for pressure equalization in the entire loop.

b. Pump Tank

The pump tank was fabricated to contain a 5 HP molten metal pump. This tank was rigidly fastened to the dynamic loop frame by bolting through a flanged plate which had been welded to the pump reservoir. This welded plate was 3/4 inch thick and in addition to providing support for the pump served as a heat transfer sink. The plate helped in conducting and radiating excessive heat that might be accumulated close to the pump shaft seal and bearings since some conduction along the walls of the pump tank and the shaft of the pump could not be avoided.

The sealing flange for the pump vessel also received close attention and was designed for water cooling by placing cooling coils around the flange since a neoprene "O" ring was used at this location which could not stand a temperature of 500°C. Metallic "O" rings were not used on this flange since the excessive weight of the pump which rested on the sealing flange caused mechanical rupture of the metal "O" ring upon mounting and seating of the flange.

Several vertical baffles (Fig. 33) were installed in the pump tank to break up vortices that formed during pumping. The vertical baffles are supported and held by support rods and a ring which was attached to the main pump assembly.

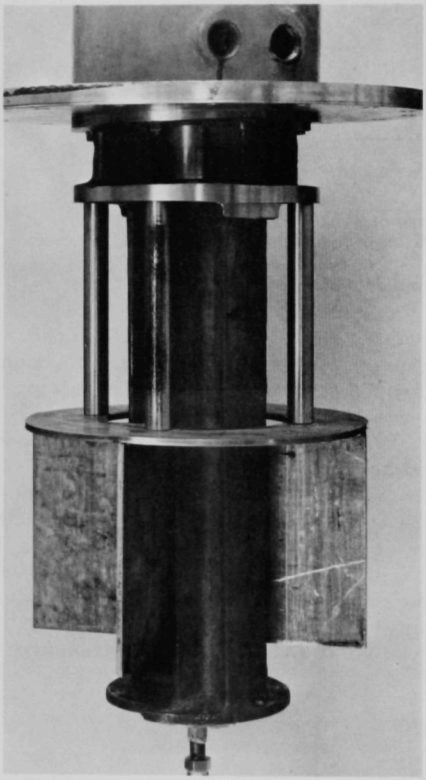

108-4947

Fig. 33. Baffle Plates for Molten Metal Pump

c. Loop Proper with Horizontal Test Section and Orifice Plates

The loop pipe (Fig. 30) was fabricated from SS 304 of 1.5 inch inside diameter, Schedule No. 80 pipe. The lower horizontal leg of the loop pipe contained bolting flanges with metal O-ring seals. One flange bolted to the exit of the pump tank. It was positioned concentrically around a sleeve insert that screwed into the pump discharge housing. The other flange served the purpose of positioning a square edge orifice plate for the measurement of flow rates of the molten cadmium. The loop conduit was doweled smooth for 5 diameters upstream from the upstream radius pressure tap at one side of the orifice, and also 2.5 diameters downstream from the orifice plate.

A radius bend through 180° directed the loop towards the reservoir tank into which the pumped cadmium discharges. Both lower and upper horizontal legs of the loop conduit were constructed 1-2 degrees from the horizontal to allow for proper draining upon dumping the molten cadmium. The upper horizontal leg was long enough to allow fully developed

flow, for about 7 feet. Immersion thermocouples were placed upstream of this specified distance and downstream of the test sample so that flow patterns remain undisturbed. The upper horizontal leg of the loop also constituted the experimental test section.

d. Reservoir or Surge Tank

The upper horizontal leg of the loop conduit was connected to a reservoir tank which provided surge volume for the pump tank as well as a separation zone for entrapped argon gas prior to entering the pump tank. Also, the reservoir tank was designed with a sampling port to allow samples to be inserted into the system and removed rapidly while prohibiting large amounts of oxygen from entering the system.

e. Sample Port and Reservoir Tank

The sample port and reservoir tank may be seen in Fig. 34. Samples were introduced into the system by utilizing a sampling rod which slides through the ball valve at G upon insertion of uranium spheres. There was a quick disconnect high vacuum coupling at J with an "O" ring seal at the flange. The flange was bolted and the sample rod held by clamps attached

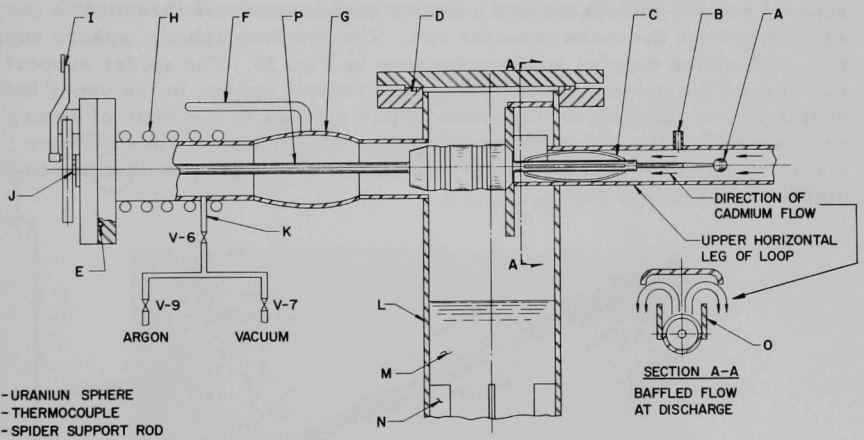

Fig. 34. Detail of Sample Port at Reservoir Tank

to the flange. The procedure for inserting and removing samples shall be discussed below:

The sample port was designed to allow uranium samples to be positioned in the experimental portion of the horizontal leg of the loop pipe. A ball valve (G, Fig. 34) was designed to allow uranium spheres to enter an inert atmosphere prior to injection into the high-temperature, experimental system. In order to insure that the upper horizontal leg of the loop pipe would remain completely filled with molten cadmium at the lowest pumping rates, a baffle was designed and placed at the end of the loop pipe as shown at section A-A, Fig. 34. Cooling coils (H, Fig. 34) were provided so that upon the completion of a mass transfer run when the uranium sphere was placed in this area, the cadmium film intact on the solid uranium surface could be rapidly solidified. This was accomplished by pulling the sample rod and uranium sphere through the high vacuum coupling (J, Fig. 34) until the uranium sphere was between the ball valve G and the flange at I. With the uranium sphere positioned in the cold zone between G and I, of Fig. 34, the high temperature, experimental system could be sealed from the cold zone by closing this valve.

A sample rod used for inserting and removing uranium test spheres was designed to mate the baffle (section A-A of Fig. 34). A support rod for the sphere and a spider support rod was threaded to the sample rod for the mass transfer run. The uranium sphere, sphere support rod, and spider support rod may be seen in Fig. 35. The spider support rod served the purpose of centering the uranium sphere in the upper horizontal pipe of the loop during a run. Four spiders in the form of an arc were welded to the rod at 90° such that the maximum distance between diametrically opposing arcs was 1 to 2 thousandths greater than the inside diameter of the loop pipe.

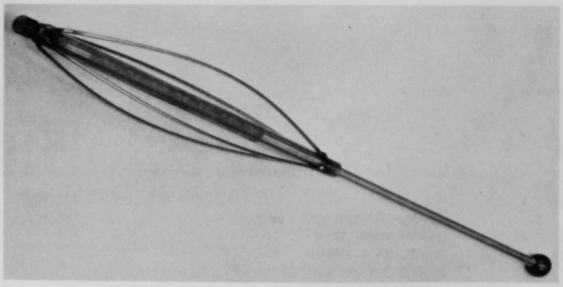

108-4229

Fig. 35. Uranium Sphere, Support Rod, and Spider Assembly

f. Orifice Plates

Orifice plates with hole diameters of 1/4, 1/2, 3/4, 1, and $1\frac{1}{4}$ inches were fabricated from stainless steel "O" rings by press fitting (through the application of heat), the orifice plate into a small recess cut into a metal oval. These orifice plates were placed in position by bolting mating flanges of the lower leg of the loop conduit which were grooved for the "O" ring. This was a metal (flange) to metal (oval and orifice) seal. The orifice and orifice plates were designed to conform to conventional recommendations[45] and a check of the orifice plates after 6 months of continuous service showed very little wear or abrasion. The orifice plate acted as a restriction to the flow of the molten cadmium and produced a pressure drop proportional to the square of the flow rate. In order to obtain pressure drop measurements across the orifice, volumetric pressure indicators and a differential pressure meter were purchased. Referring to Fig. 36 the pressure signals are transmitted from the cadmium system analogous to the cylinder through a stainless steel diaphragm to NaK which is a liquid at room temperature. The NaK actuates a pneumatically operated pressure sensing mechanism which is balanced against a 20 psi pressure-regulated air supply. The two output signals from the two pressure transmitters were fed into a differential pressure meter which was calibrated to read the correct pressure drop across the orifice plate in psi. Only one NaK pressure transmitter is shown in Fig. 36.

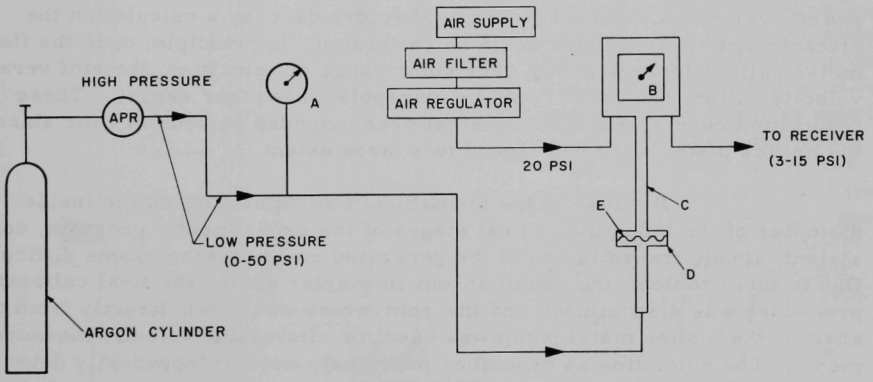

A. STANDARD TEST GAGE
B. VOLUMETRIC PRESSURE TRANSMITTER
C. NaK FILLED
D. CELL
E. DIAPHRAGM

Fig. 36. NaK Pressure Sensing Apparatus

Because of operating difficulties, the diaphragm in the volumetric cells failed, and an alternate pressure measuring system had to be installed.

In the alternate system, conventional pressure gauges were employed to measure the pressures at the orifice tops. Small cadmium dash pots (or volumetric cells) prevented cadmium from rising into gas-filled capillary tubing (1/8-inch OD) connected to the pneumatic pressure gauges. Because it was necessary to obtain the absolute pressure on either side of the orifice plate each gauge was calibrated in position in terms of a third pressure gauge. Absolute pressure differentials were then obtained by converting actual measurements to those of the reference gauge and taking the difference.

g. Electromagnetic Flowmeter

An electromagnetic flowmeter was initially employed to determine the velocity of the molten cadmium. The flowmeter was mounted on the lower leg of the loop conduit and the emf was taken from electrodes in the vertical plane while the magnetic field of the magnet was in the horizontal plane. The generated emf which was proportional to velocity was recorded on a chart recorder. Thermocouples were located on the magnet of the flowmeter to record temperature so that corrections could be applied to calibration curves. Using the pressure drop data across the orifice plate and the velocities obtained from the pressure data, by a calculation the electromagnetic flowmeter could be calibrated. In principle, once the flowmeter calibration was known over some range of velocities, the emf versus velocity calibration curve could be extrapolated to other ranges. These calibration curves remained constant over extended periods of time since the orifice plates were not eroded to a large extent.

Because of the formation of an oxide film on the inside diameter of the loop pipe in final stages of the experimental program, consistent, steady transmission of the generated emf presented some difficulty. Due to this problem, the use of an em flowmeter during the final calibration procedure was discontinued and the rpm which was taken directly from the shaft of the molten metal pump was used for alternative velocity measurements. The velocities as described previously were independently determined by calculations utilizing the pressure drops across a standard square-edge orifice.

3. Purchased Equipment for Dynamic Loop

a. Motor Drive Assembly

A Reeves varispeed meter rated at 440 volt, 3 phase, 5 hp and with a speed reduction of 8 to 1 was purchased to drive the molten

metal pump. The motor drive assembly was located on a mounting plate supported separately from the experimental equipment. Angle iron supports held the mounting plate and these were bolted to the 30-inch-thick concrete floor. It was found that using 3 different diameters of multiduty sheaves, coupled with the 8 to 1 speed reduction of the varispeed motor that the entire velocity range could be covered in the study. It was necessary, however, to throttle the pump at low velocities. A vibration reduction study is discussed for the motor drive assembly in Experimental Procedures.

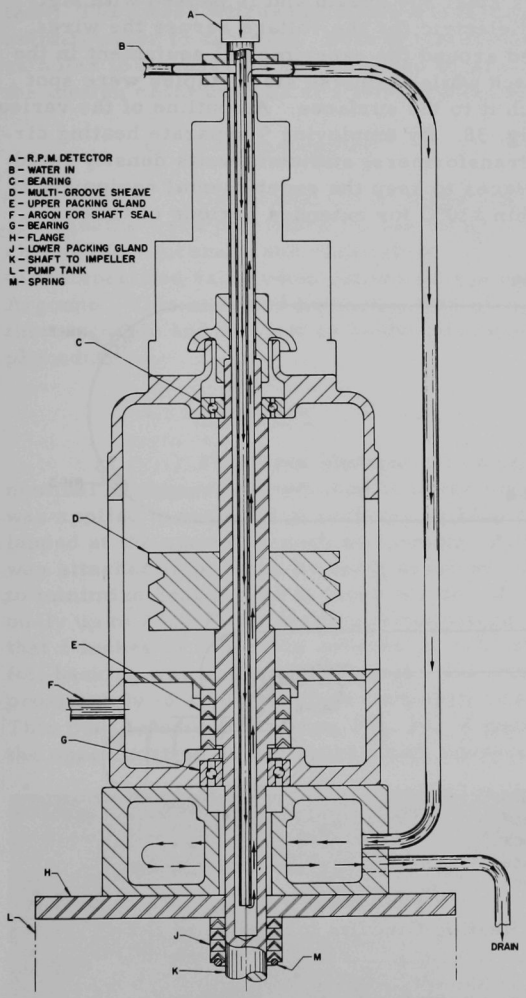

Fig. 37. Diagram of Water Cooled Shaft and High Temperature Vapor Seals

b. Molten Metal Pump

A Ruthman Gusher molten metal pump was purchased and rated at 1750 rpm at 80 gpm capacity. This pump was a mechanical, centrifugal type and was mounted vertically into the pump tank. Discharge from the pump was from the side of the impeller housing while suction into the impeller occurred from above and below the impeller housing. All parts of the pump which were exposed to the molten cadmium were fabricated from stainless steel 304. The lower bearing of the molten metal pump was cooled since the shaft of the pump was water cooled for this purpose. A schematic diagram of the water cooled shaft is shown in Fig. 37.

As indicated previously, the rpm of the molten metal pump was determined by using a tachometer which could be positioned on an extension to the shaft of the pump.

c. Resistance Heating Cable

Resistance heating wire with Nichrome leads was purchased to supply the heat to the experimental equipment. This cable consists of the conducting wire which makes a turn at the closed end of the cable and the lead wires which both protrude at one end of the cable. The conducting wire is enclosed in a stainless steel 304 sheath and is packed with MgO powder to provide sufficient dielectric for the voltage across the wires. The heating cable was wrapped around the experimental equipment in the form of a helix on a 2-inch pitch while stainless steel staples were spot welded over the cable to attach it to the surfaces. An outline of the various heater circuits is shown in Fig. 38. By employing 9 separate heating circuits and powerstat variable transformers, sufficient watts density could be supplied to the heating surfaces to keep the experimental equipment at steady-state temperature within ±10°C for extended periods of time.

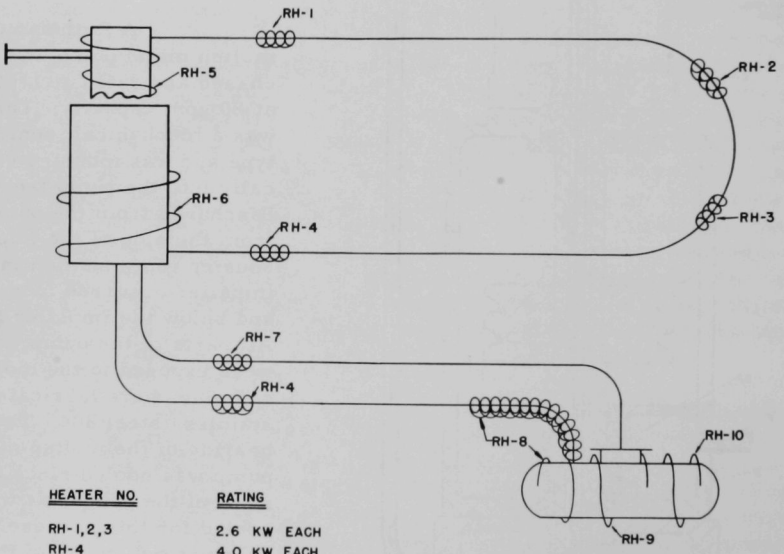

Fig. 38. Outline of Heating Circuits for Dynamic Loop

d. Ball Valves for Sampling Ports

Two ball valves were purchased. The ball valve, V-1, employed at the sample port was 3 inches in diameter with Teflon packing

as shown in Fig. 34 at G. Location of this valve at the sample port allowed the high temperature system to be isolated from the atmosphere when inserting or removing spheres. The valve, V-8, Fig. 31, was 3/4 inch in diameter and was located above the reservoir tank in a sampling tube. A high-temperature seal was utilized in this valve since samples of the molten cadmium were taken a few inches below the valve from within the reservoir tank. They were withdrawn above the valve where they then remained to solidify prior to analysis. Both of the valves V-1, and V-8 of Fig. 31 allowed samples to be inserted and removed from the experimental system while the molten cadmium was at a temperature of approximately 500°C.

e. Thermocouples

Calibrated Cr-Al thermocouples enclosed in stainless steel 304 sheaths were purchased for the loop. These thermocouples were rechecked for accuracy and calibration. They were found to be within ±1°C of the specified value when calibrated against a standard thermocouple at Argonne. This standard had been checked against a Bureau of Standards thermocouple and was set up in the laboratory for such calibration procedures.

f. Insulation

Fiberfrax alumina-silica ceramic blanket of 1/2 inch nominal thickness was obtained to cover the heating surfaces. The blanket was applied to the heating surfaces in 1/2-inch thick sections and was overlapped at the seams as each succeeding layer was applied. The blanket was attached in position by using asbestos cord and overlapped at the joints to minimize heat losses at these points. (Fiberfrax may be used continuously up to 2300°F; its melting temperature is around 3200°F.) It was found that 2 inches of Fiberfrax covered by 1/2 inch of fiberglass with aluminum foil backing was sufficient to reduce the heating losses to the surface approximately to a 50°C surface temperature on the outside of the insulation. This may be seen by viewing Fig. 39. Figure 39 shows a cross section of the upper portion of the figure which reveals the resistance heating cable,

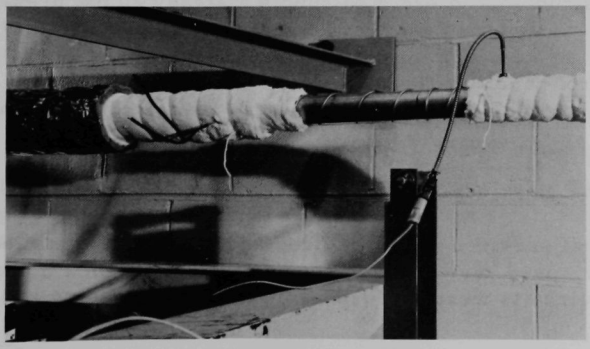

Fig. 39

Cross Section of Loop Pipe, Heating Cable, Insulation and Thermocouple

108-5062

Fiberfrax insulation and finally the fiberglass blanket. Immersion thermocouples are shown at the upper horizontal leg of the loop pipe.

g. Variable Powerstat Transformers

Eight transformers were required for the separate heating circuits. These transformers were either 220 volts or 440 volts depending upon the heating circuit and the component to be heated. The heating circuits on the pump tank, reservoir tank, and charge tank were 440 volts while the loop conduit and transfer lines operated on 220 volts. All transformers and heating circuits were properly fused to avoid circuit overload and power was shut off in case of heating element failures. The use of separate heating circuits allowed great flexibility in applying heat to the various surfaces. Once the various settings were known for the powerstats, the loop could be held isothermal for on-off controllers within ±1°C for considerable lengths of time.

h. Purity of Cadmium Used in Mass Transfer Study

The cadmium for the mass transfer study was purchased in solid billet rods of 1 inch diameter in lengths of 12 inches. The specification of cadmium purity was 99.95 percent; a typical spectrochemical analysis of the cadmium showed the various constituents and their percentage content in the cadmium. The constituents which were present in less than 0.01 percent were Al, B, Ba, Be, Bi, Ca, Co, Cr, Fe, Hg, Li, Mn, Mo, Na, Ni, Si, Sn, Ti, V, Zn, and Zr. The constituents which were present in less than 0.1 percent were As, P, Sr, and P. Faint traces were detected of Ag, Cu, Mg, Pb and a trace of Sb was detected. The analysis of cadmium was close to 99.9 percent.

4. Services for Dynamic Loop

a. Air

A separate air supply was needed for the volumetric and differential pressure instruments in order to supply a steady 20 psi pressure to the static heads. In order to supply this constant air bleed to the volumetric instruments, an air control panel was set up and an air line was installed. The control panel consisted of an air filter, valves, and a pressure regulator which could be adjusted to bleed in the air supply to the instruments.

b. Electrical Services

Electrical services were provided and a fuse box installed for the 5 hp Reeves varispeed meter which required 440 volts on a 3 phase circuit. The electrical circuits were all fused to prevent overloading and

short circuits. Also, the start, stop, and re-set button for the motor was wired through a 2 position key switch for safety purposes. Keys for the switching circuits were in the possession of operating personnel at all times when a run was not in progress. After a run was completed, the key could be removed from the switching circuit before the operator stepped on the sampling platform to remove the uranium sample from the experimental system. This provided an extra safety precaution and facilitated the sample changing process without endangering the personnel operating the loop.

c. Argon Supply for Blanket Gas

In order to avoid contamination in the system and possible creation of uranium and cadmium oxides as well as to avoid fires, the entire loop was kept under argon blanket gas. In addition, argon was used to pressurize molten cadmium during the charging operation into the experimental system. Normally, the argon blanket over the molten cadmium was kept at 5 psi except at the lowest pumping rates when the argon was increased on the system to increase head for the pump. At the highest pumping rate, a pressure of 15 psi was required on the reservoir tank to suppress the static head of molten cadmium collected there. Two cylinders were used in the supply system as shown in Fig. 32, valves V-13 and V-14. One cylinder served as a spare and could be turned on while the other cylinder was removed for refilling. The blanket gas could be turned on or off at the cylinders. The operations of charging, dumping, and making a run required operation from the general panel board. This allowed the operator some degree of protection since a leak of molten cadmium to the environment during a run could be stopped by the panelboard. This will be discussed elsewhere.

5. Instrumentation for the Dynamic Loop

a. Transformers and Controllers

Much of the instrumentation is shown on the general panelboard in Fig. 40. The variable powerstats with indicator dials for adjusting the power for the heater circuits are shown at the lower left and center of the panelboard. The dynamic loop could be held to within $\pm 1^{\circ}C$ of the experimental temperature by adjusting the requisite load for each circuit.

b. Automatic Timers

Automatic timers for the electrical system for the separate heating circuits of the dynamic loop are shown at the lower right of the panelboard. The timers serve the purpose of allowing power to be supplied to the loop at some selected time prior to the mass transfer runs.

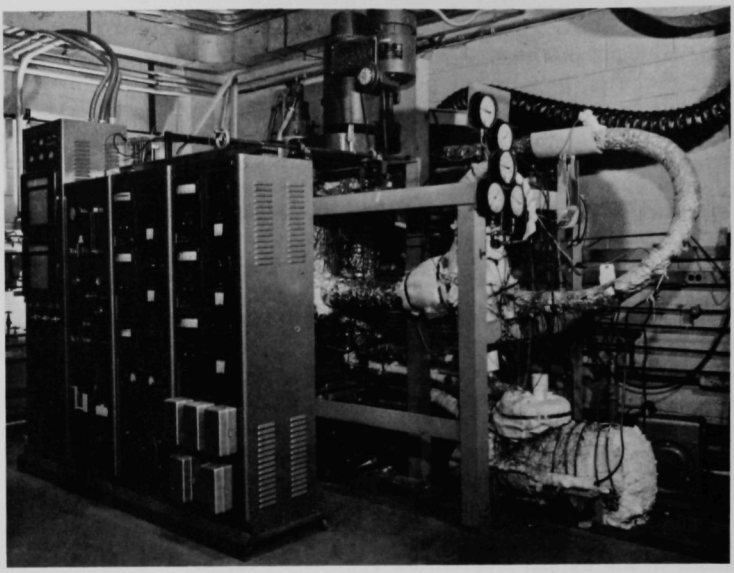

108-5853

Fig. 40. Photograph of Instrumentation Panelboard

c. Liquid Metal Level Indicators

Two types of liquid metal level indicators were developed to use in this study. These are (a) the spark plug type and (b) the gas bubble system. Neither of these are new in principle. The spark plug type has been used and described elsewhere[46] together with its advantages and disadvantages. The gas bubbler has been used for years in various forms for determining pressure at submerged depths in liquids and liquid level measurements.

(1) Spark Plug Type

Spark plugs were obtained and the plugs were modified so that a stainless steel 304 welding rod of about 1/8 inch in diameter was welded so that it became the center electrode. A 6-volt battery and an indicator light were connected to the spark in series and grounded to the equipment. The equipment and the liquid metal contacting the center electrode of the level probe completed an electrical circuit and a light connected into the circuit indicated the completed circuit signifying that liquid metal had contacted the probe. Actually, the stainless steel probe was adjusted to a certain predetermined level and the indicating light remained off until the liquid metal level in the tank was sufficiently high to make contact with

the probe. The disadvantages of this arrangement were found to be as follows: (1) two spark plug level probes had to be used to indicate high and low level in the various tanks, and (2) there was the possibility of shorting the electrical circuit on the side of the tank with the probe instead of making contact with the liquid. It was decided to replace the spark plug level probes with bleed gas bubblers which gave better results.

(2) Gas Bubble Level Probe

Argon gas was bled through a pressure regulator and needle valve through a hollow stainless steel tube (B, Fig. 41) which was free to be raised or lowered through a high-vacuum coupling into the molten cadmium. The bleed gas line was connected through a tee into one leg of a manometer whose other leg was connected into the system or tank. While the probe was raised above the liquid level (D, Fig. 41), the argon bleed was adjusted with the needle valve. When the bleed pressure balanced the system pressure in the charge tank, the manometer read zero. As the probe was lowered just beneath the liquid metal surface E, Fig. 41, an unbalance of pressure forces resulted between the charge tank and bleed and a deflection of manometer fluid was observed on the manometer. Operation of the gas bubbler may be followed by referring to Fig. 41. Argon gas is bled from the argon cylinder into the level probe at B and simultaneously into one side of the manometer. This flow rate is adjusted with the level probe at position D until the manometer reading is constant. This constant reading indicates that the pressure (or flow rate) through the level probe balances the pressure on the system which is indicated at H and connected

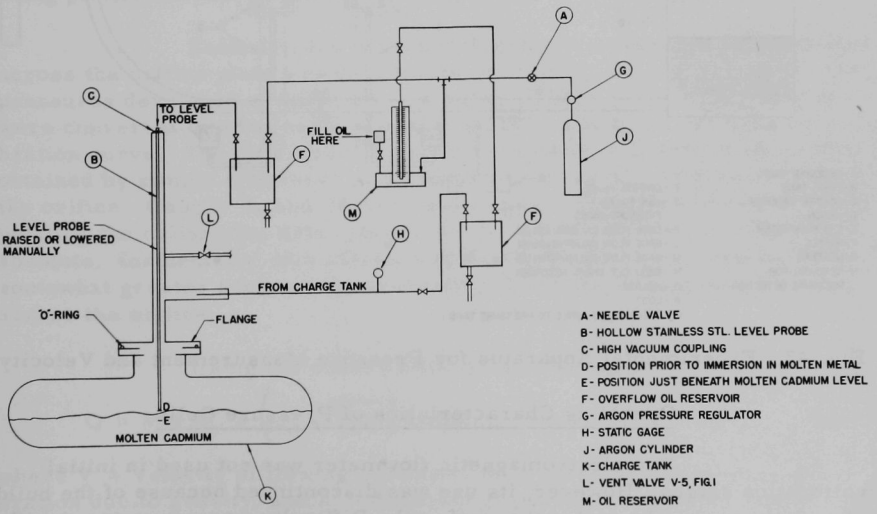

Fig. 41. Gas Bubbler Level Indicator

into the other leg of the manometer via the oil overflow reservoir at F. Measurement of the length of stainless steel probe before and after a transfer operation yielded the liquid metal level in the tanks or system by simple arithmetic calculation.

D. Velocity Calibration and Operating Procedures

1. Velocity Calibration

a. Experimental Equipment for Velocity Calibration

A sketch of the orifice location, radius pipe tape, and pressure cells is shown in Fig. 42. The figure also shows the location of the electromagnetic flowmeter (E) and millivolt chart recorder (N) for recording the voltage. The orifice plate was located at (I) and could be inserted and removed by the bolting flange. Two reservoirs for pressure detection are shown at H. Pneumatic gauges are shown at K, L, L', and M, M'. Differential pressure cells with NaK filled capillaries are shown at J. Heaters are shown at G for the radius pressure taps.

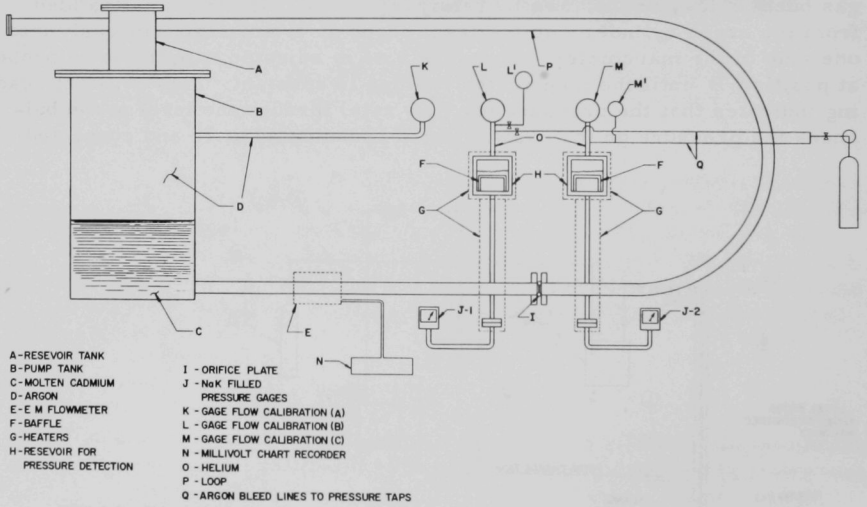

Fig. 42. Experimental Apparatus for Pressure Measurement and Velocity

b. Operating Characteristics of Pressure Cells

The electromagnetic flowmeter was not used in initial calibration stages. However, its use was discontinued because of the buildup of a slight oxide film under the pipe wall. Difficulty was encountered with the NaK filled capillaries and differential pressure cells because of diaphragm rupture.

Because of the difficulties encountered with the electromagnetic flowmeter and the NaK filled cells later in the experimental program, an alternate apparatus had to be developed to determine the flow rate. This apparatus consisted of placing reservoirs for pressure detection on either side of the orifice plate. These reservoirs were designed to hold molten metal under pressure from the dynamic loop. Argon was trapped in the capillaries at "O" and the pressure developed by the flowing cadmium was read on the gauges L,L' and M,M'. Baffles shown at F were installed in the reservoirs, H, to dampen the possibilities of metal surging into the capillaries and plugging them. An argon cylinder and argon bleed lines shown at Q were installed by making terminal corrections into the capillaries. These bleed gas lines allowed the reservoirs to be cleared prior to operation and a constant or steady head could be held on the reservoirs.

c. Calibration Procedure

The principle of the calibration procedure consists of two specific steps. Prior to operation, the pressure reservoirs, H, are calibrated in terms of an arbitrary standard gauge shown at K. This calibration is accomplished by differentially bleeding argon gas into the pump tank. During this operation, there is a continuous differential pressure buildup on gauges K, L, L' and M, M'. The pressures on these gauges are recorded at each differential increment of pressure, bled into the system.

The recorded data are then plotted with L,L' and M,M' being plotted versus the arbitrary standard K as in Fig. 43.

Secondly, the pressure difference under flowing conditions across the orifice plate was determined by reading L,L' and M,M' for the pressures developed at different flow rates. These recorded pressures were converted into the same pressure units by using the previous calibration curve. The difference in pressure between L,L' and M,M' is then obtained by simple difference and amounts to the pressure drops across the orifice. Gauges L and M are read in psig. For convenience in interpolating the calibration data, gauges K, L and M are read in MM of Hg absolute. Incidentally, this allows a smaller unit to be read and perhaps somewhat greater accuracy in calibrating the differential pressure drop across the orifice.

Using the conventional orifice formulas

$$Q = V \times A_p = \left(C_d \sqrt{2gh'}\right) \times A_p \qquad (15.1)$$

where V = velocity of flowing cadmium, A_p = area of loop pipe, g = acceleration due to gravity, and h' = differential pressure in feet of flowing fluid.

The velocities could be calculated using equation 15.1. The above equation is modified to account for the conversion of pressure units to feet when using psi units.

$$V = C_d \sqrt{\frac{2(g)\Delta p \times 144}{\rho \times 62.4}} \qquad (15.2)$$

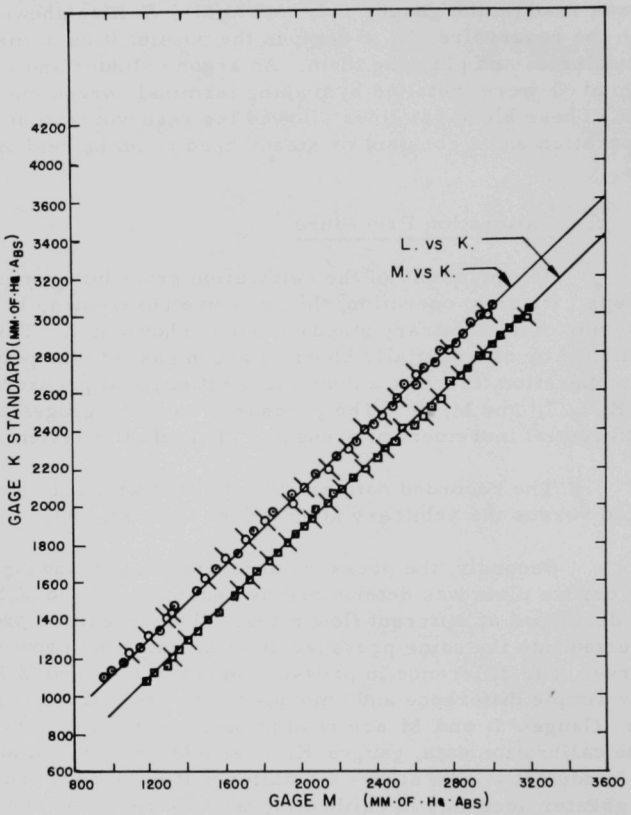

Fig. 43. Calibration Data, L' and M' Plotted Versus Arbitrary Standard Gauge K

The discharge coefficients for 4 orifice plates of different diameter were obtained experimentally by pumping water around the loop and metering with a water meter the flow rate. The water was metered in the lower horizontal leg of the loop and the pressure drop was measured across the various orifices. From this data the discharge coefficients

could be calculated. These coefficients all approach a constant value of 0.61 above an orifice Reynolds number of 10^5. The coefficients are tabulated in Chapter XVI. Using this coefficient of 0.61 the velocity of the molten cadmium could be calculated from pressure drop data obtained by the procedure outlined above. This assumes that the coefficients for water were the same as for liquid cadmium. The velocity of the molten cadmium is plotted versus the rpm of the pump shaft in Fig. 44. The data are presented in Chapter XVI for the calibration of the molten cadmium versus the velocity.

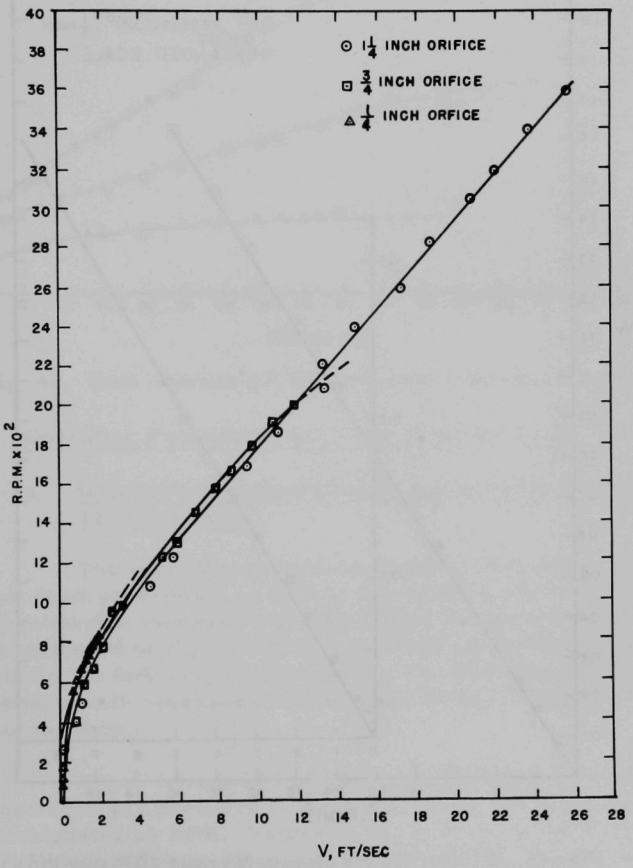

Fig. 44. Rpm of Pump Shaft Versus Velocity of Cadmium Flow in ft/sec

It is observed that above an orifice Reynolds number of 10^5, the orifice coefficients approach a constant value of 0.61. This value is used in the standard orifice equation above to calculate the velocity from known Δp data. The velocity may also be read as a function of rpm of the pump. The rpm of the pump shaft is recorded simultaneously with the pressure drop across the orifice. This was the final calibration curve used for the velocity determination. Figures 44 and 45 are plots of rpm velocity and pressure drop data used in the velocity calibration.

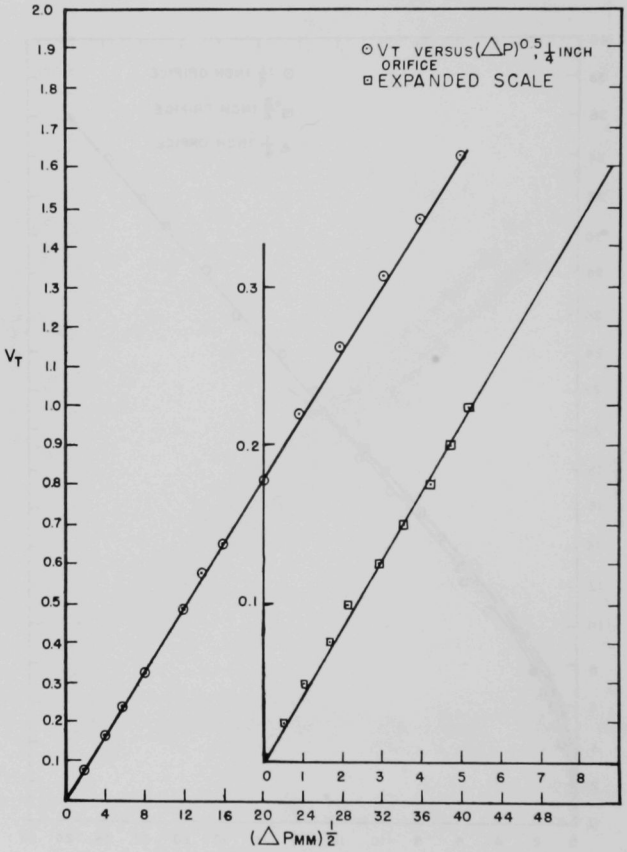

Fig. 45. Plot of Low Velocity Versus $(\Delta P \text{ mm})^{1/2}$ across the Orifice

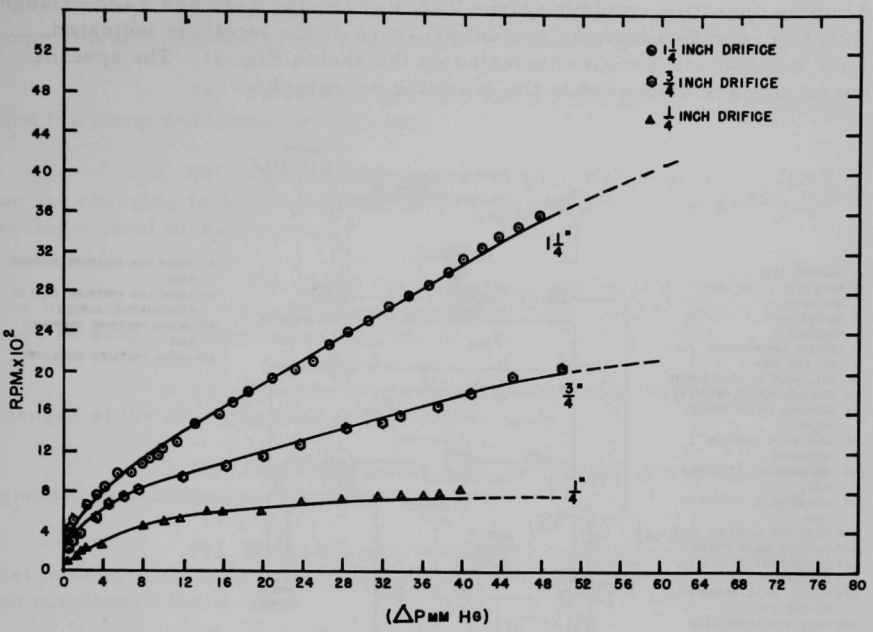

Fig. 46. Rpm Versus ΔP for Different Diameter Orifices

2. Operating Procedures for Mass Transfer Runs

a. Introduction to Operating Procedures for Making Mass Transfer Runs

The operating procedures consist of the operation, charging, normal shut down procedure, as well as the detailed procedure for making a run. These involve manipulating appropriate valves for the argon blanket gas from panelboard of Fig. 40. The flow sheet for the argon blanket gas may be seen in the following sketch as Fig. 47. The sketch includes major loop components with necessary instrumentation to accomplish successful operation of the loop.

Argon is supplied by the compression gas cylinder as shown. The argon gas pressure is first reduced by the argon high pressure regulator designated as APR. Valves V-16, V-17, V-5 and V-2 are involved in the charging operation as discussed in that section. Gauge G-1 is used to read the pressure on the charge tank. The sketch indicates the safety relief provided for the charging operation. Valves V-6, V-7, and V-21 are used when operating the vacuum pump. Valves V-19, V-20, V-6, V-7, and V-21 as well as V-18 are employed in the gas leak test operation. The

dumping operation employs valves V-2, V-5, V-16, V-17 and V-22. Gauges G-1, G-2, and G-3 indicate system pressure at the locations indicated. Loop components are also indicated on the sketch Fig. 31. The specific operations are discussed in the following paragraphs.

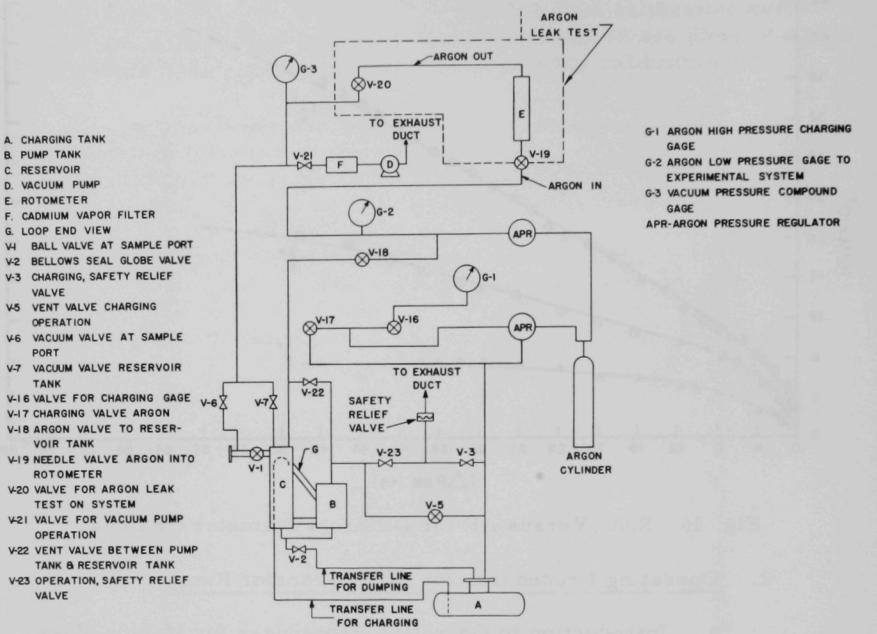

Fig. 47. Argon Blanket Gas Flow Sheet

b. Charging Procedure for Molten Cadmium

The charging procedure refers to the specific operation where the molten cadmium was forced upwards by high pressure argon gas through the transfer line into the surge reservoir of the experimental system.

The detailed sequence of steps in a charging operation may be listed and followed by referring to Figs. 30, 31, 32, and 40.

(1) The temperature recorder and the individual controller temperature were checked to see if the experimental system was up to operating temperature.

(2) Valve V-2, the dumping valve, was closed.

(3) A sample rod with dummy sphere was placed in the experimental position at the sample port according to the run procedure.

(4) Valve V-5, the vent valve between the charging tank and the pump reservoir, was closed.

(5) The leveling device, that is, the argon gas bubbler, on the charging tank was adjusted to its initial position preliminary to taking a level measurement.

(6) The argon valves to the experimental system, including the high pressure argon valves on panelboard No. 2 were closed. These may be seen by referring to Fig. 40.

(7) The portable exhaust ducts were positioned at the flanges of the charging tank and reservoir tank.

(8) Operating personnel assumed positions in front of the general instrumentation panelboard.

(9) Using the argon pressure regulator the pressure was set for charging the molten cadmium and was read at the charging gauge on panelboard No. 2.

(10) Charging of molten cadmium to the loop was initiated by opening the charging valve on panelboard No. 2, and the pressure gauges were watched during charging.

(11) After sufficient time had elapsed to complete the charging procedure, the liquid level in the charging tank was checked using the leveling probe.

(12) Valve V-8 which discharged directly into the exhaust duct was opened and allowed the release of argon gas accumulated in the experimental system during charging.

(13) The charging procedure was terminated and special notes observed during charging were recorded.

c. Detailed Procedure for Making a Run

After the molten cadmium was charged to the experimental system, the next procedure consisted of the preparation and completion of a specific run. The following detailed steps were executed during this operation. Again refer to Figs. 31, 34, 40.

(1) A dummy sphere of SS 304, the same size of the uranium test sphere, was placed in the dissolving position. A dummy sphere was used to enable velocity adjustments to be made without dissolving the test sphere.

(2) The molten cadmium was transferred from the charging tank into the experimental system under high pressure argon placed on the charging tank.

(3) The cadmium flow rate was adjusted by using the emf versus pumping rate calibration curve previously established for cadmium.

(4) The pump was shut off and the cadmium allowed to become quiescent in the two reservoirs. This allowed the liquid level in the loop to drop to a position below the sphere.

(5) The dummy sphere was removed from the experimental position by pulling the sample rod back through a Cenco high vacuum fitting until the dummy sphere was behind the ball valve V-1 at the sample port. The ball valve, shown in Fig. 31 as V-1, was then closed.

(6) The dummy sphere was allowed to cool for about 20 minutes to approximately room temperature in this small sealed chamber. After cooling, the flange on the sampling port was removed and the dummy sphere detached from the sampling rod.

(7) A uranium test sphere already pre-wet with cadmium was then attached to the sampling rod. The flange and sampling rod were again placed in position. The uranium test sphere in this position was located in the small sealed chamber between the flange and ball valve V-1.

(8) The chamber which contained the sphere between the valve V-1 and the flange was then evacuated and flushed three times with argon to eliminate air.

(9) Valve V-1 was then opened and the uranium test sphere was positioned in the experimental location in the upper horizontal leg of the 1.5 inch conduit.

(10) The pump was turned on after the uranium sphere was placed in the dissolving position. Molten cadmium flowed past the uranium sphere and dissolved it to some extent.

(11) After a prescribed time interval for the experimental run, the pump was shut off and the molten cadmium was allowed to become quiescent in the two reservoir tanks.

(12) The uranium test sphere was then removed from the experimental position in the same manner that the dummy sphere was removed.

(13) The uranium test sphere was detached from the sample rod and weighed. From the weight loss of the sphere and appropriate equations, the dissolution correlations were established as a function of cadmium velocity and temperature.

d. Normal Shut Down Procedures

After specific mass transfer runs were completed, or in order to repair some malfunction in the equipment, the molten cadmium was dumped from the experimental system to the charge tank where it solidified. The detailed procedure for normal shut down may be itemized as follows:

(1) The pump was shut off by shutting off the motor drive assembly.

(2) After the pump had coasted down, the molten cadmium was allowed to become quiescent in the system.

(3) Vent valves were opened to allow for necessary pressure equalization between tanks as the molten cadmium flowed to the charge tank.

(4) Valve V-2, the bellow-sealed globe valve as shown in Fig. 31, was opened to commence the dumping operation.

(5) The next step consisted of watching pressure gauges for pressure equalization, and using the liquid metal level probe in the charge tank to obtain level.

(6) Liquid metal level probes on the charge tank and the surge reservoir tank showed that all of the cadmium was in the charge tank, and the valve V-2 was closed. The normal dumping operation was then terminated.

3. Analytical Procedure for Obtaining Weight Loss from Sphere

a. Weighing techniques as regards the analysis of the uranium spheres were carefully worked out in demonstration runs. It is shown elsewhere in the treatment of data that the dissolution analysis is based upon the weight loss of the uranium spheres during a mass transfer run. The pertinent weights of the uranium spheres were recorded in accordance with the following detailed steps:

(1) The initial weight of the uranium spheres were recorded before the removal of oxide films as discussed in the wetting procedure.

(2) The weights of the uranium spheres were recorded after step (1) was completed and the weights of the SS 304 support rods were recorded separately.

(3) After wetting, the sphere plus the Zn coating and the SS 304 support rod were stored until ready for a run. Analysis was made of the Zn melt for the uranium content which might be present. The content of Zn and U was found to be negligible.

(4) After a mass transfer run was completed, the cadmium coating on the uranium sphere was removed by dilute H_2SO_4. (Sulfuric acid[65] attacks Cd but not U.)

(5) The cadmium coating removed as in step (4). The weight loss during dissolution was obtained by subtracting the weight of the clean uranium sphere after a run from the weight obtained from step (2).

4. Procedure for Uranium Analysis

In the laboratory analysis, samples which contained uranium were all checked for uranium content. Uranium was determined spectrophotometrically with 1.3-diphenyl-1-3 propanedione using modifications of the procedures listed by Francois,[66] and Maeck.[67] This required a pH adjustment and the extraction of uranium using hexone as the extractant. The uranium was extracted as tetrapropyl ammonium uranyl nitrate from acid deficient aluminum nitrate. Further treatment of the hexone phase was accomplished by adding this phase to an acetone-water solution which contained dibenzoyl methane and pyridine. The absorbance was measured at 410 mu using 1 cm cells. The experimental error involved in the test was ±5%.

5. Safety Considerations

The most serious considerations concerning the exposure of human beings to cadmium compounds in this operation consisted of the possible leakage of cadmium either as a liquid or vapor from the system. It was considered unlikely that cadmium could spew out as a liquid through the heavy layer of insulation. However, the following safety precautions were practiced in this operation:

a. Safety Precautions Taken While Melting Cadmium Charge

In this case it was anticipated that a leak of cadmium from the charge tank, or a leak of cadmium vapors might occur during the melting process. In the event of such an emergency, the operating personnel were instructed to shut down the power to the heating circuits, reduce the argon gas pressure, and place portable exhaust lines at the source of leakage. Personnel were instructed to then leave the area.

Leakage of argon gas, except when argon was deliberately being supplied could be detected by argon flow through a rotameter on the argon supply system. The system was leak checked prior to a run by determining if the pressure remained constant in the system over some prescribed time interval. Industrial Hygiene section of the Chemical Engineering Division monitored in the area by taking periodic air samples.

b. Safety Precautions Taken during an Experimental Run

An emergency situation during a run would be leakage of cadmium liquid or vapors from the experimental system. Operating personnel were instructed to shut off the pump, open the valve V-2 of Fig. 31 for dumping the molten cadmium to the charge tank and then to leave the area.

c. Pressure Control and Relief

Argon gas was supplied to the experimental system through argon pressure regulators. Generally the operating pressure never exceeded 15 psi. However, during the operation of the experimental loop with the exception of the charging operation, the argon gas lines were connected to a pressure relief valve set at 50 psi which if ruptured would exit all gas to the exhaust duct.

d. General Safety Procedures Summary

The general safety philosophy was based upon performing rapid shutdown of the equipment by relatively few operations (drainage of loop, shutdown of pump and power, and reduction of pressure) and evacuation of personnel. Assault masks were located and used by operating personnel for certain operations, particularly for inserting and removing samples.

E. Vibration Reduction of Motor and Mounting Supports

1. Statement of Problem

It was necessary to determine the extent of mechanical vibrations which might be transmitted to the dynamic loop from the motor and

drive assembly. The dynamic loop was designed so that the upper horizontal leg of the loop connected into the reservoir tank as shown in Fig. 2. Because of the operating temperature of about 500°C, allowance had to be made for thermal expansion in the tank and reservoir tank. This constituted placing the reservoir tank on coasters which rested on the loop supports. Because the molten metal pump was mounted vertically and driven from the side (the same horizontal place as that in which the coasters were contained) it was necessary to mount the motor and drive assembly separate from the rest of the experimental equipment. In addition, a study was initiated after mounting the motor separately to further reduce the vibration index transmitted from the motor. The pump was belt driven by the motor which helped dampen some of the vibration level. However, the motor and drive assembly which constituted the source of vibrations had to be properly isolated. This result is described in the following paragraph.

2. Methods Employed to Reduce Vibrations

Rubber absorber padding was obtained and sandwiched between aluminum plates, each about 0.125 inches thick. These absorber units were placed between the terminal points of the mounting braces and the wall. Figure 48 shows the location of the absorber unit after installation. A vibration absorber tube was made and attached to the mounting plate at a 45° angle with the horizontal and the wall. The absorption tube acted as a vibration dampener and could be adjusted using a turn buckle at one end. A torque wrench was used to indicate the torque in inch-pounds that was applied

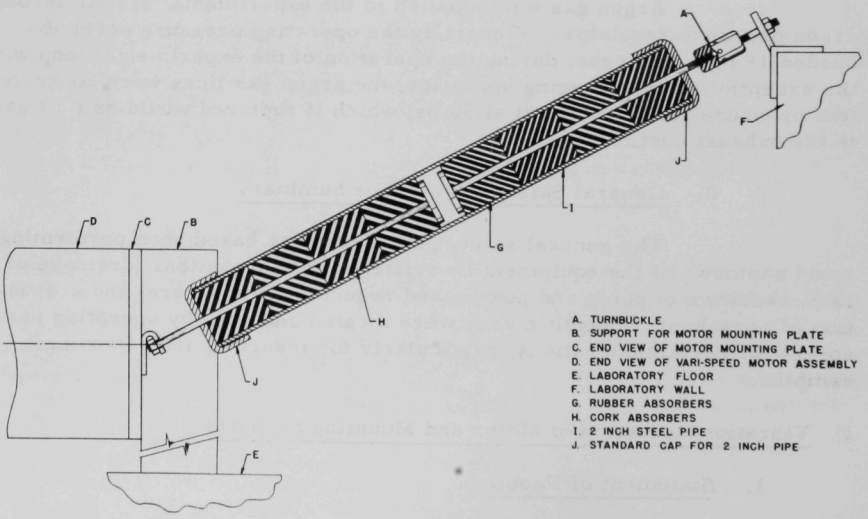

Fig. 48. Vibration Absorber Tube

to the terminal connection. The interior of the tube consisted of rubber sections which acted as cushions between the terminal ends of the tube.

3. Experimental Procedure and Technique

It was immediately recognized that some detection device had to be fabricated to detect the effect of the vibration absorbers, and the effect of placing different torques on the dampening tube.

a. Transducer for Detecting Vibrations

The vibrations were detected by employing a transducer to pick up the vibrations, which in turn transmitted a signal to a pre-amplifier; from the pre-amplifier, the signal was fed to a linear amplifier and finally to a scaler for counting. A sketch of the experimental set-up is shown in Fig. 49. The transducer consisted of a small cylindrical plate suspended inside a cup. This may be viewed in Figs. 50 and 51. The small plate was suspended on an arm which was connected to one side of the electrical circuit while the cup was connected to the other electrical lead. The cup was mounted on an accoustical pad which was about 3 by 6 inches in dimensions. The transducer assembly was attached to the motor at the location where it was desired to pick up the vibrations. In this position the vibration index of the running motor could be detected. Completion of the electrical circuit introduced a signal to the pre-amplifier, secondly to the amplifier, and finally to the scaler for counting.

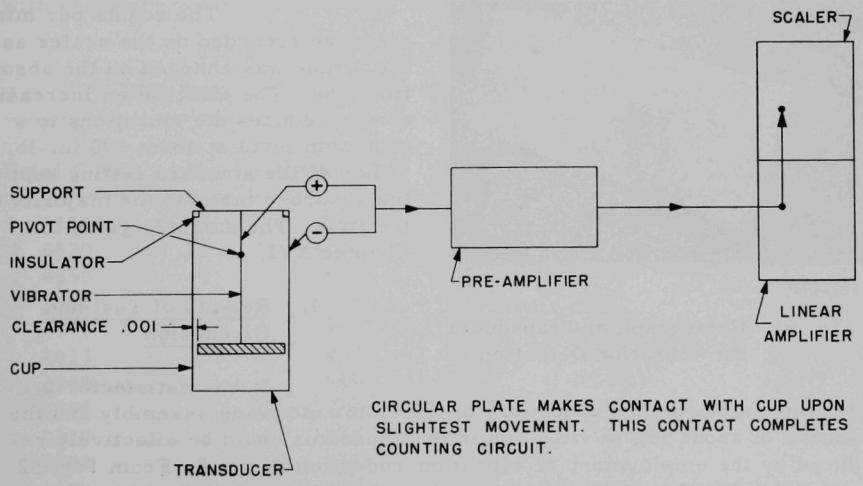

Fig. 49. Vibration Detector

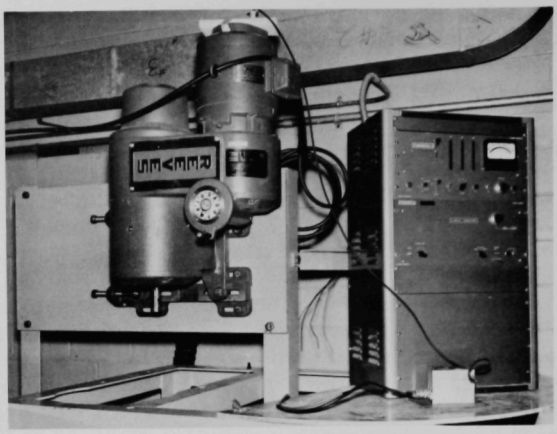

108-4839

Fig. 50. Equipment for Vibration Detection

b. Experimental Procedure

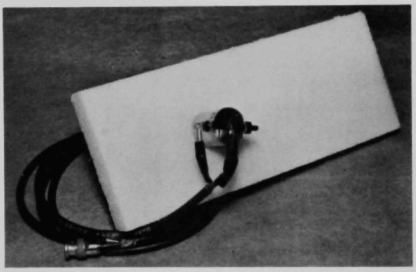

108-4841

Fig. 51. Photograph of Transducer for Vibration Detection

The counts per minute were recorded on the scaler as the torque was changed on the absorption tube. The effect of an increasing torque reduces the vibrations to a minimum level at about 600 in.-lb. This was the standard setting kept on the absorber tube for the majority of the runs. The data are given in Chapter XVI.

4. Results of Test and Discussion

It was satisfactorily demonstrated that the vibrations of the motor mounting assembly and the source of about 95% of vibration in the apparatus could be effectively reduced by the employment of vibration reduction devices. From Fig. 52 and Table XVIII it is observed that the relative vibration could be reduced by about 50% when 600 in.-lb of torque was applied to the absorber tube rather than 100 in.-lb. Also the figure demonstrates a steady decrease in the vibrations with increasing torque. No effort was made to determine the

exact effect of the vibration index on the mass transfer data. It was considered sufficient to keep a torque of about 600 in.-lb on the tube since this value seemed to be the most desirable at all speeds to hold a minimum vibration index. It should be recognized that a separate mass transfer study would be of academic interest which would determine the effects of vibration sources on mass transfer rates from single spheres.

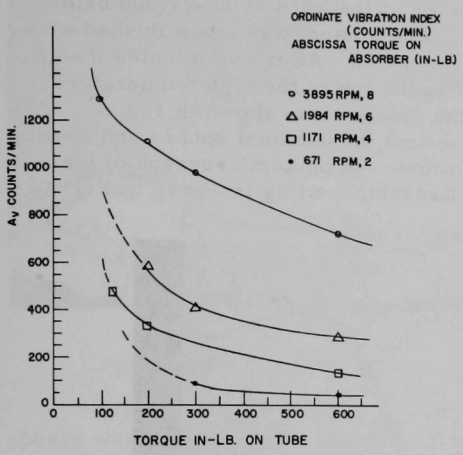

Fig. 52. Effect of Vibration Absorber Tube

F. Description of Ultrasonic Equipment and Procedures for Conducting Physical Wetting Experiment

A furnace capable of reaching 600°C was set up and a small crucible filled with solid cadmium placed inside. A small wire was attached to the crucible and was made to exit the furnace as shown in Fig. 53 through a side arm and vacuum fitting. The procedure prior to wetting the uranium with cadmium consisted of bolting the transducer on the high temperature

TABLE XVIII. Vibration Reduction Data

Data from Vibration Test (with Adjustable Dampener)

Total Count	Min	Count/Min	RPM	T, Torque (in.-lb)	N (Vari-Speed)
6192	5	1296	3895	100	8
5530	5	1106	3895	200	8
4950	5	980	3895	300	8
3692	5	738	3895	600	8
1479	5	296	1984	600	6
2013	5	402	1984	300	6
2940	5	588	1984	200	6
4350	5	870	1984	100	6
2310	5	478	1171	100	4
1646	5	348	1171	200	4
1450	5	290	1171	300	4
960	5	133	1171	600	4
400	5	80	671	300	2
200	5	40	671	600	2

vessel, evacuating the furncae, flushing with argon, melting the cadmium, and holding the molten cadmium at 550°C for wetting. As soon as 550°C was reached, the uranium sphere was attached to the magnetostrictive device by a pin in the smaller diameter of the horn as described below. The set screws were then tightened. The system was again flushed with argon and the ultrasonic generator turned on. After two minutes the crucible of molten cadmium was pulled to the top of the high temperature vessel by pulling the wire through the side arm as shown in Fig. 53. The molten cadmium at 550°C was now around the uranium sphere and wetting was accomplished in less than one minute. A photomicrograph of the uranium-cadmium interface after ultrasonic wetting is shown in Fig. 54.

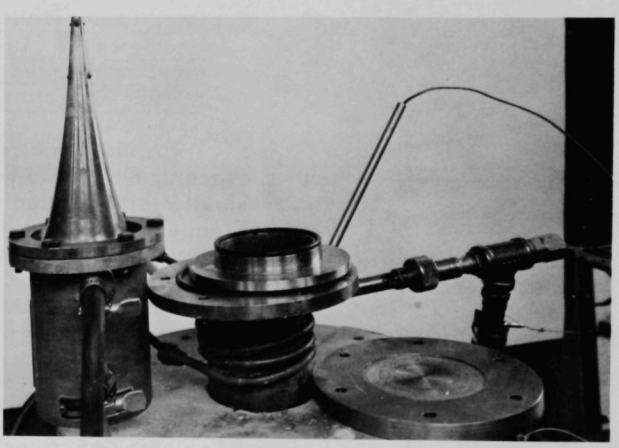

108-4908

Fig. 53. Exponential Horn for Attenuating Ultrasonic Energy

The ultrasonic transducer was a magnetostrictive device about 5 inches long with a cylindrical nickel core provided for connections for water cooling.

An exponential horn made from SS 304 was designed and then made by the shops. It was attached to the magnetostrictive device to attenuate the energy into the liquid metal.

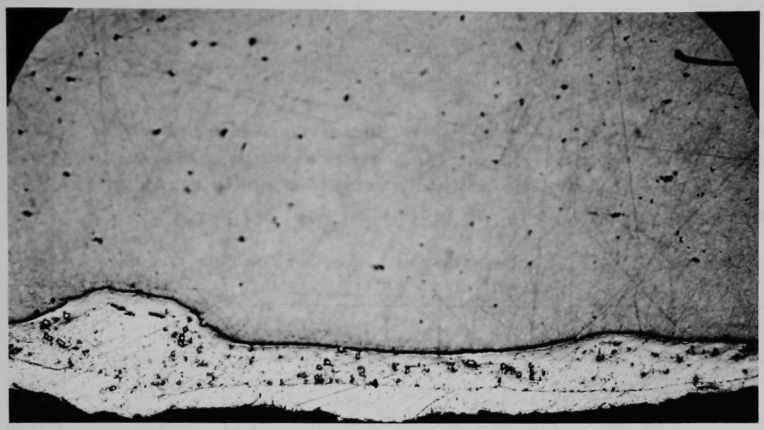

187.5X

Fig. 54. Photomicrograph of Uranium-Cadmium Interface after Ultrasonic Wetting

In the application of the ultrasonic horn for this study the uranium sphere was attached to the smaller diameter of the magnetostrictive device. A small stainless steel 304 pin about one inch slipped along the axis of the horn into a small recess. It was held in position by set screws from the periphery of the smaller diameter of the horn at angles 120° apart. The uranium sphere was attached to the threaded end of the small pin which protrudes from the horn by about 1/4 inch. The overall setup for ultrasonic wetting is shown in Fig. 55.

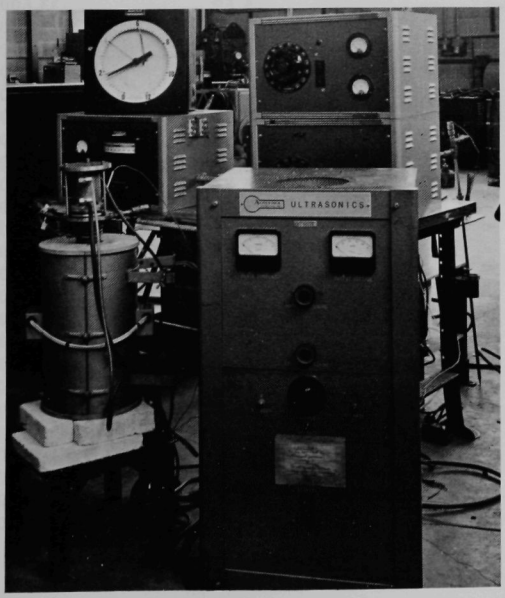

Fig. 55

Ultrasonic Generator for Providing Energy for Ultrasonic Wetting Experiment

108-4907

XVI. TABLES OF EXPERIMENTAL AND DERIVED MASS TRANSFER DATA

The following section presents a tabulation of the individual data tables and the important variables used for the several mass transfer correlations. Only the data for the primary variables and dimensionless number moduli are tabulated in the individual data tables.

TABLE XIX. Selected Values of J_d for Organic Solutes Dissolving in Water[22]

Run No.	Solute	Solvent	$J_d(N_{Sc}^{0.666}) \times 10^3$	$N_{Re,s}$
30	2-naphthol	Water	4.16	40,200
31			4.04	62,200
41			3.61	31,100
42			3.87	22,400
43			3.97	53,400
44			3.61	76,100
45			2.99	95,400
54t			3.51	35,700
55t			3.57	62,000
56t			2.80	136,500
57t			3.27	31,800
83			8.93	2,300
76			6.77	5,640
91			19.5	788
92			13.02	1,545
100			4.30	29,800
4	Cinnamic Acid	Water	5.98	33,600
5			5.59	33,600
6			7.42	57,100
8			5.37	102,000
9			6.40	62,500
11			7.18	72,900
12			7.11	80,300
13			6.99	81,500
14			6.05	84,700
15			5.83	92,500
16			5.84	96,000
18			5.77	47,700
22			6.85	16,900
23			6.68	54,800
24			7.01	77,300
27			7.11	82,500
28			6.94	61,300
29			6.19	40,200
66			5.52	24,300
67			5.22	28,500
74			13.81	3,370
75			7.86	10,100
77			9.90	5,350
78			9.18	9,700
79			13.5	3,380

TABLE XIX. (Contd.)

Run No.	Solute	Solvent	$J_d(N_{Sc}^{0.666}) \times 10^3$	$N_{Re,s}$
80	Cinnamic Acid	Water	15.2	2,240
86			9.2	6,150
87			30.7	727
88			33.8	632
32	Benzoic Acid	Water	8.37	16,350
33			7.06	21,500
34			6.46	26,100
35			6.65	31,100
46			8.12	23,800
47			7.15	32,900
48			7.73	38,600
49			8.56	74,500
50			7.92	52,900
98w			10.45	9,320
99w			20.2	2,680
89			36.6	718
90			21.0	1,600

TABLE XX. Summary of J_d Values for Correcting the Exponent of the Schmidt Number

Solute	Solvent	T	N_{Sc}	$N_{Sc}^{0.666}$	$N_{Sc}^{0.58}$
Benzoic Acid	Water	25°C	1000	100	54.96
Cinnamic Acid	Water	25°C	900	92.79	51.68
2-naphthol	Water	25°C	750	82.18	44.80
Uranium	Cadmium	500°C	151.8	28.36	18.413

Solute	Solvent	T	N_{Sc}	$J_d(N_{Sc}^{0.666})$	$J_d(N_{Sc}^{0.58})$	$N_{Re,s}$
Benzoic Acid	Water			0.015	0.00823	4×10^3
				0.0130	0.00713	5×10^3
				0.0120	0.00659	6×10^3
				0.0110	0.00603	8×10^3
Cinnamic Acid	Water	25°C		0.0120	0.00670	4×10^3
				0.010	0.00614	5×10^3
				0.0096	0.00535	6×10^3
				0.0086	0.00480	8×10^3
2-naphthol	Water	25°C		0.0160	0.00872	1×10^3
				0.010	0.00545	2×10^3
				0.0061	0.00332	4×10^3
				0.0040	0.00218	1×10^4
				0.0038	0.00207	2×10^4
				0.0033	0.00179	3×10^4
				0.0042	0.00228	5×10^4
				0.0046	0.00250	6×10^4
				0.0040	0.00218	8×10^4
				0.0030	0.00163	9×10^4
				0.0028	0.00152	1×10^5

TABLE XXI. Calibration Data for Gauges K, L, M

Trial No.	Gauge K, mm of Hg	Gauge L, mm of Hg	Gauge M, mm of Hg
1	1100	950	1180
2	1130	1000	1010
3	1180	1075	1090
4	1265	1155	1175
5	1360	1250	1275
6	1475	1335	1365
7	1575	1450	1465
8	1675	1550	1575
9	1760	1650	1665
10	1875	1750	1770
11	1980	1860	1875
12	2075	1960	1975
13	2160	2055	2065
14	2260	2190	2205
15	2340	2295	2300
16	2430	2390	2400
17	2530	2480	2482
18	2630	2575	2585
19	2650	2600	2580
20	2700	2630	2630
21	2735	2675	2675
22	2750	2700	2680
23	2800	2740	2740
24	2850	2800	2800
25	2900	2860	2860
26	3000	2950	3160
27	3050	3000	3200
28	3180	3280	3240
29	3300	3360	3300
30	3400	3400	3360
31	3700	3560	3500
32	3750	3580	3530
33	3800	3620	3560
34	3900	3670	3610
35	3950	3680	3630
36	4100	3720	3660
37	1425	1300	1320
38	1475	1340	1380
39	1625	1500	1520
40	1725	1610	1620
41	1825	1720	1730
42	1320	1180	1200
43	1220	1080	1120
44	1925	1820	1810
45	2020	1960	1950
46	2100	2030	2010
47	2200	2150	2140
48	2300	2250	2240
49	2400	2360	2340
50	2490	2440	2440
51	2575	2530	2520
52	2700	2620	2630
53	2800	2790	2790
54	3000	2975	2980

TABLE XXII. Activity Data for Uranium Cadmium System

Atom Fraction Uranium	Weight Fraction	log (a)
1.476×10^{-3}	$0.30\ (10^{-2})$	-0.9864
4.861×10^{-3}	$0.92\ (10^{-2})$	-0.4087
7.018×10^{-3}	$1.47\ (10^{-2})$	-0.2097
7.863×10^{-3}	$1.65\ (10^{-2})$	-0.1458

TABLE XXIII. Differential Pressure and Velocity Data for $1\frac{1}{4}$ inch Orifice

Trial No.	L	L', psi	M	M', psi	ΔP, psi	$(\Delta P)^{0.5}$, $psi^{0.5}$	V, ft/sec
1	5.8	20.5	5.5	20.2	0.3	0.548	2.19
2	9.5	24.2	9.0	23.7	0.5	0.70	2.78
3	10.5	25.2	9.5	24.2	1.0	1.0	3.98
4	12.0	26.7	10.1	24.8	1.9	1.38	5.52
5	12.5	27.2	2.5	24.7	2.5	1.58	6.32
6	14.0	28.7	9.5	24.2	4.5	2.13	8.50
7	15.4	30.1	11.5	26.2	3.9	1.97	7.86
8	26.0	40.7	10.0	24.7	16.0	4.0	15.8
9	36.4	51.1	12.5	27.2	23.9	4.88	19.3
10	58.0	72.7	14.0	28.7	44.0	6.54	26.0

TABLE XXIV. Differential Pressure and Velocity Data for 3/4 inch Orifice

Trial No.	L, mm Hg	L', mm Hg	M, mm Hg	M', mm Hg	L'-M', mm Hg	$(L'-M')^{1/2}$ $(mm\ Hg)^{0.5}$	L'-M', inches Hg	Z, lb/ft^2	V, ft/sec
1	1190	1305	1198	1300	5	2.23	0.197	6.07	0.53
2	1200	1330	1200	1321	9	3.00	0.354	10.75	0.864
3	1270	1375	1280	1362	13	3.61	1.41	15.6	0.86
4	1300	1410	1260	1375	35	5.92	1.38	42.2	1.42
5	1340	1450	1290	1397	53	7.28	2.09	63.9	1.75
6	1375	1492	1300	1410	82	9.06	3.23	98.4	2.17
7	1450	1550	1340	1425	125	11.19	4.93	150.3	2.68
8	1550	1650	1360	1450	200	14.4	7.88	241	3.41
9	1630	1725	1375	1460	265	16.29	10.44	319	3.92
10	1740	1862	1360	1475	387	19.67	15.22	464	4.72
11	1860	1950	1380	1487	463	21.6	18.2	554	5.16
12	2060	2150	1390	1490	660	25.7	25.9	790	6.18
13	2145	2210	1400	1500	710	26.6	27.9	850	6.39
14	2290	2350	1400	1525	825	28.7	32.5	994	6.93
15	2390	2462	1460	1562	900	30.0	35.4	1080	7.22
16	2660	2737	1520	1612	1100	33.2	43.3	1349	8.08
17	2780	2825	1540	1625	1200	34.7	47.3	1440	8.32
18	2940	2992	1580	1675	1317	36.3	51.8	1582	8.71
19	3240	3275	1600	1700	1575	39.7	62.2	1899	9.52
20	3660	3700	1675	1775	1925	43.8	75.7	2310	10.53

TABLE XXV. Differential Pressure and Velocity Data for 1/2 inch Orifice

Trial No.	L	M	L-M	Z'	V
1	9.3	8.0	1.3	1.245	0.140
2	8.9	7.6	1.3	1.245	0.140
3	10.6	6.1	4.1	2.055	0.411
4	10.0	7.5	2.5	1.603	0.293
5	11.0	6.0	5.0	2.27	0.497
6	11.2	6.1	5.1	2.29	0.501
7	14.3	5.8	8.5	2.96	0.653
8	14.3	6.6	7.7	2.81	0.618
9	19.6	6.0	13.6	3.72	0.820
10	19.5	6.0	13.5	3.73	0.809
11	31.2	4.7	26.5	5.22	1.14
12	31.2	4.3	26.9	5.27	1.16

TABLE XXVI. Differential Pressure and Velocity Data for 1/4 inch Orifice

Trial No.	ΔP, mm Hg	X, inches Hg	P, ft Hg	Z	0.1325Z	$(0.1325Z)^{0.5}$	0.103 $(\sqrt{0.1325x})$, ft/sec
1	1600	63	5.24	1890	251	15.85	1.632
2	1448	58.3	4.84	1740	231	15.21	1.570
3	1295	51.2	4.26	1530	203	14.24	1.470
4	1160	45.7	3.81	1370	181.5	13.47	1.380
5	1025	40.3	3.35	1205	160.0	12.66	1.305
6	900	35.5	2.96	1070	142	11.92	1.32
7	784	30.8	2.57	920	122	11.04	1.14
8	676	26.6	2.21	796	105	10.25	1.055
9	577	22.7	1.89	682	90.4	9.51	0.979
10	484	19.05	1.585	571	75.6	8.70	0.894
11	400	15.75	1.305	472	62.4	7.90	0.814
12	324	12.75	1.063	384	51.0	7.14	0.736
13	256	10.05	0.837	301	37.9	6.31	0.650
14	196	7.73	0.643	231	30.7	5.54	0.572
15	144	5.66	0.472	169	22.4	4.73	0.487
16	100	3.95	0.329	118.5	15.7	3.96	0.408
17	64	2.53	0.211	76	10.005	3.17	0.326
18	36	1.41	0.1174	42.3	5.58	2.36	0.243
19	16	0.63	0.0523	18.8	2.49	1.578	0.162
20	4	0.157	0.0131	0.390	0.0525	0.229	0.0236
21	3.24	0.127	0.0106	0.381	0.0507	0.225	0.0231
22	3.06	0.122	0.0101	0.309	0.0411	0.202	0.0208
23	2.25	0.0886	0.0074	0.221	0.0293	0.171	0.0176
24	1.57	0.0622	0.00518	0.156	0.0207	0.144	0.01485
25	1.44	0.0568	0.00473	0.141	0.0188	0.137	0.0141
26	1.21	0.0478	0.00398	0.119	0.0158	0.126	0.0129
27	1.10	0.043	0.00361	0.108	0.0143	0.119	0.0122

TABLE XXVII. Tabulation of Orifice Coefficients

(C_0 Determined Experimentally Using Water and Given Orifices)

D_0	ΔP, #/in.^{2}	V, ft/sec	$(\Delta P \times 144)^{1/2}$	γ	C_0
1/2 in.	1.5	0.498	14.6	9.35	0.3189
	2.5	1.03	18.97		0.5076
	4.5	1.584	25.45		0.5819
	7.5	2.22	32.86		0.6317
	13.3	3.115	43.70		0.6664
	25.1	4.325	62.76		0.6442
3/4 in.	1.5	1.513	14.69	3.88	0.3933
	2.9	2.545	20.42		0.4760
	4.8	3.56	26.28		0.5174
	6.7	4.75	31.04		0.5845
	11.0	6.23	39.74		0.5988
	20.0	8.63	53.66		0.6433
1 in.	1.5	1.24	14.69	2.21	0.1839
	2.1	2.73	17.37		0.3425
	2.7	4.27	19.69		0.4726
	3.8	5.99	23.38		0.5583
	5.7	8.01	28.63		0.6097
	9.3	11.32	36.60		0.6740
1 1/4 in.	1.5	1.47	14.69	1.019	0.1000
	1.8	2.99	16.09		0.1858
	2.0	4.64	16.97		0.2734
	2.1	6.60	17.37		0.3780
	2.3	8.90	18.19		0.4892
	3.2	12.24	21.44		0.5708

TABLE XXVIII. Mass Transfer Data at 500°C for Random Spheres

Run No.	4*	5	6*	7*	8*	21*	22*	23*	24*
$\bar{\epsilon}$	0.54		0.47	0.44	0.41	0.43	0.41	0.53	0.57
T_e	500	500	500	500	500	500	500	500	500
θ'	5.8		3.9	4.2	5.1	5.1	7.0	5.3	6.3
$\mu \times 10^2$	1.84	1.84	1.84	1.84	1.84	1.84	1.84	1.84	1.84
ρ	7.82	7.82	7.82	7.82	7.82	7.82	7.82	7.82	7.82
$D_V \times 10^5$	1.55	1.55	1.55	1.55	1.55	1.55	1.55	1.55	1.55
N_{Sc}	151.8	151.8	151.8	151.8	151.8	151.8	151.8	151.8	151.8
V_a, ft/sec	1.79	2.86	3.22	5.38	5.74	3.93	6.8	1.79	2.5
V_s, ft/sec	2.013	3.21	3.62	6.05	6.47	4.43	7.65	2.013	2.81
d_s	1.223	1.231	1.202	1.179	1.239	1.262	1.255	1.231	1.242
$N_{Re,s}$	31,800	51,300	56,400	92,200	103,800	72,400	124,000	32,100	45,300
RPM	750	950	1050	1250	1300	1100	1450	750	850
Δw (measured)	1.535	3.493	6.646	7.799	2.955	4.085	0.8290	3.1455	1.9103
θ	300	300	300	300	300	120	60	474	180
A_s	4.72	4.78	4.57	4.39	4.81	4.97	4.73	4.78	4.84
C_s	0.167	0.167	0.167	0.167	0.167	0.167	0.167	0.167	0.167
C_1	0.0	0.0	0.0	0.0	0.0	0.0	0.0	0.0	0.0
k_1	6.46×10^{-3}	1.46×10^{-2}	3.02×10^{-2}	3.51×10^{-2}	1.225×10^{-2}	4.07×10^{-2}	1.725×10^{-2}	8.41×10^{-3}	1.305×10^{-2}
k_1/V_s	2.23×10^{-4}	1.499×10^{-4}	2.71×10^{-4}	1.915×10^{-4}	0.623×10^{-4}	3.02×10^{-4}	0.753×10^{-4}	13.75×10^{-5}	1.519×10^{-4}
J_d	0.00636	0.00424	0.00767	0.00546	0.00168	0.00857	0.00215	0.00378	0.00432

Run No.	25*	26*	27*	28*	29*	30*	31*	32*
$\bar{\epsilon}$	0.44	0.53	0.42	0.41	0.41	0.54	0.53	0.55
T_e	500	500	500	500	500	500	500	500
θ'	7.2	5.5	4.2	5.0	7.1	6.1	5.8	3.8
$\mu \times 10^2$	1.84	1.84	1.84	1.84	1.84	1.84	1.84	1.84
ρ	7.82	7.82	7.82	7.82	7.82	7.82	7.82	7.82
$D_V \times 10^5$	1.55	1.55	1.55	1.55	1.55	1.55	1.55	1.55
N_{Sc}	151.8	151.8	151.8	151.8	151.8	151.8	151.8	151.8
V_a ft/sec	3.22	3.93	5.38	6.30	6.5	1.68	1.19	0.89
V_s ft/sec	3.62	4.43	6.05	7.10	7.32	1.89	1.34	1.00
d_s	1.251	1.242	1.251	1.242	1.242	1.259	1.262	1.262
$N_{Re,s}$	58,600	71,200	98,100	118,900	118,000	30,800	21,900	16,310
RPM	1350	1100	1250	1375	1400	790	700	400
Δw (measured)	3.9629	4.2450	1.946	2.5195	1.3402	2.3862	1.6060	1.2350
θ	120	120	60	60	60	360	360	360
A_s	4.80	4.84	4.93	4.84	4.84	4.97	4.91	4.97
C_s	0.167	0.167	0.167	0.167	0.167	0.167	0.167	0.167
C_1	0.0	0.0	0.0	0.0	0.0	0.0	0.0	0.0
k_1	4.13×10^{-2}	4.35×10^{-2}	3.91×10^{-2}	5.13×10^{-2}	2.76×10^{-2}	7.98×10^{-2}	5.36×10^{-3}	4.13×10^{-3}
k_1/V_s	3.74×10^{-4}	3.22×10^{-4}	2.11×10^{-4}	2.370×10^{-4}	1.405×10^{-4}	1.385×10^{-4}	1.311×10^{-4}	1.361×10^{-4}
J_d	106.2×10^{-4}	0.00916	0.00602	0.00674	0.00402	0.00393	0.00373	0.00386

TABLE XXVIII. (Contd.)

Run No.	33°	34°	35°	36°	37°	38°	39°
$\bar{\epsilon}$	0.57	0.56	0.43	0.42	0.42	0.46	0.46
T_e	500	500	500	500	500	500	500
θ'	3.5	3.4	3.0	3.3	2.9	2.8	2.7
$\mu \times 10^2$	1.84	1.84	1.84	1.84	1.84	1.84	1.84
ρ	7.82	7.82	7.82	7.82	7.82	7.82	7.82
$D_v \times 10^5$	1.55	1.55	1.55	1.55	1.55	1.55	1.55
N_{Sc}	151.8	151.8	151.8	151.8	151.8	151.8	151.8
V_a, ft/sec	0.48	0.24	0.06	0.04	0.0301	0.0156	0.00984
V_s, ft/sec	0.54	0.27	0.0675	0.045	0.0340	0.0176	0.0110
d_s	1.257	1.262	1.265	1.257	1.269	1.230	1.267
$N_{Re,s}$	8,730	4,420	1,110	733	561	280	183
RPM	375	370	180	150	125	100	90
Δw (measured)	0.9430	0.6383	0.2546	0.1660	0.1140	0.1130	0.5200
θ	420	420	480	480	300	300	300
A_s	4.96	4.97	5.02	4.96	5.02	4.76	5.02
C_s	0.167	0.167	0.167	0.167	0.167	0.167	0.167
C_1	0.0	0.0	0.0	0.0	0.0	0.0	0.0
k_1	2.72×10^{-3}	1.835×10^{-3}	6.37×10^{-4}	4.17×10^{-4}	4.53×10^{-4}	4.72×10^{-4}	2.075×10^{-5}
k_1/V_s	2.02×10^{-4}	2.23×10^{-4}	3.09×10^{-4}	3.27×10^{-4}	4.38×10^{-4}	7.86×10^{-4}	5.99×10^{-4}
J_d	0.00576	0.00637	0.0088	0.00931	0.0125	0.0223	0.0170
$1/k_1/V_s$				3080			

Run No.	40	41	43	44	45	46	47°	48°
$\bar{\epsilon}$							0.41	0.45
T_e	500	500	550	550	600	600	500	500
θ'							7.5	7.5
$\mu \times 10^2$	1.84	1.84	1.72	1.72	1.54	1.54	1.84	1.84
ρ	7.82	7.82	7.77	7.77	7.72	7.72	7.82	7.82
$D_v \times 10^5$	1.55	1.55	1.82	1.82	2.10	2.10	1.55	1.55
N_{Sc}	151.8	151.8	122	122	94.7	94.7	151.8	151.8
V_a, ft/sec	0.00447	0.00624	0.00624	0.04	0.00624	0.04	8.99	13.45
V_s, ft/sec	0.00503	0.00704	0.00704	0.045	0.00704	0.045	10.103	15.15
d_s	1.232	1.251	1.267	1.262	1.265	1.259	1.262	1.262
$N_{Re,s}$	80	114	115	736	115	735	1.799×10^5	2.465×10^5
RPM	80	85	85	150	80	150	1725	2250
Δw (measured)	0.0570	0.0353	0.0425	0.1510	0.0596	0.1610	4.260	0.5350
θ	300	300	300	300	300	300	300	300
A_s	4.76	4.93	5.02	4.97	5.02	4.97	4.97	4.97
C_s	0.167	0.167	0.167	0.167	0.167	0.167	0.167	0.167
C_1	0.0	0.0	0.0	0.0	0.0	0.0	0.0	0.0
k_1	2.39×10^{-2}	0.144×10^{-3}	0.169×10^{-3}	0.606×10^{-3}	0.237×10^{-3}	0.646×10^{-3}	1.708×10^{-2}	2.14×10^{-2}
k_1/V_s	9.03×10^{-4}	0.686×10^{-3}	0.807×10^{-3}	0.443×10^{-3}	1.110×10^{-3}	0.472×10^{-3}	4.93×10^{-5}	4.69×10^{-5}
J_d	0.0257	0.0195	0.0198	0.0115	0.00227	0.00979	0.00140	0.00133
$1/k_1/V_s$		1460	1240	2270	902	2110		

TABLE XXVIII. (Contd.)

Run No.	49*	50*	55	56	57*	58*	63	64
$\bar{\epsilon}$	0.53	0.43			0.41	0.41		
T_e	500	500	500	500	500	500	500	500
θ'	7.5	7.5			7.2	7.3		
$\mu \times 10^2$	1.84	1.84	1.84	1.84	1.84	1.84	1.84	1.84
ρ	7.82	7.82	7.82	7.82	7.82	7.82	7.82	7.82
$D_v \times 10^5$	1.55	1.55	1.55	1.55	1.55	1.55	1.55	1.55
N_{Sc}	151.8	151.8	151.8	151.8	151.8	151.8	151.8	151.8
V_a, ft/sec	17.9	22.4	0.104	0.208	7.56	8.91	3.25	5.33
V_s, ft/sec	20.206	25.258	0.1175	0.234	8.50	10.00	3.65	6.0
d_s	1.265	1.251	1.255	1.239	1.255	1.265	1.187	1.111
$N_{Re,s}$	3.310×10^5	4.080×10^5	1.905×10^3	3.73×10^3	1.381×10^5	1.641×10^5	56,100	86,300
RPM	2650	3300	690	810	1660	1700	1060	1270
Δw (measured)	7.631	8.860	2.5910	0.0332	0.6060	0.6320	6.5093	8.9300
θ	300	300	360	360	60	60	300	300
A_s	5.02	4.93	4.96	4.78	4.96	5.02	4.46	3.94
C_s	0.167	0.167	0.167	0.167	0.167	0.167	0.167	0.167
C_1	0.0	0.0	0.0	0.0	0.0	0.0	0.0	0.0
k_1	3.04×10^{-2}	3.56×10^{-2}	0.866×10^{-2}	11.55×10^{-4}	1.22×10^{-3}	1.255×10^{-2}	2.91×10^{-2}	4.52×10^{-2}
k_1/V_s	4.96×10^{-5}	4.63×10^{-5}	24.2×10^{-5}	1.625×10^{-4}	4.37×10^{-5}	4.13×10^{-5}	2.61×10^{-4}	2.47×10^{-4}
J_d	0.00142	0.00132	0.00666	0.00521	0.00124	0.00117	0.00743	0.00707

Run No.	65	66	67	68	69	70	73
$\bar{\epsilon}$							
T_e	500	500	500	500	500	500	500
θ'							
$\mu \times 10^2$	1.84	1.84	1.84	1.84	1.84	1.84	1.84
ρ	7.82	7.82	7.82	7.82	7.82	7.82	7.82
$D_v \times 10^5$	1.55	1.55	1.55	1.55	1.55	1.55	1.55
N_{Sc}	151.8	151.8	151.8	151.8	151.8	151.8	151.8
V_a, ft/sec	6.01	1.68	2.84	1.55	1.085	0.833	0.00898
V_s, ft/sec	6.75	1.89	3.20	1.75	1.22	0.94	0.0101
d_s	1.220	1.173	1.262	1.239	1.241	1.191	1.257
$N_{Re,s}$	107,500	28,700	52,400	28,100	20,600	14,400	165
RPM	1340	740	940	725	710	442	90
Δw (measured)	2.9310	3.5010	3.493	2.3862	1.6060	1.2350	0.9230
θ	300	470	300	360	360	360	600
A_s	4.67	4.34	4.97	4.81	4.84	4.46	4.96
C_s	0.167	0.167	0.167	0.167	0.167	0.167	0.167
C_1	0.0	0.0	0.0	0.0	0.0	0.0	0.0
k_1	12.55×10^{-3}	10.15×10^{-3}	1.411×10^{-2}	8.24×10^{-3}	5.49×10^{-3}	4.61×10^{-3}	1.855×10^{-3}
k_1/V_s	0.611×10^{-4}	1.791×10^{-4}	1.451×10^{-4}	1.545×10^{-4}	1.515×10^{-4}	1.615×10^{-4}	5.97×10^{-4}
J_d	0.00174	0.00511	0.00413	0.00439	0.00429	0.00461	0.0169

*Values calculated from equations 17.1, 17.2, 17.3 before coast-down correction.

TABLE XXIX. Mass Transfer Data with Knurled Spheres for Random Orientation

Run No.	87	88	Run No.	87	88
$\bar{\epsilon}$			$N_{Re,s}$	330	8,800
T_e	500	500	RPM	337	700
θ'			Δw (measured)	0.8142	2.681
$\mu \times 10^2$	1.84	1.84	θ	600	660
ρ	7.82	7.82	A_s	4.97	4.97
$D_v \times 10^5$	1.55	1.55	C_s	0.167	0.167
N_{Sc}	151.8	151.8	C_l	0.0	0.0
V_a, ft/sec	0.0176	0.480	k_l	1.62×10^{-3}	4.88×10^{-3}
V_s, ft/sec	0.200	0.537	k_l/V_s	4.18×10^{-4}	2.98×10^{-4}
d_s	1.261	1.261	J_d	0.0119	0.00850

TABLE XXX. Mass Transfer Data at 500°C for 1/4 and 3/8 inch Spheres (Random Orientation)

Run No.	110*	111*	112*	113*	114*
$\bar{\epsilon}$	0.56	0.55	0.53	0.42	0.41
T_e	500	500	500	500	500
θ'	3.7	3.8	4.6	7.0	7.2
$\mu \times 10^2$	1.84	1.84	1.84	1.84	1.84
ρ	7.82	7.82	7.82	7.82	7.82
$D_v \times 10^5$	1.55	1.55	1.55	1.55	1.55
N_{Sc}	151.8	151.8	151.8	151.8	151.8
V_a, ft/sec	0.00946	0.0706	0.393	4.78	7.92
V_s, ft/sec	0.01015	0.0736	0.422	5.13	8.47
d_s	0.946	0.945	0.945	0.921	0.949
$N_{Re,s}$	124	903	5,160	61,100	104,000
RPM	375	395	500	1200	1680
Δw (measured)	0.0127	0.0163	0.1092	1.750	2.720
θ	120	60	120	120	120
A_s	2.81	2.81	2.81	2.66	2.82
C_s	0.167	0.167	0.167	0.167	0.167
C_l	0.0	0.0	0.0	0.0	0.0
k_l	2.25×10^{-4}	5.79×10^{-4}	1.945×10^{-3}	3.27×10^{-2}	4.83×10^{-2}
k_l/V_s	7.28×10^{-4}	2.51×10^{-4}	1.515×10^{-4}	2.09×10^{-4}	1.865×10^{-4}
J_d	0.0207	0.00713	0.00431	0.00597	0.00532

Run No.	115*	116*	117*	118*	119*
$\bar{\epsilon}$	0.55	0.53	0.55	0.42	0.41
T_e	500	500	500	500	500
θ'	3.7	4.6	3.8	7.0	7.2
$\mu \times 10^2$	1.84	1.84	1.84	1.84	1.84
ρ	7.82	7.82	7.82	7.82	7.82
$D_v \times 10^5$	1.55	1.55	1.55	1.55	1.55
N_{Sc}	151.8	151.8	151.8	151.8	151.8
V_a, ft/sec	0.01369	0.533	0.1093	7.11	11.97
V_s, ft/sec	0.0141	0.538	0.1125	7.32	12.35
d_s	0.621	0.626	0.624	0.611	0.597
$N_{Re,s}$	114	4,330	905	57,900	95,600
RPM	385	500	395	1200	1680
Δw (measured)	0.00416	0.0314	0.0109	0.4720	0.7030
θ	60	60	60	60	60
A_s	1.21	1.23	1.23	1.17	1.12
C_s	0.167	0.167	0.167	0.167	0.167
C_l	0.0	0.0	0.0	0.0	0.0
k_l	3.51×10^{-4}	2.54×10^{-3}	0.888×10^{-3}	4.03×10^{-2}	6.29×10^{-2}
k_l/V_s	8.17×10^{-4}	1.362×10^{-4}	0.259×10^{-3}	1.805×10^{-4}	1.67×10^{-4}
J_d	0.0232	0.00387	0.00739	0.00514	0.00477

*Values calculated from equations 17.1, 17.2, 17.3 before coast-down correction.

TABLE XXXI. Mass Transfer Data for Grain Orientation and Ultrasonic Effects

Run No.	NR-1*	NR-2*	NR-3*	NR-1R	US-1**	US-2**	US-3**
$\bar{\epsilon}$							
T_e	500	500	500	500	500	500	500
θ'							
$\mu \times 10^2$	1.84	1.84	1.84	1.84	1.84	1.84	1.84
ρ	7.82	7.82	7.82	7.82	7.82	7.82	7.82
$D_v \times 10^5$	1.55	1.55	1.55	1.55	1.55	1.55	1.55
N_{Sc}	151.8	151.8	151.8	151.8	151.8	151.8	151.8
V_a, ft/sec	0.0419	3.46	6.07	0.467	0.0597	0.478	1.83
V_s, ft/sec	0.0474	3.91	6.83	0.524	0.0707	0.535	2.01
d_s	1.261	1.120	1.220	1.261	1.261	1.261	1.261
$N_{Re,s}$	773	56,600	108,000	8,530	1,150	8,680	33,100
RPM	370	890	1420	495	180	497	820
Δw (measured)	0.0387	0.7930	1.5950	0.3770	0.2240	0.6900	1.5750
θ	420	420	420	420	480	420	300
A_s	4.97	3.94	4.67	4.97	4.97	4.97	4.97
C_s	0.167	0.167	0.167	0.167	0.167	0.167	0.167
C_1	0.0	0.0	0.0	0.0	0.0	0.0	0.0
k_1	1.110×10^{-4}	2.87×10^{-3}	4.87×10^{-3}	1.080×10^{-3}	5.63×10^{-4}	1.97×10^{-3}	6.33×10^{-3}
k_1/V_s	0.770×10^{-4}	2.41×10^{-5}	2.34×10^{-5}	0.678×10^{-4}	2.61×10^{-4}	1.201×10^{-4}	1.025×10^{-4}
J_d	21.9×10^{-4}	68.7×10^{-5}	66.6×10^{-5}	0.001930	0.00743	0.00343	0.00293

*Nonrandom.

**Ultrasonically wetted.

TABLE XXXII. Data for Variation of Driving Force

Run No.	89	90	91	92	93	94
T_e	500	500	500	500	500	500
$\mu \times 10^2$	1.84	1.84	1.84	1.84	1.84	1.84
ρ	7.82	7.82	7.82	7.82	7.82	7.82
$D_v \times 10^5$	1.55	1.55	1.55	1.55	1.55	1.55
N_{Sc}	151.8	151.8	151.8	151.8	151.8	151.8
V_a, ft/sec	0.04	0.04	3.51	3.51	0.04	0.04
V_s, ft/sec	0.045	0.045	3.95	3.95	0.045	0.045
$N_{Re,s}$	732	733	6.41×10^4	6.39×10^4	742	734
RPM	450	450	550	550	450	450
Δw (measured)	0.4056	0.1765	0.5748	0.4844	0.3550	0.3448
d_s	1.253	1.259	1.255	1.250	1.265	1.255
θ	480	480	540	540	480	480
A_s	4.93	4.97	4.94	4.92	5.01	4.95
C_s	0.167	0.167	0.167	0.167	0.167	0.167
C_1	0.004	0.004	0.004	0.004	0.014	0.014
ΔC	0.163	0.163	0.163	0.163	0.153	0.153
k_1	1.05×10^{-3}	4.55×10^{-4}	1.315×10^{-3}	1.120×10^{-3}	0.966×10^{-3}	0.949×10^{-3}
k_1/V_s	0.782×10^{-3}	3.33×10^{-4}	1.11×10^{-5}	0.936×10^{-5}	0.706×10^{-3}	0.693×10^{-3}
J_d	21.8×10^{-3}	95.0×10^{-4}	28.9×10^{-5}	26.7×10^{-5}	20.1×10^{-3}	19.75×10^{-3}

TABLE XXXII. (Contd.)

Run No.	95	96	98	99	100	102
T_e	500	500	500	500	500	500
$\mu \times 10^2$	1.84	1.84	1.84	1.84	1.84	1.84
ρ	7.82	7.82	7.82	7.82	7.82	7.82
$D_v \times 10^5$	1.55	1.55	1.55	1.55	1.55	1.55
N_{Sc}	151.8	151.8	151.8	151.8	151.8	151.8
V_a, ft/sec	3.51	3.51	0.04	3.51	3.51	0.04
V_s, ft/sec	3.95	3.95	0.045	3.95	3.95	0.045
$N_{Re,s}$	6.43×10^4	6.43×10^4	731	6.43×10^4	6.41×10^4	734
RPM	548	548	450	550	550	450
Δw (measured)	0.4074	0.1990	0.5053	0.2736	0.8708	0.4506
d_s	1.255	1.255	1.252	1.259	1.255	1.255
θ	540	540	480	540	540	480
A_s	4.95	4.95	4.93	4.96	4.93	4.94
C_s	0.167	0.167	0.167	0.167	0.167	0.167
C_1	0.014	0.014	0.020	0.020	0.020	0.050
ΔC	0.153	0.153	0.147	0.147	0.147	0.117
k_1	0.989×10^{-3}	0.484×10^{-3}	1.449×10^{-3}	6.93×10^{-4}	2.30×10^{-3}	1.632×10^{-3}
k_1/V_s	0.816×10^{-5}	0.403×10^{-5}	1.055×10^{-3}	5.73×10^{-6}	1.86×10^{-5}	1.19×10^{-3}
J_d	23.2×10^{-5}	11.5×10^{-5}	30×10^{-3}	16.3×10^{-6}	53.1×10^{-5}	31.7×10^{-3}

Run No.	103	104	105	107	108	109
T_e	500	500	500	500	500	500
$\mu \times 10^2$	1.84	1.84	1.84	1.84	1.84	1.84
ρ	7.82	7.82	7.82	7.82	7.82	7.82
$D_v \times 10^5$	1.55	1.55	1.55	1.55	1.55	1.55
N_{Sc}	151.8	151.8	151.8	151.8	151.8	151.8
V_a, ft/sec	0.04	3.51	3.51	0.04	0.04	3.51
V_s, ft/sec	0.045	3.95	3.95	0.045	0.045	3.95
$N_{Re,s}$	733	6.47×10^4	6.43×10^4	733	732	6.38×10^4
RPM	450	550	550	450	450	550
Δw (measured)	0.6420	1.4869	0.2636	1.0230	0.2928	0.7910
d_s	1.260	1.259	1.257	1.252	1.255	1.249
θ	480	480	480	540	600	480
A_s	4.99	4.96	4.96	4.93	4.95	4.87
C_s	0.167	0.167	0.167	0.167	0.167	0.167
C_1	0.050	0.050	0.050	0.097	0.097	0.097
ΔC	0.117	0.117	0.117	0.070	0.070	0.070
k_1	2.31×10^{-3}	5.36×10^{-3}	0.946×10^{-3}	5.47×10^{-3}	1.375×10^{-3}	4.84×10^{-3}
k_1/V_s	1.69×10^{-3}	4.43×10^{-5}	0.788×10^{-5}	3.99×10^{-3}	1.01×10^{-3}	4.03×10^{-5}
J_d	48.2×10^{-3}	126.1×10^{-5}	22.4×10^{-5}	113.5×10^{-3}	28.7×10^{-3}	115×10^{-5}

TABLE XXXII. (Contd.)

Run No.	130	131	132	133
T_e	500	500	500	500
x 10^2	1.84	1.84	1.84	1.84
	7.82	7.82	7.82	7.82
D_v x 10^5	1.55	1.55	1.55	1.55
N_{Sc}	151.8	151.8	151.8	151.8
V_a, ft/sec	0.04	0.04	3.51	3.51
V_s, ft/sec	0.045	0.045	3.95	3.95
$N_{Re,s}$	734	733	6.42×10^4	6.43×10^4
RPM	540	480	480	480
w (measured)	0.3148	0.3613	0.5597	0.2316
d_s	1.259	1.259	1.255	1.259
A_s	4.97	4.97	4.95	4.97
C_s	0.167	0.167	0.167	0.167
C_1	0.142	0.142	0.142	0.142
C	0.025	0.025	0.025	0.025
k_1	4.67×10^{-3}	6.06×10^{-3}	9.41×10^{-3}	3.87×10^{-3}
k_1/V_s	3.42×10^{-3}	4.43×10^{-3}	7.86×10^{-5}	3.23×10^{-5}
J_d	97.6×10^{-3}	126.5×10^{-3}	224×10^{-5}	92.1×10^{-5}

XVII. APPENDIX: SAMPLE CALCULATIONS OF MASS TRANSFER DATA AND ERROR ANALYSIS

A. Typical Analysis and Data for Run 25

1. Run No. 25

Length of Run θ = 120 sec. Coast-down θ' = 7.2 sec.

Average Cadmium Velocity 3.22 ft/sec; 98.3 cm/sec.

Velocity at Sample, V_s 3.62 ft/sec; 110.41 cm/sec.

Average Temperature Reservoir Tank	500°C
Average Temperature Pump Tank	500°C
Temp TC No. 1	499°C
Temp TC No. 2	499°C
Temperature Sphere	499°C
Orifice Pressure, mm of Hg Abs	$217\Delta P$ $14.8\Delta P^{1/2}$
C_s, Concentration at Saturation	0.167 g/cc, constant from 500 to 600°C
C_l, Concentration at Bulk Liquid	0.00 g/cc

2. Physical Properties at Temperature of Run

Temperature at Sample	499°C
Density of Solution	7.82 g/cc
Viscosity of Solution	1.84 cp
Molecular Diffusivity of Uranium in Cadmium at Run Temperature	$D_v \times 10^5$, 1.54 cm^2/sec
Solubility	C_s, 0.167 g/cc

3. Sphere Properties and Pertinent Measurements (inches)

Before Run: Longitudinal Diameter 0.501; Transverse Diameter 0.499

After Run: Longitudinal Diameter 0.472; Transverse Diameter 0.478

Average Sphere Diameter 0.487

4. Analysis of Sphere by Weight Measurement

Weight Sphere before Run (Before Electropolish)	20.2291 g
Weight Sphere before Run (After Electropolish)	20.2180 g
Weight Sphere plus Cadmium Coating	17.0482 g
Weight Sphere after Acid Cleaned	16.2551 g
Weight Cadmium Coating Dissolved Off	0.7931 g
Net Weight of Uranium Dissolved during Mass Transfer Run plus Coast-down Time ($\theta + \theta'$)	3.9629 g
Average Uranium in Zinc and Flux Phases	0.008 g

B. Computation

1. Calculation of J_d without Coast-down Corrections Applied

From the data and using equation 9.2 the mass transfer coefficient is calculated as

$$k_1 = \frac{3.9629}{(4.8019)(120)(0.167)} = 4.13 \times 10^{-2} \qquad (17.1)$$

using equation 9.4 the dimensionless ratio, k_1/V_s may be calculated

$$\frac{k_1}{V_s} = \frac{4.13\ (10^{-2})}{110.41} = 3.74\ (10^{-4}) \qquad (17.2)$$

Using equation 9.6 with the Schmidt number, 151.8, raised to the 2/3 exponent, or 28.45, the J_d factor is calculated as

$$J_d = 3.74\ (10^{-4})(28.45) = 106.2\ (10^{-4}) \qquad (17.3)$$

The preceding figure represents the apparent J_d factor without any corrections for the effective mass transferred during coast-down. The effective velocity past the sphere in this case is $\bar{\epsilon}V_s$ or $0.436 \times V_s$.

2. Sample Calculation of J_d with Coast-down Corrections Applied

The average diameter of the sphere, 0.478 inches is used to calculate an average surface area as

$$A_s = \pi d_s^2 = 3.14(0.237)(6.45) = 4.8019\ cm^2. \qquad (17.4)$$

The effective mass transferred during the coast-down time may be calculated by employing the apparent k_l/V_s which was calculated above in part 1. The average effective velocity at coast-down is taken as the velocity at the sphere multiplied by $\bar{\epsilon}$. The effective mass transferred during θ' is subtracted from the weight loss from the sphere during $(\theta + \theta')$ seconds and an actual J_d factor is calculated using the corrected weight. The effective mass transferred in this case is

$$\Delta w' = \left(\frac{k_l}{V_s}\right) \times \bar{\epsilon} \times V_s \times \Delta C \times A_s \times \theta' \tag{17.5}$$

$$\Delta w' = 3.74(10^{-4})(0.436)(110.41)(0.167)(4.8019)(7.2)$$

$$\Delta w' = 0.1053 \text{ g} \tag{17.6}$$

The actual mass transferred, therefore, was

$$\Delta w = \Delta w \text{ measured} - \Delta w' \tag{17.7}$$

$$\Delta w = 3.9629 - 0.1053$$

The actual $\left(\frac{k_l}{V_s}\right)$ amounts to

$$\frac{3.8576}{110.41 \times (0.167)(4.8019)(120)} = 3.63 \times 10^{-4} \tag{17.8}$$

The actual J_d factor amounts to

$$J_d = (3.63 \times 10^{-4})(28.456) = 103.6 \times 10^{-4} \tag{17.9}$$

The percentage change in J_d which results from the coast-down is

$$\frac{\Delta w}{w} \times 100 = \frac{0.1053}{3.9629} \times 100 = \frac{10.53}{3.9629} = 2.67\% \tag{17.10}$$

In all the experimental runs, the maximum change in J_d because of coast-down was 4.8% in run 22. In the majority of runs, the change in J_d due to coast-down was less than 1 to 2%. Hence, the coast-down correction was not applied in Tables XXVIII to XXXII.

C. Summary of All Errors for J_d Calculation for Run 25

1. Summary of Measurements and Properties

The experimental data for the mass transfer study were correlated by using the Chilton-Colburn J_d factor equation. The range of accuracy

of the data is dependent upon the precision and accuracy with which other measurements may be taken and also upon the range of accuracy of other physical data needed for the determination of the Schmidt number and the mass transfer coefficient. The following calculation is based upon known and probable or estimated errors for the various properties needed for the J_d calculation. The following table lists the property and the range of accuracy of the property as considered in this report.

TABLE XXXIII. Summary of Probable Errors

Measurement or Property	Probable Error	Measurement or Property	Probable Error
Micrometer Reading	±0.001 inch	Solubility	±1%
Temperature, T°C	±1°C	Area of Sphere	±1%
Molecular Diffusivity	±15%	Weight Loss	±0.0001 g
Cadmium Velocity	±2%	Viscosity	±2%
Schmidt Number	±19%	Density	±2%

2. Calculation of Probable Errors in J_d

The calculation of the probable error in J_d is done using the data for run 25 and equation 17.11.

$$J_d = \frac{k_l}{V_s}\left(\frac{\mu}{\rho D_v}\right)^{0.666} \tag{17.11}$$

The k_l/V_s is calculated from equation 17.8. The error in k_l/V_s is the sum of the errors in V_s, A_s, C_s, and Δw.

$$\text{Error in } k_l/V_s = 2.0 + 1.0 + 1.0 + 0 = \pm 4.0\%. \tag{17.12}$$

To calculate the error in J_d it is obtained by differentiating equation 17.11 and inserting the errors in each variable.

$$\text{Error in } J_d = 4.0 + 0.666(19.0) = \pm 14.6\%. \tag{17.13}$$